

Comprehensive Mapping of PERIOD2 Expression Patterns
in the Rat Forebrain Across the 24-hr Day

Valerie Harbour

A Thesis

In the Department

of

Psychology

Presented in Partial Fulfillment of the Requirements

For the Degree of

Doctor of Philosophy (Psychology)

Concordia University

Montreal, Quebec, Canada

December 2011

© Valerie Harbour, 2011

**CONCORDIA UNIVERSITY
SCHOOL OF GRADUATE STUDIES**

This is to certify that the thesis prepared

By: Valerie Harbour

Entitled: Comprehensive Mapping of PERIOD2 Expression Patterns in the Rat
Forebrain Across the 24-hr Day

and submitted in partial fulfillment of the requirements for the degree of

Doctor of Philosophy

complies with the regulations of the University and meets the accepted standards with respect to originality and quality.

Signed by the final examining committee:

_____ Chair

____Dr. Mongrain_____ External Examiner

____Dr. Courtemanche_____ External to Program

____Dr. Woodside_____ Examiner

____Dr. Shalev_____ Examiner

____Dr. Amir_____ Thesis Supervisor

Approved by

Chair of Department or Graduate Program Director

Dean of Faculty

ABSTRACT

Comprehensive Mapping of PERIOD2 Expression Patterns in the Rat Forebrain Across the 24-hr Day

Valerie Harbour, Ph.D.

Concordia University, 2011

In mammals, a light-entrainable circadian clock located in the suprachiasmatic nucleus (SCN) regulates circadian behavioural and physiological rhythms by synchronizing oscillators throughout the brain and body. Synchrony between these multiple oscillators is believed to be essential for normal daily functions, and disruptions of the phase relationships between them are associated with several disorders and disease.

Importantly, the nature of the relationship between the master SCN clock and subordinate oscillators in the rest of the brain is not well defined. We performed an unparalleled high temporal resolution analysis of potential extra-SCN brain oscillators by analyzing the expression of the clock protein PERIOD2 (PER2) throughout the forebrain of the inbred Lewis (LEW/Crl) rat. In addition, we analyzed the transcript levels of two core clock genes, *Per2* and *Bmal1*, and a clock-controlled gene, *Dbp*, in the SCN and two limbic forebrain regions. Eighty-four LEW/Crl male rats were individually housed in cages equipped with running wheels and were entrained to a regular 12-hr:12-hr light/dark cycle. After 3-4 weeks on this schedule, rats were perfused every 30 min across the 24-hr day, giving a total of 48 time-points ($n=1-4/\text{time-point}$). In this thesis, I report the

presence of circadian rhythms in clock gene expression in brain areas important for locomotion, stress, emotion, motivation, and learning and memory, and further explore the relationship between these rhythms. Twenty-two brain areas showed PER2 expression including the SCN, bed nucleus, and several regions of the amygdala, hippocampus, striatum, and cortex. Of these, 20 structures displayed circadian rhythms in PER2 expression. Remarkably, none of the PER2 rhythms in any of the regions analyzed were in phase with the SCN. Instead, an intricate network of brain oscillators with clock gene expression peaking at different times throughout the day was revealed. Furthermore, *Per2*, *Bmal1*, and *Dbp* were rhythmic in the SCN, CEAl, and DG, albeit to different degrees, consistent with the presence of a functional circadian clock in these regions. The data demonstrate the presence of complex and previously unappreciated associations of clock phases throughout the mammalian brain. This comprehensive atlas of clock gene rhythms in the normal rat brain will provide a sound baseline for studies of circadian clock function in animal models of disease.

ACKNOWLEDGEMENTS

First and foremost, I would like to thank my supervisor, Dr. Amir, for sharing his wealth of knowledge on circadian rhythms, his constant support, and for believing in me. Thanks Shimmy.

I would also like to thank Dr. Woodside for commenting on drafts of the thesis and for her genuine interest in my work, and me, throughout my graduate studies.

Thank you to Barry Robinson for teaching me all the laboratory procedures necessary for my experiments and to Yuval Weigl for showing me the PCR ropes.

Thank you to Dr. Shizgal and Dr. Conover for their generous and much appreciated help with the statistics applied in this thesis. I now know all about Akaike and his information criterion!

Thank you to Beata, Elaine, and Alex for their comments and discussions on the PCR related aspects of this thesis. Your help was greatly appreciated!

Thank you to the outstanding CSBN/Psychology staff (past and present) for all of their help and support throughout my studies: Shirley, Phyllis, Elizabeth, Heshmat, Isabelle, Pat, Dave, Steve, Aileen, and Andrea.

I have made some wonderful friends at the CSBN over the past years; thank you to each and every one of you for your help/support, enthusiastic science related discussions, and especially, for the fun times and laughs, which is probably what kept me (somewhat) sane through this process!! Thank you especially to (in no particular order): Lauren, May, Suzanne, Elaine, Laura, Katuschia, Stephanie, Dema, Sherin, Dean, Patrick, Sherri, and Yannick. Alex, thank you for your help with (unfortunately

unsuccessful) experiments, volleyball captain'ing, rants on the economy (hey, you got me to invest in silver!!), and most of all for your friendship. To my fellow student Amir lab mates (past and present); thanks for making it such a great place to work!

Thank you to my family (my parents: Steve and Lucie, my grand-parents: Ina, Percy, Madeleine, and Gérard, and my Beaulé in-laws) and hometown friends (especially, Nancy, Tricia, and Serita) for their constant support and love. To Chris, my future hubby, love of my life, thank you a million times over for your support, countless thesis editing and related discussions, encouragement, and love throughout this process. I couldn't have done it without you! Je t'aime.

Finally, I would like to thank FRSQ and Concordia for funding during my doctoral degree.

CONTRIBUTION TO DATA

Dr. Shimon Amir, Dr. Yuval Weigl, and Valerie Harbour designed the experiments. Weigl, Harbour, and Barry Robinson performed the perfusions and tissue slicing. All IHC, microscopy, and data analysis for Chapter 1 as well as the tissue punching for qRT-PCR was performed by Harbour. Weigl and Harbour performed all procedures related to qRT-PCR and the analysis of these data (Chapter 2).

TABLE OF CONTENTS

	Page
List of Figures	ix
List of Tables	xxii
Notes on Nomenclature	xxvi
List of Abbreviations	xxvii
Introduction	1
Chapter 1: PERIOD2 protein	25
Methods	25
Results	32
Summary of results	79
Chapter 2: mRNA	83
Methods	83
Results	89
Summary of results	97
Discussion	106
References	127
Appendix	145

LIST OF FIGURES

	Page
Figure 1. Molecular clock.	10
Simplified schematic diagram of the circadian molecular clock. <i>Genes are in italic</i> , PROTEINS ARE CAPITALIZED, P= phosphorylation, ----+ = activation, — = inhibition, →= transcription, →= translation.	
Figure 2. Wheel-running activity.	33
Representative single-plotted actograms from 4 rats showing stable entrainment to the 24-hr LD cycle. White and grey backgrounds indicate lights on or off, respectively. Black vertical marks indicate periods of activity of at least 10 wheel revolutions/10 min. Successive days are plotted from top to bottom.	
Figure 3. Individual differences in wheel-running activity.	34
Average number of wheel revolutions (\pm SEM) for the light (ZT0-ZT12) and dark (ZT12- ZT24) periods of the last 7 days of activity for each group ($n= 12$ /group).	
Figure 4. Schematic diagram of the rat brain (sagittal view).	35
Depiction of the five major brain areas (SCN: ☆, Amygdala: □, Hippocampus: ◇, Striatum: ○, and Cortex: ▲) that were analyzed for this study. In total, 22 different sub- regions were examined.	
Figure 5. Suprachiasmatic Nucleus (SCN).	36

A) Schematic diagrams of the SCN, coronal view (left) and sagittal view (right), number corresponds to level in the Swanson atlas. B) Representative photomicrographs (square in A) of PER2 expression at ZT1 and ZT13. C) Mean number of PER2-immunoreactive cells in the SCN of each individual rat (diamonds) across 48 *zeitgeber* times. White and grey backgrounds indicate lights on and off, respectively. R²= Goodness of fit value for given sine wave. n= 81 (1 outlier removed, red diamond).

Figure 6. PERIOD2 in the SCN.

38

Representative photomicrographs of PER2 expression in the SCN every hour across the 24-hr day. *Zeitgeber* time (ZT) 0 denotes lights on, ZT12 lights off.

Figure 7. SCN core and shell.

39

A) Representative photomicrograph of PER2 expression at ZT19. Arrows highlight the core and shell regions. Mean number of PER2-immunoreactive cells in the SCNsh (B) and SCNc (C) of each individual rat (diamonds) across 48 *zeitgeber* times. White and grey backgrounds indicate lights on and off, respectively. R²= Goodness of fit value for given sine wave. n= 81 (1 outlier removed, red diamond).

Figure 8. Suprachiasmatic Nucleus.

43

A) Sine-fitted PER2 expression patterns in the SCN core and shell across 48 *zeitgeber* times. Solid line: 24-hr fit, dotted line: <28-hr fit. B) Amplitudes (mean number \pm SEM of PER2 immunoreactive cells) measured from peak to trough, in the core and shell compared to the whole SCN, Symbols indicate statistical significance ($p < .001$) as

follows: *: whole SCN compared to both subdivisions, †: core compared to shell. C) Rhythmicity index values for the SCN core and shell normalized to the whole SCN.

Figure 9. Oval Nucleus of the Bed Nucleus of the Stria Terminalis (BNSTov). 44

A) Schematic diagrams of the BNSTov, coronal view (left) and sagittal view (right), number corresponds to level in the Swanson atlas. B) Representative photomicrographs (square in A) of PER2 expression at ZT1 and ZT13. C) Mean number of PER2-immunoreactive cells in the BNSTov of each individual rat (black diamonds) across 48 *zeitgeber* times. White and grey backgrounds indicate lights on and off, respectively. R^2 = Goodness of fit value for given sine wave. $n= 84$

Figure 10. Central Nucleus of the amygdala, lateral (CEAl). 46

A) Schematic diagrams of the CEAl, coronal view (left) and sagittal view (right), number corresponds to level in the Swanson atlas. B) Representative photomicrographs (square in A) of PER2 expression at ZT1 and ZT13. C) Mean number of PER2-immunoreactive cells in the CEAl of each individual rat (black diamonds) across 48 *zeitgeber* times. White and grey backgrounds indicate lights on and off, respectively. R^2 = Goodness of fit value for given sine wave. $n= 84$

Figure 11. Basolateral Amygdala (BLA). 47

A) Schematic diagrams of the BLA, coronal view (left) and sagittal view (right), number corresponds to level in the Swanson atlas. B) Representative photomicrographs (square in A) of PER2 expression at ZT1 and ZT13. C) Mean number of PER2-immunoreactive

cells in the BLA of each individual rat (black diamonds) across 48 *zeitgeber* times. White and grey backgrounds indicate lights on and off, respectively. R^2 = Goodness of fit value for given sine wave. $n= 84$

Figure 12. Medial Amygdala, posteriodorsal (MEApd). 49

A) Schematic diagrams of the MEApd, coronal view (left) and sagittal view (right), number corresponds to level in the Swanson atlas. B) Representative photomicrographs (square in A) of PER2 expression at ZT1 and ZT13. C) Mean number of PER2-immunoreactive cells in the MEApd of each individual rat (black diamonds) across 48 *zeitgeber* times. White and grey backgrounds indicate lights on and off, respectively. R^2 = Goodness of fit value for given sine wave. $n= 84$

Figure 13. Amygdala. 50

A) Sine-fitted PER2 expression patterns in all 4 regions of the amygdala across 48 *zeitgeber* times. B) Amplitudes (mean number \pm SEM of PER2 immunoreactive cells) measured from peak to trough, in each region of the amygdala, compared to the SCN. Symbols indicate statistical significance ($p<.05$) as follows: *: SCN compared to all other regions, †: CEAl compared to all other regions, ‡: MEApd compared to all other regions. C) Rhythmicity index values for the 4 regions of the amygdala normalized to the SCN.

Figure 14. Dentate Gyrus (DG). 53

A) Schematic diagrams of the DG, coronal view (left) and sagittal view (right), number corresponds to level in the Swanson atlas. B) Representative photomicrographs (square in

A) of PER2 expression at ZT1 and ZT13. C) Mean number of PER2-immunoreactive cells in the DG of each individual rat (diamonds) across 48 *zeitgeber* times. White and grey backgrounds indicate lights on and off, respectively. R^2 = Goodness of fit value for given sine wave. $n= 78$ (6 outliers removed, red diamonds)

Figure 15. CA1.

54

A) Schematic diagrams of the CA1, coronal view (left) and sagittal view (right), number corresponds to level in the Swanson atlas. B) Representative photomicrographs (square in A) of PER2 expression at ZT1 and ZT13. C) Mean number of PER2-immunoreactive cells in the CA1 of each individual rat (black diamonds) across 48 *zeitgeber* times. White and grey backgrounds indicate lights on and off, respectively. R^2 = Goodness of fit value for given sine wave. $n= 84$

Figure 16. CA3.

55

A) Schematic diagrams of the CA3, coronal view (left) and sagittal view (right), number corresponds to level in the Swanson atlas. B) Representative photomicrographs (square in A) of PER2 expression at ZT1 and ZT13. C) Mean number of PER2-immunoreactive cells in the CA3 of each individual rat (diamonds) across 48 *zeitgeber* times. White and grey backgrounds indicate lights on and off, respectively. R^2 = Goodness of fit value for given sine wave. $n= 82$ (2 outliers removed, red diamonds)

Figure 17. Hippocampus.

57

A) Sine-fitted PER2 expression patterns in all 3 regions of the hippocampus across 48 *zeitgeber* times. Solid line: 24-hr fit, dotted line: <28-hr fit. B) Amplitudes (mean number \pm SEM of PER2 immunoreactive cells) measured from peak to trough, in each region of the hippocampus, compared to the SCN. Symbols indicate statistical significance ($p < .01$) as follows: *: SCN compared to all other regions, †: DG compared to all other regions. C) Rhythmicity index values for the 3 regions of the hippocampus normalized to the SCN.

Figure 18. Anterior striatum, dorsal (ASd). 59

A) Schematic diagrams of the ASd, coronal view (left) and sagittal view (right), number corresponds to level in the Swanson atlas. B) Representative photomicrographs (square in A) of PER2 expression at ZT1 and ZT13. C) Mean number of PER2-immunoreactive cells in the ASd of each individual rat (black diamonds) across 48 *zeitgeber* times. White and grey backgrounds indicate lights on and off, respectively. R^2 = Goodness of fit value for sine wave. $n = 84$

Figure 19. Anterior striatum, medial (ASm). 60

A) Schematic diagrams of the ASm, coronal view (left) and sagittal view (right), number corresponds to level in the Swanson atlas. B) Representative photomicrographs (square in A) of PER2 expression at ZT1 and ZT13. C) Mean number of PER2-immunoreactive cells in the ASm of each individual rat (black diamonds) across 48 *zeitgeber* times. White and grey backgrounds indicate lights on and off, respectively. R^2 = Goodness of fit value for sine wave. $n = 82$

Figure 20. Posterior striatum, dorsal (PSd).

62

A) Schematic diagrams of the PSd, coronal view (left) and sagittal view (right), number corresponds to level in the Swanson atlas. B) Representative photomicrographs (square in A) of PER2 expression at ZT1 and ZT13. C) Mean number of PER2-immunoreactive cells in the PSd of each individual rat (diamonds) across 48 *zeitgeber* times. White and grey backgrounds indicate lights on and off, respectively. R^2 = Goodness of fit value for sine wave. $n= 83$ (1 outlier removed, red diamond)

Figure 21. Posterior striatum, medial (PSm).

63

A) Schematic diagrams of the PSm, coronal view (left) and sagittal view (right), number corresponds to level in the Swanson atlas. B) Representative photomicrographs (square in A) of PER2 expression at ZT1 and ZT13. C) Mean number of PER2-immunoreactive cells in the PSm of each individual rat (black diamonds) across 48 *zeitgeber* times. White and grey backgrounds indicate lights on and off, respectively. R^2 = Goodness of fit value for sine wave. $n= 82$

Figure 22. Nucleus Accumbens, core (NAcc).

64

A) Schematic diagrams of the NAcc, coronal view (left) and sagittal view (right), number corresponds to level in the Swanson atlas. B) Representative photomicrographs (square in A) of PER2 expression at ZT1 and ZT13. C) Mean number of PER2-immunoreactive cells in the NAcc of each individual rat (black diamonds) across 48 *zeitgeber* times. White and grey backgrounds indicate lights on and off, respectively. R^2 = Goodness of fit value for given sine wave. $n= 74$

Figure 23. Nucleus Accumbens, shell (NAcsh).

65

A) Schematic diagrams of the NAcsh, coronal view (left) and sagittal view (right), number corresponds to level in the Swanson atlas. B) Representative photomicrographs (square in A) of PER2 expression at ZT1 and ZT13. C) Mean number of PER2-immunoreactive cells in the NAcsh of each individual rat (black diamonds) across 48 *zeitgeber* times. White and grey backgrounds indicate lights on and off, respectively. R^2 = Goodness of fit value for sine wave. $n= 74$

Figure 24. Striatum.

67

A) Sine-fitted PER2 expression patterns in all 6 regions of the striatum across 48 *zeitgeber* times. B) Amplitudes (mean number \pm SEM of PER2 immunoreactive cells) measured from peak to trough, in each region of the striatum, compared to the SCN. Symbols indicate statistical significance ($p<.01$) as follows: *: SCN compared to all other regions, †: NAcc compared to all other regions, ‡: NAcsh compared to all other regions. C) Rhythmicity index values for the 6 regions of the striatum normalized to the SCN.

Figure 25. Endopiriform cortex, dorsal (EPd).

69

A) Schematic diagrams of the EPd, coronal view (left) and sagittal view (right), number corresponds to level in the Swanson atlas. B) Representative photomicrographs (square in A) of PER2 expression at ZT1 and ZT13. C) Mean number of PER2-immunoreactive cells in the EPd of each individual rat (black diamonds) across 48 *zeitgeber* times. White and grey backgrounds indicate lights on and off, respectively. R^2 = Goodness of fit value for given sine wave. $n= 84$

Figure 26. Piriform cortex, pyramidal layer (PIR2).

70

A) Schematic diagrams of the PIR2, coronal (left) and sagittal view (right), number corresponds to level in the Swanson atlas. B) Representative photomicrographs (square in A) of PER2 expression at ZT1 and ZT13. C) Mean number of PER2-immunoreactive cells in the PIR2 of each individual rat (diamonds) across 48 *zeitgeber* times. White and grey backgrounds indicate lights on and off, respectively. R^2 = Goodness of fit value for sine wave. $n= 78$ (6 outliers removed, red diamonds)

Figure 27. Anterior Cingulate Area, ventral (ACAv).

72

A) Schematic diagrams of the ACAv, coronal view (left) and sagittal view (right), number corresponds to level in the Swanson atlas. B) Representative photomicrographs (square in A) of PER2 expression at ZT1 and ZT13. C) Mean number of PER2-immunoreactive cells in the ACAv of each individual rat (black diamonds) across 48 *zeitgeber* times. White and grey backgrounds indicate lights on and off, respectively. R^2 = Goodness of fit value for given sine wave. $n= 83$ (1 outlier removed, red diamond)

Figure 28. Agranular Insular cortex, posterior (AIp).

73

A) Schematic diagrams of the AIp, coronal view (left) and sagittal view (right), number corresponds to level in the Swanson atlas. B) Representative photomicrographs (square in A) of PER2 expression at ZT1 and ZT13. C) Mean number of PER2-immunoreactive cells in the AIp of each individual rat (black diamonds) across 48 *zeitgeber* times. White and grey backgrounds indicate lights on and off, respectively. R^2 = Goodness of fit value for given sine wave. $n= 84$

Figure 29. Entorhinal cortex, lateral, superficial layers (ENTIs). 74

A) Schematic diagrams of the ENT1 sup, coronal view (left) and sagittal view (right), number corresponds to level in the Swanson atlas. B) Representative photomicrographs (square in A) of PER2 expression at ZT1 and ZT13. C) Mean number of PER2-immunoreactive cells in the ENT1 sup of each individual rat (black diamonds) across 48 *zeitgeber* times. White and grey backgrounds indicate lights on and off, respectively. R^2 = Goodness of fit value for given sine wave. $n= 79$

Figure 30. Entorhinal cortex, lateral, deep layers (ENTId). 75

A) Schematic diagrams of the ENT1 deep, coronal view (left) and sagittal view (right), number corresponds to level in the Swanson atlas. B) Representative photomicrographs (square in A) of PER2 expression at ZT1 and ZT13. C) Mean number of PER2-immunoreactive cells in the ENT1 deep of each individual rat (black diamonds) across 48 *zeitgeber* times. White and grey backgrounds indicate lights on and off, respectively. R^2 = Goodness of fit value for given sine wave. $n= 79$

Figure 31. Cortex. 77

A) Sine-fitted PER2 expression patterns in all 6 regions of the cortex across 48 *zeitgeber* times. Solid line: 24-hr fit, dotted line: <28-hr fit. B) Amplitudes (mean number \pm SEM of PER2 immunoreactive cells) measured from peak to trough, in each region of the cortex, compared to the SCN. Symbols indicate statistical significance ($p<.05$) as follows: *: SCN compared to all other regions, †: PIR2 compared to all other regions, ‡: A1p

compared to EPd, ACAv, and ENTls. C) Rhythmicity index values for the 6 regions of the cortex normalized to the SCN.

Figure 32. Summary: Comparing phase between all regions. 80

A) Sine-fitted PER2 expression patterns in all 22 regions analyzed across 48 *zeitgeber* times. B) 24-hr circular diagram displaying peak PER2 expression in all 20 rhythmic regions. Numbers around the ‘clock’ are in ZT time. ☆: SCN, □: amygdala, ◇: hippocampus, ○: striatum, ▲: cortex.

Figure 33. Summary: Comparing amplitude and strength of rhythms between all regions. 82

A) Amplitudes (mean number \pm SEM of PER2 immunoreactive cells) measured from peak to trough, in all brain regions. B) Rhythmicity Index for each brain region normalized to the SCN.

Figure 34. Suprachiasmatic Nucleus (SCN). 90

Relative mRNA levels of A) *Per2* B) *Bmal1* and C) *Dbp* in the SCN of each individual rat (black diamonds) across 48 *zeitgeber* times. White and grey backgrounds indicate lights on and off, respectively. R^2 = Goodness of fit value for given sine wave. $n= 73$ for each graph

Figure 35. Summary: Comparing phase between all regions and genes. 92

Sine fitted *Per2*, *Bmall*, and *Dbp* expression patterns in the SCN (A), CEAl (B), and DG (C) across 48 *zeitgeber* times.

Figure 36. Central amygdala, lateral (CEAl). 94

Relative mRNA levels of A) *Per2* B) *Bmall* and C) *Dbp* in the CEAl of each individual rat (black diamonds) across 48 *zeitgeber* times. White and grey backgrounds indicate lights on and off, respectively. R²= Goodness of fit value for given sine wave. n= 74 for each graph

Figure 37. Dentate gyrus (DG). 96

Relative mRNA levels of A) *Per2* B) *Bmall* and C) *Dbp* in the DG of each individual rat (black diamonds) across 48 *zeitgeber* times. White and grey backgrounds indicate lights on and off, respectively. R²= Goodness of fit value for given sine wave. n= 74, except for *Per2* where n=73

Figure 38. *Period2*. 99

A) Sine-fitted *Per2* expression patterns in all 3 regions across 48 *zeitgeber* times. B) Amplitudes (mean number ± SEM of relative *Per2* mRNA) measured from peak to trough, in each region. Symbol indicates statistical significance ($p<.05$) as follows: *: CEAl compared to all other regions.

Figure 39. PER2 protein vs *Per2* mRNA. 100

Sine-fitted *Per2* mRNA (light blue) versus PER2 protein expression in the A) suprachiasmatic nucleus B) central amygdala, lateral and C) dentate gyrus across 48 *zeitgeber* times. Solid lines: 24-hr fit, dotted lines: <28-hr fit.

Figure 40. *Bmal1*. 102

A) Sine-fitted *Bmal1* expression patterns in all 3 regions across 48 *zeitgeber* times. B) Amplitudes (mean number \pm SEM of relative *Bmal1* mRNA) measured from peak to trough, in each region.

Figure 41. *Dbp*. 104

A) Sine-fitted *Dbp* expression patterns in all 3 regions across 48 *zeitgeber* times. B) Amplitudes (mean number \pm SEM of relative *Dbp* mRNA) measured from peak to trough, in each region.

Figure 42. Summary: Comparing phase between regions. 105

24-hr circular diagram displaying peak *Per2* (A), *Bmal1* (B), and *Dbp* (C) expression in the SCN, CEAL, and DG. Numbers around the 'clock' are in *zeitgeber* time.

LIST OF TABLES

	Page
Table 1. Summary of statistical tests conducted on sine wave data.	41
Values in bold are statistically significant ($p < .05$), except for AIC results which don't have a p value, here values in bold are deemed to be meaningfully different based on the Evidence Ratio.	
Notes:	42
N/A: not applicable, for these regions the <28-hr model could not be fitted to the data.	
Outliers were found using the ROUT method (which combines R obust regression with O utlier removal) with a False Discovery Rate of 1% (recommended by Prism) and removed from all analyses (Motulsky & Brown, 2006).	
Akaike Information Criterion (AIC): The data were fit with two models, Model 1: frequency =24-hrs, Model 2: frequency is <28-hrs, and compared using the AIC. The AIC quantifies how well each model fit the data (based on goodness-of-fit, i.e. sum of squares, and the number of parameters in each model), and determines the preferred model (column 1 in AIC). The difference in AIC is what matters and tells us the likelihood that a model is correct (column 2, Prism calculates the corrected AIC (AICc) which corrects for low sample size), and with the Evidence Ratio (the probability that model 1 is correct over the probability that model 2 is correct, column 3), qualifies the difference between the models. We followed the guidelines in the Prism manual that state that an Evidence Ratio of 12 or less suggests no meaningful differences between the models (Motulsky & Christopoulos, 2003).	
D'Agostino-Pearson omnibus K^2 test (i.e. normality test): This test determines the skewness and kurtosis for a given data set and quantifies how far from Gaussian the	

distribution is (in terms of asymmetry and shape) and calculates how far each of these values differs from the value expected with a Gaussian distribution. A data set **fails** the normality test when the ***p* value is ≤ 0.05** , meaning that it deviates significantly from a normal distribution.

Wald-Wolfowitz Runs Test (i.e. Runs test): This test determines whether the fitted curve deviates systematically from the data (i.e. it looks for patterns in the residuals). A run is a consecutive series of data points whose residuals are either all positive or all negative (a small number of runs would indicate patterns in the residuals). A data set **fails** the Runs test when the ***p* value is ≤ 0.05** , meaning that the data points are not randomly distributed along the curve.

Table 2. Correlations of PER2 expression in the amygdala. 51

Pearson r values comparing regions of the amygdala and the master SCN clock across the 24-hr day. Values in bold are statistically significant ($p < 0.05$). The MEApd has been omitted since it is arrhythmic.

Table 3. Correlations of PER2 expression in the hippocampus. 58

Pearson r values comparing regions of the hippocampus and the master SCN clock across the 24-hr day. Values in bold are statistically significant ($p < 0.05$).

Table 4. Correlations of PER2 expression in the striatum. 68

Pearson r values comparing regions of the striatum and the master SCN clock across the 24-hr day. Values in bold are statistically significant ($p < .05$). The NAcsh has been omitted since it is arrhythmic.

Table 5. Correlations of PER2 expression in the cortex. 78

Pearson r values comparing regions of the cortex and the master SCN clock across the 24-hr day. Values in bold are statistically significant ($p < .05$).

Table 6. Primer/ Probe sequences and Amplicon length of target clock genes. 87

Table 7. Correlations between *Per2*, *Bmal1*, and *Dbp* expression. 93

Pearson r values comparing clock genes in the SCN (A), CEAl (B), and DG (C) across the 24-hr day. Values in bold are statistically significant ($p < .05$).

Table 8. Correlations between the SCN, CEAl, and DG. 101

Pearson r values comparing brain regions for *Per2* (A), *Bmal1* (B), and *Dbp* (C) expression across the 24-hr day. Values in bold are statistically significant ($p < .05$).

NOTES ON NOMENCLATURE

In order to readily differentiate between genes and proteins, mRNA or anything other than the final protein product are *Italicized* with the first letter capitalized, whereas proteins are written in CAPITAL letters. This has been made consistent throughout the thesis

Only rats were used in this thesis, thus the “r” before a given gene or protein has been omitted. When there is mention of clock genes in another species, it is explicitly specified.

LIST OF ABBREVIATIONS

ACAv	Anterior cingulate area, ventral
AIp	Agranular insular cortex, posterior
ASd	Anterior striatum, dorsal
ASm	Anterior striatum, medial
AVP	Arginine vasopressin
BLA	Basolateral amygdala
<i>Bmal1</i> , BMAL1	Brain and muscle Arnt-like <i>gene</i> , protein 1
BNSTov	Bed nucleus of the stria terminalis, oval nucleus
CA1	Field CA1, Ammon's horn
CA3	Field CA3, Ammon's horn
CCG	Clock-controlled gene
CEAl	Central amygdala, lateral
CK1 δ , ϵ	Casein kinase 1 delta, epsilon
<i>Clock</i> , CLOCK	Circadian locomotor output cycles kaput <i>gene</i> , protein
<i>Cry</i> , CRY	Cryptochrome <i>gene</i> , protein
<i>Dbp</i>	albumin promoter D-site binding protein <i>gene</i>
DG	Dentate gyrus
ENK	Enkephalin
ENTld	Entorhinal cortex, lateral, deep layers (IV-VI)
ENTls	Entorhinal cortex, lateral, superficial layers (I-III)
EPd	Endopiriform cortex, dorsal

GRP	Gastrin-releasing peptide
GSK3	Glycogen synthase kinase 3
IHC	Immunohistochemistry
KO	Knockout
LD	Light/dark cycle
MEApd	Medial amygdala, posterodorsal
NAc	Nucleus accumbens
NAcc	Nucleus accumbens core
NAcsh	Nucleus accumbens shell
OB	Olfactory bulb
<i>Per2</i> , PER2	Period2 <i>gene</i> , protein
PIR2	Piriform cortex, pyramidal layer 2
qRT-PCR	Quantitative Real-Time polymerase chain reaction
PSd	Posterior striatum, dorsal
PSm	Posterior striatum, medial
RF	Restricted feeding
SCN	Suprachiasmatic nucleus
SCNc	Suprachiasmatic nucleus core
SCNsh	Suprachiasmatic nucleus shell
VIP	Vasoactive intestinal polypeptide
WRA	Wheel-running activity
ZT	<i>Zeitgeber</i> time

INTRODUCTION

To adapt to the 24-hr light/dark (LD) cycle imposed by the Earth's rotation on its axis most living organisms have developed an internal timing mechanism, modulated by light, that regulates daily rhythms in physiology and behaviour. This daily time keeping allows organisms to anticipate day/night transitions and establish the best time for activities and processes such as leaf movements in plants, cell division and DNA replication in eukaryotes, and foraging and sleeping in vertebrates, thereby increasing survivability.

In mammals, this timing mechanism, also known as the 'biological clock', regulates nearly all physiological processes essential for normal organismal functioning, from gene expression, hormone secretion, and body temperature, to mood, feeding, and most notably, the sleep/wake cycle (Cassone, Warren, Brooks, & Lu, 1993; Reppert & Weaver, 2002). The importance of these 'circadian' (from the Latin *circa diem* meaning 'about a day') rhythms is underscored by the evidence that their disruption can lead to a myriad of health and behavioural problems such as metabolic, sleep, and mood disorders, and even cancer (Arble, Ramsey, Bass, & Turek, 2010; Lamont, James, Boivin, & Cermakian, 2007). A familiar example of the consequences of circadian disruption is the general malaise felt in relation to jet lag and rotating shift work (Bunney & Bunney, 2000).

Mammalian circadian rhythms are thought to be regulated by central and peripheral circadian oscillators that are under the synchronizing control of a light-entrainable master clock, located in the suprachiasmatic nucleus (SCN) of the hypothalamus (Lowrey & Takahashi, 2000). In recent years, a great deal has been learned

about the core ‘clock’ genes and molecular programs responsible for the generation of circadian rhythms at the cell and tissue levels, and about the cellular and neural mechanisms mediating circadian rhythms in the SCN. In contrast, very little is known about the nature, regulation, and function of circadian oscillators outside the SCN.

Using the core clock protein, PERIOD2 (PER2), as a functional marker (Akashi, Ichise, Mamme, & Takumi, 2006; Zheng et al., 1999), our laboratory has previously characterized novel SCN-driven circadian oscillators in four anatomically and functionally interconnected regions of the limbic forebrain: the oval nucleus of the bed nucleus of the stria terminalis (BNSTov), the lateral central amygdala (CEAl), the basolateral amygdala (BLA), and the dentate gyrus (DG) of the hippocampus (Amir, Lamont, Robinson, & Stewart, 2004; Lamont, Robinson, Stewart, & Amir, 2005). Remarkably, the rhythms in PER2 in the BNSTov and CEAl peaked at opposite time of day than those found in the BLA and DG, revealing that distinct phase relationships exist between subordinate brain oscillators. A leading hypothesis is that the network organization of extra-SCN oscillators defines the normal functioning state of the brain. However, their number, the extent of their distribution, and the phase relationship they establish between themselves and with the SCN still remains unclear. Using a high temporal resolution analysis of PER2 expression, the aim of this thesis was to identify novel circadian oscillators in the rat forebrain and characterize their phase relationships. A brief review of the circadian system pertinent to this thesis is given below.

The suprachiasmatic nucleus

The SCN is a bilateral structure located in the anterior hypothalamus above the optic chiasm on either side of the third ventricle. Each nucleus is composed of approximately 10,000 neurons, most of which are considered to be self-sustained autonomous oscillators (Reppert & Weaver, 2001; Welsh, Logothetis, Meister, & Reppert, 1995). The SCN can be divided into two sub-structures, the ventrolateral core and dorsomedial shell (Moore, Speh, & Leak, 2002; Van den Pol, 1980). The cells in the core are retinorecipient and play a key role in photic entrainment, whereas, the cells in the shell act as the main output system of the SCN communicating timing signals to the rest of the brain (Drouyer, LeSauter, Hernandez, & Silver, 2010; Leak, Card, & Moore, 1999). In addition to direct retinal input through the retinohypothalamic tract (RHT), containing glutamate and pituitary adenylate cyclase-activating polypeptide (PACAP, (Moore & Lenn, 1972), the core also receives indirect input from the retina via projections from the retinorecipient thalamic intergeniculate leaflet (containing neuropeptide Y and gamma-aminobutyric acid, GABA) (Morin & Blanchard, 2001; Pickard, 1985), and serotonergic projections from the median raphe nucleus (Moga & Moore, 1997). The shell receives non-visual moderate to sparse projections from multiple areas, including the surrounding hypothalamic regions, thalamus, basal forebrain, limbic cortex, and brainstem (Moga & Moore, 1997; Moore, Speh, & Leak, 2002). Thus, efferents from the core send circadian timing signals to the shell carrying information about external light-cues, while projections from the shell send signals that integrate timing information from the core along with non-visual information from multiple brain areas (Moore, Speh, & Leak, 2002). While the core projects mostly to the shell, the shell projects heavily to the subparaventricular zone and also to other regions in the adjoining

hypothalamus, such as the dorsomedial and ventromedial nuclei, paraventricular nucleus, and medial preoptic area, with few efferent projections to the SCN core (Leak & Moore, 2001; Watts & Swanson, 1987). There has also been some evidence for sparse projections from the SCN to the BNST (Leak & Moore, 2001; Watts & Swanson, 1987) and medial amygdala (Canteras, Ribeiro-Barbosa, Goto, Cipolla-Neto, & Swanson, 2011; Watts & Swanson, 1987).

Although most, if not all, neurons in the SCN are GABAergic (Moore & Speh, 1993), clear distinctions can be made between the core and shell subdivisions based on their respective distribution of neuropeptides. Neurons in the core mostly express vasoactive intestinal polypeptide (VIP) or gastrin-releasing peptide (GRP), while neurons in the shell mostly express arginine vasopressin (AVP) (Moore, Speh, & Leak, 2002). In addition, other neuropeptides co-localized with GABAergic neurons are produced distinctly within the subdivisions of the SCN in smaller quantities. Specifically, neurons in the core also express calbindin, neurotensin, or substance P, while neurons in the shell also express calretinin, enkephalin (ENK), or somatostatin (Moore, Speh, & Leak, 2002).

In both nocturnal and diurnal rodents, most SCN neurons display 24-hr rhythms in firing rate with peak activity occurring during the subjective day and low levels of firing during the subjective night (Inouye & Kawamura, 1979; Smale, Nunez, & Schwartz, 2008; van Esseveldt, Lehman, & Boer, 2000; Welsh, Logothetis, Meister, & Reppert, 1995). *In vivo* simultaneous recordings of multiunit activity have revealed circadian changes in firing rates in other brain regions in both rats and hamsters, such as the thalamus, hypothalamus, dorsal and ventral striatum, raphe nucleus, and visual cortex, that peak in antiphase with the firing rate seen in the SCN, in the subjective night (Inouye

& Kawamura, 1979; Yamazaki, Kerbeshian, Hocker, Block, & Menaker, 1998). In contrast, firing rates in the BNSTov were found to peak in phase with the SCN, during the subjective day (Yamazaki, Kerbeshian, Hocker, Block, & Menaker, 1998). These data are consistent with the unique phase relationship seen in PER2 protein expression between the SCN and BNSTov (Amir, Lamont, Robinson, & Stewart, 2004).

The SCN possesses all the necessary characteristics of a circadian pacemaker: intrinsic rhythmicity (Abe et al., 2002; Green & Gillette, 1982; Yamazaki et al., 2000), an endogenous (i.e. free running) period of approximately 24-hrs (Groos & Hendriks, 1982; Inouye & Kawamura, 1979; Yamazaki, Kerbeshian, Hocker, Block, & Menaker, 1998), entrainment to external time cues, an ability to keep accurate time across varying temperatures (described as ‘temperature compensation’) (Herzog & Huckfeldt, 2003; Ruby, Burns, & Heller, 1999), and an ability to drive rhythms in physiology and behaviour. For example, the diurnal rhythm in locomotor activity is driven by the SCN. Furthermore, the pineal hormone, melatonin, displays a 24-hr rhythm that is regulated by the SCN and is suppressed by light, and also feeds back onto the SCN playing a key role in the regulation of the expression of certain clock genes (Jilg et al., 2005; Uz, Akhisaroglu, Ahmed, & Manev, 2003; von Gall et al., 2002). Rhythmic cortisol (corticosterone in rodents) secretion from the adrenal glands is also under the control of the SCN, showing peak levels at the time of awakening with minimal levels early in the inactive phase (Weitzman et al., 1971). The diurnal rhythm of core body temperature is also driven by the SCN, with the lowest values seen a few hours before awakening (Refinetti & Menaker, 1992).

The master clock is appropriately named in that lesions of the SCN result in complete behavioural and physiological arrhythmicity (Abe, Kroning, Greer, & Critchlow, 1979; Stephan & Zucker, 1972). Confirmation of the role of the SCN as the master clock comes from experiments where fetal SCN transplants were found to restore locomotor rhythmicity in SCN-ablated recipients, and importantly, to do so with the period of the donor (Lehman et al., 1987; Ralph, Foster, Davis, & Menaker, 1990). The finding that periodicity is contained within the cells of the SCN and that rhythm properties of the donor can be communicated to host tissue established the SCN as both necessary and sufficient for circadian function. Notably, these transplant experiments also established that the SCN relies on both diffusible signals and synaptic transmission to regulate rhythms throughout the brain and body. Knife-cut isolation of the SCN, which sever efferent axonal projections, induce arrhythmicity in locomotor behaviour, sleep wakefulness, and electrical firing rates in the brain, while the rhythm in the stress hormone corticosterone remains unaffected (Honma, Honma, & Hiroshige, 1984; Inouye & Kawamura, 1979). Conversely, encapsulating an SCN graft in a semi-permeable membrane, which only allows diffusible signals to pass through, restores circadian activity rhythms of SCN-ablated recipients to some degree, highlighting the involvement of both synaptic transmission and humoral factors (Silver, LeSauter, Tresco, & Lehman, 1996).

More recently, a series of elegant *in vitro* experiments further confirmed the role for neuronal and diffusible signals in the coordination of circadian rhythms by the SCN. For example, diffusible signals from cultured SCN can sustain rhythmicity in cultured astrocytes, which normally lose rhythmicity after a few cycles *in vitro* (Prolo, Takahashi,

& Herzog, 2005). Importantly, this ability appears specific to the SCN since a slice of cortex is unable to sustain rhythms in other cells (Prolo, Takahashi, & Herzog, 2005). The cultured SCN can also induce circadian oscillations in a genetically arrhythmic SCN. Maywood and colleagues (2011) showed that a wild type SCN could induce rhythmicity in a genetically arrhythmic SCN using diffusible (paracrine) signals (Maywood, Chesham, O'Brien, & Hastings, 2011). These diffusible signals were able to rescue arrhythmicity induced either by lack of an essential coupling agent (VIP) or by lack of essential clock genes (*Cry1* and *Cry2* null). In agreement with the transplantation studies cited above, the period induced in the arrhythmic SCN (host) was determined by the graft (donor) (Maywood, Chesham, O'Brien, & Hastings, 2011). Although diffusible signals play a clear role in rhythmic coordination, direct neuronal contact also controls circadian parameters in specific brain areas. Using a slice model previously developed (Trudel & Bourque, 2003), it was found that direct synaptic communication between the SCN and the supraoptic nucleus (SON) controls circadian changes in the sensing of osmotic challenges (Trudel & Bourque, 2010). This is done through presynaptic silencing of osmosensory afferent synapses in the SON (Trudel & Bourque, 2010). Thus, both diffusible and direct synaptic signals from the SCN are critical for temporally coordinating circadian rhythms among multiple oscillating structures.

Entrainment to the 24-hr day

In the absence of external time cues, outputs of the master clock, such as rhythmic locomotor activity, display an endogenous 'free running' rhythm slightly different from 24-hrs. For example, humans and rats have a daily endogenous period slightly longer

than 24-hrs, approximately 24.2-hrs (Czeisler et al., 1999; Stephan, 1983), whereas mice have a shorter endogenous period of approximately 23.5-hrs (Pittendrigh & Daan, 1976b). In order for circadian rhythms to be in tune with the solar cycle, the master clock in the SCN needs to be synchronized (entrained) to the LD cycle. Light is the major environmental synchronizer, or *zeitgeber* (ZT; time giver), that entrains the SCN on a daily basis (Rusak & Zucker, 1979). Importantly, the SCN responds almost exclusively to light, and therefore buffers the entire system against perturbations. As previously noted, light is communicated to the SCN directly from the retina via the RHT and induces daily adjustments (resetting) of the SCN clock ensuring synchrony with the 24-hr LD cycle. The response of the SCN clock to light varies according to the phase of the circadian cycle. In rodents housed in constant darkness, light presented during the subjective day (the inactive phase of the cycle) has no effect on circadian rhythms, whereas light presented during the subjective night (the active phase of the cycle) causes phase shifts. Specifically, light presented early in the night (which would correspond to dusk in a LD cycle) causes phase delays, while light presented in the late night (near dawn in a LD cycle) causes phase advances (Dann & Pittendrigh, 1976). Following entrainment, endogenous rhythms establish a stable phase relationship with the external *zeitgeber*.

Conversely, extra-SCN oscillators have been shown to respond and entrain to non-photoc cues, allowing for flexibility within the circadian system, thereby optimizing survival (review: Mrosovsky, 1996). Examples of some non-photoc time cues include the scheduled presentation of food (Stephan, 2002; Stephan, Swann, & Sisk, 1979; Waddington Lamont et al., 2007), odors (Amir, Cain, Sullivan, Robinson, & Stewart, 1999; Funk & Amir, 2000; Governale & Lee, 2001), and exercise (reviewed in

Mistlberger & Skene, 2005). While these *zeitgebers* have little to no effect on the SCN, they can influence circadian rhythms in physiology and behaviour (Amir & Stewart, 2009b), and even dissociate rhythms in subordinate clocks from the SCN, which remains synchronized to the LD cycle (e.g. Masubuchi et al., 2000; Waddington Lamont et al., 2007). However, the inviolability of the SCN is dependent on context. For example, in conditions of constant light, rhythms in the SCN are abolished, resulting in physiological and behavioural arrhythmicity. Under these conditions, the restriction of food presentation to a brief period during the day (restricted feeding, RF), can re-entrain a rhythm in the SCN clock (Lamont, Diaz, Barry-Shaw, Stewart, & Amir, 2005).

Molecular clockwork

The molecular program responsible for the generation of circadian rhythms at the cellular level has been well established in mammals and is similar across different species. Every cell in the mammalian SCN is thought to contain this oscillatory machinery (Herzog, Takahashi, & Block, 1998; Welsh, Logothetis, Meister, & Reppert, 1995). At its most basic level, circadian rhythms are generated by a small set of core clock genes that are driven by transcription/translation auto-regulatory feedback loops (see Fig.1 for a schematic diagram of the following description). The positive arm of the primary feedback loop is comprised of the basic helix-loop-helix (bHLH)-PAS (PER-ARNT-SIM) transcription factors CLOCK (circadian locomotor output cycles kaput) and BMAL1 (Brain and muscle Arnt-like 1) (Hogenesch et al., 1997; Yu, Nomura, & Ikeda, 2002). The negative arm of the primary feedback loop is comprised of the protein products of the *Period* (*Per* 1, 2, 3) and *Cryptochrome* (*Cry* 1, 2) genes (Kume et al.,

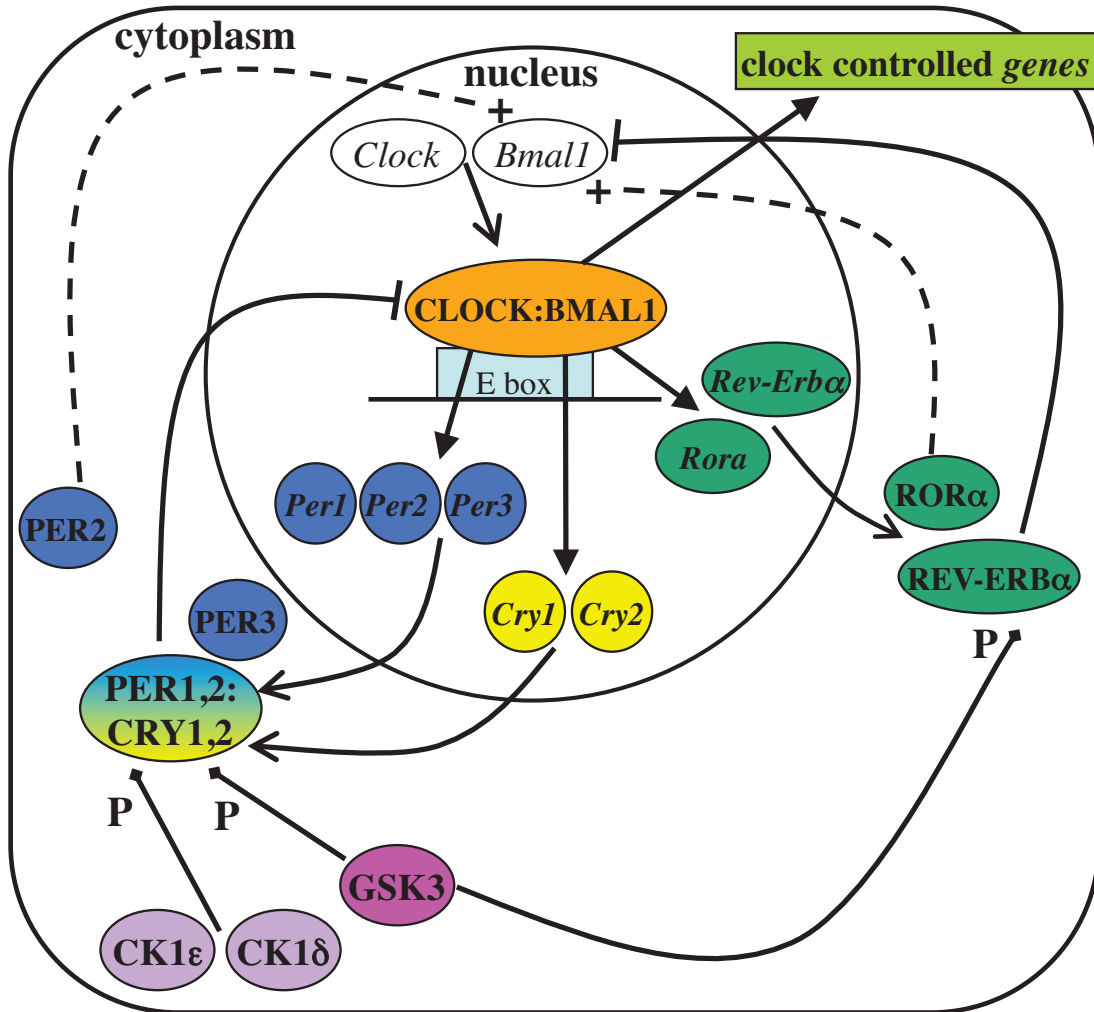


Figure 1. Molecular clock. Simplified schematic diagram of the circadian molecular clock. *Genes are in italic*, PROTEINS ARE CAPITALIZED, P= phosphorylation, - - + = activation, —| = inhibition, —> = transcription, —> = translation.

1999; Reppert & Weaver, 2001; Shearman et al., 2000). Specifically, CLOCK and BMAL1 heterodimerize and activate the transcription of the *Per* and *Cry* genes through E-box enhancers highly selective for the CACGTG nucleotide sequence. The resulting protein products form PER:CRY heterodimers that translocate back to the nucleus and act on the CLOCK:BMAL1 complex to inhibit their own transcription (Shearman et al., 2000; Yu, Nomura, & Ikeda, 2002). In addition, PER2 acts on its own to activate *Bmal1*, contributing to the positive arm of the feedback loop (Kume et al., 1999; Reppert & Weaver, 2001; Shearman et al., 2000; Zheng et al., 1999).

Another, secondary, feedback loop is created by CLOCK:BMAL1 heterodimers activating the transcription of the retinoic acid-related orphan nuclear receptor (ROR) genes, *Rev-erba* and *Rora* (Preitner et al., 2002; Sato et al., 2004; Ueda et al., 2002). The resulting REV-ERB α and ROR α proteins actively compete for binding at the ROR response elements in the BMAL1 promoter, where REV-ERBs repress (Preitner et al., 2002) and RORs activate (Akashi & Takumi, 2005; Sato et al., 2004) *Bmal1* transcription. Although this feedback loop is not necessary for circadian rhythmicity, it helps to stabilize and fine-tune the oscillations (Akashi & Takumi, 2005; Preitner et al., 2002; Sato et al., 2004).

An overview of the timeframe of the interacting genes and proteins of the primary and secondary feedback loops in the SCN is as follows: In the absence of time cues (most notably light), the 24-hr day is measured in circadian time (CT) based on endogenous activity rhythms. At the beginning of the circadian day (CT0) accumulation of the CLOCK:BMAL1 heterodimers initiates the transcription of the *Per*, *Cry*, *Rora*, and *Rev-Erba* genes. The timing of peak mRNA expression of these genes is spread out, with the

rhythm of *Per1* and *Rev-Erb α* peaking between CT4-6, followed by *Per3* (CT4-8), *Ror α* (CT6-10), *Per2* (CT8-10), and *Cry1* at around CT10. The protein product of these genes peak approximately 4 to 6-hrs later (Reppert & Weaver, 2001). The expression of *Clock* is constitutive and the expression of *Cry2* is weak with no clear rhythm (Lowrey & Takahashi, 2000). REV-ERB α inhibits *Bmal1* transcription causing a decrease in BMAL1 protein levels. By the middle of the 24-hr day (CT12) both PER and CRY proteins are expressed at high levels in the nucleus, where CRY, and to a lesser degree PER2, inhibit CLOCK:BMAL1 mediated transcription. At the same time, PER2 and ROR α work to enhance *Bmal1* transcription, leading to peak *Bmal1* expression between CT15-18. The rhythm in BMAL1 protein subsequently peaks 4 to 6-hrs later, from CT22-24, which then starts a new cycle of gene transcription at the beginning of the circadian day (CT0) (Ko & Takahashi, 2006; Reppert & Weaver, 2001; Yu, Nomura, & Ikeda, 2002).

These auto-regulatory feedback loops take approximately 24-hrs to complete one cycle and underlie the 24-hr rhythmicity seen in physiology and behaviour (Kalsbeek, Perreau-Lenz, & Buijs, 2006). Post-transcriptional modifications such as phosphorylation and ubiquitination also play critical roles in the generation of the delay in protein expression necessary to maintain these 24-hr rhythms, influencing the period and phase of oscillations. For example, the enzymes casein kinase 1 epsilon (CK1 ϵ) and delta (CK1 δ) phosphorylate the PER proteins, affecting dimerization with the CRY proteins, movement between the cytoplasm and nucleus, and lead to their degradation (Dunlap, Loros, & DeCoursey, 2004; Reppert & Weaver, 2001). The *Drosophila shaggy* homologue, glycogen synthase kinase 3 (GSK3), is another enzyme that phosphorylates

the PER proteins as well as REV-ERB α , and is thought to be an important regulator of the circadian clock and necessary for proper circadian function (Iitaka, Miyazaki, Akaike, & Ishida, 2005). The genes, proteins, and enzymes of the molecular clock all work together to regulate circadian oscillations, and abnormalities, such as clock gene mutations, can have profound effects on both physiology and behaviour. In addition, CLOCK:BMAL1 can potentially regulate the expression of any gene that contains an E-box sequence in their promoter region, thus having effects outside of 'classical clock function'.

One way in which the circadian system can modulate some of these non-clock functions is through clock-controlled genes (CCG) (Reppert & Weaver, 2001), which are dependent on the primary feedback loop for their own transcription, but are not themselves critical for the functioning of the circadian clock. It is well established that CLOCK:BMAL1 activate the transcription of numerous CCGs (Jin et al., 1999), which can in turn moderately influence the clock, but more importantly, can intensify the influence of the clock on numerous target genes. The CCG, *Dbp* (albumin gene D-site binding protein), a PAR leucine zipper transcription factor, shows a robust rhythm in the SCN, with peak expression occurring during the subjective day, as well as in other brain areas, such as the striatum and cortex, but with a phase that is delayed by 4 to 8-hrs compared to the SCN (Yamaguchi et al., 2000; Yan, Miyake, & Okamura, 2000). *Dbp* is also highly rhythmic in the liver with peak expression occurring 4-hrs later than in the SCN (Lopez-Molina, Conquet, Dubois-Dauphin, & Schibler, 1997). The expression of CCGs is often used to assess the functionality of the underlying molecular clock.

Genetic disruption of clock genes

The importance of proper clock gene function becomes evident when examining the consequences of clock gene disruptions. Two methods have been used to induce these disruptions: mutations, which modify a part of a gene leading to the expression of a non-functional protein, and knockouts (KO), which delete a gene (or its start sequence) entirely, resulting in the absence of the protein. Numerous clock gene disruptions in rodents lead to abnormal circadian activity rhythms by either shortening or lengthening the circadian period, and sometimes causing complete behavioural arrhythmicity. The *tau* mutant hamster discovered in 1988 was found to have a shortened wheel-running period; 22-hrs in heterozygotes and 20-hrs in homozygotes (Ralph & Menaker, 1988). The mutation was later found to reside in the CK1 ϵ enzyme (Lowrey et al., 2000). Decreases in the period of cortisol and melatonin rhythms are also apparent in these mutants (Lucas, Stirland, Darrow, Menaker, & Loudon, 1999). *Cryptochrome* KO mice display opposing effects depending on the gene affected; *Cry1* KO have a shorter period (by ~1-hr), whereas *Cry2* KO have a period that is approximately 1-hr longer (van der Horst et al., 1999; Vitaterna et al., 1999). *Period1* mutants have a shorter free running period, whereas *Per2* mutants initially have a longer period and then become arrhythmic (Zheng et al., 2001; Zheng et al., 1999). *Period3* KO mice have a very mild phenotype with a free-running period only slightly shorter than normal (Shearman, Jin, Lee, Reppert, & Weaver, 2000). When housed in constant darkness, animals with disruptions in both *Cry1/Cry2* or *Per1/Per2* become completely arrhythmic, as do *Bmal1* KO mice (Bunger et al., 2000; van der Horst et al., 1999; Vitaterna et al., 1999).

CLOCK KO mice surprisingly show only a mild phenotype, with some changes in clock gene expression but no effect on wheel-running behaviour (Debruyne et al., 2006). This is most likely due to the presence of NPAS2, a CLOCK analog (Reick, Garcia, Dudley, & McKnight, 2001), compensating for the absence of CLOCK. In contrast, mice with a mutation in the *Clock* gene (which acts as a dominant negative) have a longer free running period compared to wild types (Vitaterna et al., 1994). They also show numerous alterations in physiology and behaviour including, hyperphagia, greater consumption of their daily food intake during the day, obesity, and have elevated levels of cholesterol, leptin, lipids, glucose, and decreased levels of insulin (Turek et al., 2005; Williams & Schwartz, 2005). *Clock* mutants also show behavioural phenotypes that are similar to mania; they are hyperactive, sleep less, are less anxious compared to wild types, and show increased sensitivity to cocaine (McClung et al., 2005; Roybal et al., 2007). Thus, it appears that disruptions in the molecular circadian machinery have far reaching implications for overall health and behaviour. For instance, disturbances in circadian rhythms are commonly seen in mental illness, especially in mood disorders such as major depression and bipolar disorder, and in sleep disorders (Cermakian & Boivin, 2003). Interestingly, recent evidence has linked mutations in specific clock genes with these disorders in humans (reviewed in Waddington Lamont, Legault-Coutu, Cermakian, & Boivin, 2007). For example, variations in *Per2*, *Bmall*, and *NPAS2* have been associated with seasonal affective disorder (Partonen et al., 2007), and variations in the 3111C *Clock* gene allele have been linked with bipolar disorder (Benedetti et al., 2003; Serretti et al., 2003). Moreover, the rhythms in melatonin, cortisol, and core body

temperature described earlier are all commonly disrupted in these psychopathologies (Bunney & Bunney, 2000).

The multifaceted roles of Period

Although their task within the molecular clockwork of the biological timing system is well characterized, *Per* genes appear to be pleiotropic, having roles outside the machinery associated with circadian rhythms. Mutations in the *Per* genes have been linked to numerous abnormalities in physiology and behaviour. For example, *Period2* mutants show alterations in the glutamatergic system, which is accompanied by an increase in ethanol preference in these mice (Spanagel et al., 2005). Interestingly, in humans, there is an association between alcoholism and variations in the *Per2* gene (Spanagel et al., 2005). Mice with genetic modifications in either *Per1* or *Per2* show opposing responses to cocaine exposure; cocaine sensitization is absent in *Per1* KO mice while it is potentiated in the *Per2* KO, implicating these genes in reward (Abarca, Albrecht, & Spanagel, 2002). Furthermore, *Per1* KO mice fail to show conditioned place preference for cocaine (Abarca, Albrecht, & Spanagel, 2002). *Period2* mutant mice also lack the ability to show food anticipation (Feillet et al., 2006), further demonstrating the importance of this gene in the regulation of motivated behaviours. *Period2* mutant mice also respond abnormally to Gamma-irradiation and are more likely to develop tumors than wild type mice, suggesting a tumor suppressive role for *Per2* (Fu, Pelicano, Liu, Huang, & Lee, 2002; Lee, 2006). This finding is further confirmed by human data showing that *Per1*, *Per2*, and *Per3* expression is abnormal in breast cancer cells (Chen et

al., 2005). In addition, over-expression of *Per2* has been shown to induce apoptosis in cancer cells (Hua et al., 2006).

Mutations in the human *Per2* gene have also been linked to sleep abnormalities. Familial advanced sleep phase syndrome, a sleep disorder affecting a person's wake and sleep times, has been linked to a serine to glycine mutation within the CK1 ϵ binding region of the PER2 protein, resulting in a decrease in phosphorylation, faster accumulation of PER2, an acceleration of the molecular feedback loops, and consequently, a shorter period (Toh et al., 2001). In another study, a missense mutation in the *Ckl8* gene, also resulting in a reduction of PER2 phosphorylation, was found to be associated with this syndrome (Xu et al., 2005).

Nuclear receptors play important roles in regulating the expression of multiple genes important for functions such as reproduction, development, and metabolism (Yang et al., 2006), and importantly, PER2 has been found to act as a nuclear receptor co-regulator (Ripperger, Schmutz, & Albrecht, 2010). Specifically, PER2 interacts with REV-ERB α and peroxisome proliferator-activated receptor alpha (PPAR α) modulating *Bmal1* expression (Ripperger, Schmutz, & Albrecht, 2010; Schmutz, Ripperger, Baeriswyl-Aebischer, & Albrecht, 2010). In addition, PER2 can provide circadian information to non-rhythmic nuclear receptors, such as *Hnf4 α* in the liver, directly modulating metabolic functions (Ripperger, Schmutz, & Albrecht, 2010; Schmutz, Ripperger, Baeriswyl-Aebischer, & Albrecht, 2010).

In conclusion, *Period* genes appear to play an important role in numerous physiological and behavioural processes that go beyond what would be considered 'classical circadian functions'.

Extra-SCN oscillators

Although the SCN is considered the master pacemaker, circadian oscillators have recently been observed in other regions of the brain (Abe et al., 2002; Amir, Lamont, Robinson, & Stewart, 2004; Guilding & Piggins, 2007; Lamont, Robinson, Stewart, & Amir, 2005) and in peripheral organs and tissues (Hogenesch, Panda, Kay, & Takahashi, 2003; Yamazaki et al., 2000; Yoo et al., 2004). The SCN is thought to act as a master conductor, synchronizing rhythms in these subordinate oscillators (Yoo et al., 2004).

Yamazaki et al (2000) have shown circadian rhythms in rat peripheral tissues using continuous bioluminescence recording in *Per1-luciferase* transgenic rats. Cultured explants of the liver, lung, and skeletal muscle continued to oscillate for two to seven days without input from the SCN before damping out (Yamazaki et al., 2000). Importantly, this damping was not due to cell death, as rhythmicity could be reinstated with medium change. It seems that without input from the SCN, rhythms in peripheral tissue remain synchronized for short periods of time before becoming uncoupled. Also using the *Per1-luciferase* transgene as a marker for circadian oscillations, Abe and colleagues (2002) found that although many structures in the brain exhibit some rhythms *in vitro*, only four structures besides the SCN, the olfactory bulbs, the arcuate nucleus, and the pineal and pituitary glands, showed near 24-hr oscillations and continued to do so for more than three cycles before damping out (Abe et al., 2002).

Using semiquantitative *in situ* hybridization in the rat, Shieh (2003) found clock gene mRNA expression in 50 out of 83 brain regions examined (Shieh, 2003). Importantly, *Per1*, *Per2*, and *Clock* were all concurrently present, with the exception of

the SON of the hypothalamus and the superior olivary nucleus of the brain stem, which showed *Clock* expression only. Surprisingly, the BLA and BNST, regions that we have shown to express rhythms in PER2 protein, were found to express very low to no levels of these clock genes. However, it is important to note that only one time-point was examined per region (either ZT4 or ZT6), the possibility therefore remains that these clock genes peak at a different time in these regions. In another study, *Per1* expression at ZT4 was also found to be similarly expressed throughout the hamster brain (Yamamoto et al., 2001).

Although important, the studies mentioned above either use organotypic tissue explants or only look at one time-point. The first method, by definition, isolates the tissue sample from all connections, while the second method only establishes if a gene or protein is expressed at that specific time, and hence gives no temporal expression profile information. Consequently, these experiments fail to provide any insight about the presence or absence of a rhythm or about phase relationships between subordinate oscillators in the intact animal.

Subordinate oscillators in the forebrain

As previously mentioned, using a low temporal resolution analysis of PER2 expression, our laboratory identified several circadian oscillators in limbic forebrain areas known to be involved in emotion, motivation, and learning and memory; the BNSTov, CEAl, BLA, and DG (Amir, Lamont, Robinson, & Stewart, 2004; Lamont, Robinson, Stewart, & Amir, 2005). Uniquely amongst subordinate oscillators, it was established that the BNSTov and CEAl have PER2 rhythms that are in phase with that of the SCN, with

peak expression occurring at the beginning of the dark phase of the LD cycle, at ZT13 (Amir, Lamont, Robinson, & Stewart, 2004; Lamont, Robinson, Stewart, & Amir, 2005). Whereas the BLA and DG have PER2 rhythms that are 180° out of phase, with PER2 expression peaking at the beginning of the light phase, at ZT1 (Lamont, Robinson, Stewart, & Amir, 2005).

The BNSTov and CEAl are two regions that are highly anatomically interconnected, and neurochemically and functionally related (Day, Curran, Watson, & Akil, 1999; Swanson, 2003). Together, these regions are commonly referred to as the central extended amygdala (Alheid, 2003), and have been shown to be involved in multiple behavioural systems including: feeding (Petrovich & Gallagher, 2003); drug addiction and relapse (Day et al., 2001; Erb, Salmaso, Rodaros, & Stewart, 2001; Erb, Shaham, & Stewart, 2001); and fear and anxiety (Davis, 1998; Lee & Davis, 1997). In contrast, the BLA resembles the neighboring cortex more than the rest of the amygdala, and mainly projects to the medial CEA and other regions in the amygdala, the cortex, and the hippocampus through the entorhinal cortex (Dong, Petrovich, & Swanson, 2001; Dong, Petrovich, Watts, & Swanson, 2001; Petrovich, Canteras, & Swanson, 2001), but does not have dense connections to the BNSTov (Dong, Petrovich, & Swanson, 2001). The hippocampus sends extensive projections to most of the amygdala (Petrovich, Canteras, & Swanson, 2001) and has been implicated in the stress pathway, affective disorders, and learning and memory through long-term potentiation (LTP) and neurogenesis in the DG (Gould, Tanapat, Hastings, & Shors, 1999; Malberg & Duman, 2003; McEwen, 2001). Together, the hippocampus and amygdala are thought to play an important role in the integration of learning and memory of emotional states.

Studies of the mechanisms that control the rhythms of PER2 expression in these limbic forebrain areas have shown that they are all under the control of the SCN. Lesioning the SCN completely blunts PER2 rhythms in these regions (Lamont, Diaz, Barry-Shaw, Stewart, & Amir, 2005). It has also been shown that unilateral SCN lesions blunt rhythmic PER2 expression in the BNSTov ipsilateral to the lesioned SCN, suggesting that the rhythm in PER2 expression observed in the BNSTov is due, in part, to ipsilateral neural connections from the SCN (Amir, Lamont, Robinson, & Stewart, 2004). Bilateral adrenalectomy was also found to blunt PER2 rhythms in the BNSTov and CEAl, but not in BLA and DG (Amir, Lamont, Robinson, & Stewart, 2004; Segall, Perrin, Walker, Stewart, & Amir, 2006) and this effect was found to be reversed by rhythmic corticosterone self-administration via the drinking water but not via a constant release pellet (Segall, Perrin, Walker, Stewart, & Amir, 2006). These data suggest that the PER2 rhythm in the BNSTov and CEAl depend on the rhythm rather than the mere presence of corticosterone in the circulation. Finally, it was found that the rhythms of PER2 expression in the limbic forebrain are sensitive to treatments that disrupt energy balance. Specifically, daily restricted feeding schedules, which are known to induce food anticipatory behavioural and physiological rhythms, including body temperature and corticosterone secretion (Boulos & Terman, 1980; Mistlberger, 1994; Stephan, 2002), can entrain PER2 rhythms in the BNSTov, CEA, BLA and DG and uncouple them from the SCN (Lamont, Diaz, Barry-Shaw, Stewart, & Amir, 2005; Waddington Lamont et al., 2007).

The striatum is a large sub-cortical structure within the forebrain that functions as the major input system of the basal ganglia (Gerfen, 2004). It consists of the dorsal

striatum (also known as caudate putamen), and the ventral striatum, which can be further divided into the nucleus accumbens (NAc) core and shell. Notably, circadian rhythms in the expression of core clock genes have been found, by our laboratory and others, in the dorsal striatum, a region important for motor control, reward, and learning (Amir, Harbour, & Robinson, 2006; Imbesi et al., 2009; Shieh, 2003). The rhythm of PER2 expression in this region followed the pattern seen in the BLA and DG with peak expression occurring at the beginning of the light phase (ZT1) (Amir, Harbour, & Robinson, 2006). Furthermore, the neurotransmitter dopamine was found to be involved in the regulation of both PER2 protein and *Per2* mRNA (Hood et al., 2010), BMAL1 protein, and the clock-controlled gene, *Dbp* (Sahar, Zocchi, Kinoshita, Borrelli, & Sassone-Corsi, 2010) in the dorsal striatum. Interestingly, the effect of dopamine on PER2 rhythms in the dorsal striatum was found to be mediated by the D2 dopamine receptor (Hood et al., 2010), and preliminary work in our laboratory shows that PER2 is co-localized within neurons expressing dopamine D2 receptors or ENK in the dorsal striatum (Hood, 2010). Clock gene expression is also rhythmic in the ventral striatum, a region important for reward and addiction. Rhythms in PER1 protein show similar phase patterns in both the NAc core and shell subdivisions with peak expression occurring at the end of the dark portion of the LD cycle (Angeles-Castellanos, Mendoza, & Escobar, 2007). Li and colleagues (2009) have also shown that the NAc exhibits rhythmic expressions in *Per1* and *Per2* mRNA, peaking at the beginning-middle of the light phase in the NAc core, and at the end of the dark phase in the NAc shell, showing differential clock gene expression within the whole striatum (Li, Liu, Jiang, & Lu, 2009).

Although the striatum is cytoarchitecturally homogenous, with 90-95% of neurons being GABAergic medium spiny neurons, the afferents to the striatum (mostly cortical) differ considerably (Gerfen, 2004). It is interesting that most research tends to group the whole dorsal striatum, sometimes even including the ventral striatum, into one structure when there are potentially functional differences due to distinct cortical inputs. However, one study went to the extreme by dividing the striatum into 26 segments and reported differences in cocaine-induced changes in gene regulation between certain subdivisions (Willuhn, Sun, & Steiner, 2003).

The present thesis

The mammalian brain contains multiple areas that exhibit circadian oscillations in clock gene expression and electrical activity. This suggests that a tightly regulated interplay between oscillators is responsible for normal, daily brain function. The studies previously mentioned are limited by the small number of time-points (usually 4-8) used to assess rhythms in clock genes. Due to their limited temporal resolution, it is possible that numerous aspects of these rhythms, such as their genuine phase and amplitude, remain hidden. A more detailed analysis is necessary to reveal the relationships of rhythmic brain areas in order to get a clear understanding of clock gene expression patterns and their possible tissue-specific functions. We therefore embarked on an extensive mapping of the rhythmic expression of the clock protein PER2 in brain areas important for stress, emotion, motivation, and learning and memory. The resulting atlas will present a fine grain analysis of PER2 rhythms in the normal rat brain and provide a

baseline for studying the role of tissue-specific rhythms in cognitive and appetitive disorders.

The objectives for this thesis were four fold: First, re-examine and refine PER2 expression patterns in the SCN and the five regions of the forebrain previously mentioned, the BNSTov, CEAl, BLA, DG, and striatum. This was done using an unprecedented high temporal resolution IHC analysis of PER2 expression every 30 min across the 24-hr day, resulting in 48 time-points. Second, to characterize the presence of other PER2 containing regions in the amygdala, hippocampus, and striatum as well as in regions of the cortex. Third, to establish the phase relationships between all regions and between these regions and the master SCN clock. A fundamental question was whether all regions would fall into one of the two PER2 expression patterns previously described (peaking either near ZT1 or ZT13). These first three objectives make up Chapter 1.

Finally, the fourth objective was to confirm the presence of the circadian molecular machinery by measuring mRNA expression of the core clock genes *Per2* and *Bmal1*, and a clock-controlled gene, *Dbp*, using quantitative real-time polymerase chain reaction (qRT-PCR). This was done in order to 1) establish the phase relationship between PER2 protein and *Per2* mRNA in the SCN and two limbic forebrain regions (the CEAl and DG) and 2) to compare different clock gene expression profiles in these regions. The qRT-PCR data make up Chapter 2. The results from this thesis have been presented at scientific conferences and published in abstract form (Harbour, Weigl, Robinson, & Amir, 2010, 2011; Weigl, Harbour, Robinson, Dufresne, & Amir, 2010).

CHAPTER 1: PERIOD2 protein

METHODS

Animals and Housing

Eighty-four male inbred Lewis (LEW/Crl) rats weighing 150-200 grams upon arrival (Charles River, St-Constant, QC) were used. Rats arrived in seven successive batches of 12 with each batch (i.e. group) housed in the same experimentation room. Rats were individually housed in cages (9.5 in wide x 8 in. height x 16 in. deep) equipped with running wheels and had *ad libitum* access to rat chow and water. Each cage was housed within a custom-built ventilated, sound and light-tight isolation chamber (17.5 in wide x 27.5 in height x 27.5 in deep) equipped with a computer-controlled lighting system (VitalView software; Mini Mitter Co. Inc., Sunriver, OR). Wheel-running activity (WRA) was recorded continuously and displayed in 10-min bins using VitalView software. Single plotted actograms were created to display and analyze WRA rhythms using Circadia software (v2.1.6). All procedures were carried out in accordance with the Canadian Council on Animal Care guidelines and were approved by the Animal Care Committee of Concordia University.

Procedure

Rats were kept on one of four 12-hr:12-hr LD cycles (lights on at 3:00, 9:00, 15:00, or 21:00; light = 100 lux at cage bottom) to facilitate the time of perfusions. After three to four weeks rats were perfused every 30 min across the 24-hr day to give a total of 48 *zeitgeber* times (ZT; where ZT0 denotes lights on and ZT12 denotes lights off) with

an *n* of 1-4 per time-point. Within each of the seven groups, rats were assigned perfusion times spread across the 48 time-points in order to have a representative distribution of ZTs in each group.

Tissue Preparation

At the appropriate time, rats were deeply anesthetized with sodium pentobarbital (~100mg/kg, *i.p.*) and perfused transcardially with 300ml of cold saline (0.9% NaCl) followed by 300ml of cold paraformaldehyde (4% in a 0.1M phosphate buffer, pH 7.3). Brains were removed and post-fixed overnight in paraformaldehyde at 4°C. Three sets of serial coronal sections (50µm thick) through regions of interest were collected using a Vibratome tissue slicer (St-Louis, MO) and stored in Watson's Cryoprotectant (Watson, Wiegand, Clough, & Hoffman, 1986) at -20°C until processed for immunohistochemistry (IHC) or quantitative real-time polymerase chain reaction (qRT-PCR).

Immunohistochemistry

Free-floating sections from the 1st set of brain slices were rinsed (6 x 10 min) in cold 0.9% Trizma buffered saline (TBS; pH 7.6) and incubated in a hydrogen peroxide quench solution (3% H₂O₂ in TBS) for 30 min at room temperature. Sections were then rinsed (3 x 10 min) in TBS and incubated in a pre-block solution made of 0.3% Triton X-100 in TBS (Triton-TBS) and 5% Normal Goat Serum (NGS), for one hour at 4°C, and then directly transferred into the primary solution. Sections were incubated in PER2 polyclonal antibody raised in rabbit (Alpha Diagnostic International, San Antonio, TX) diluted 1:800 in Triton-TBS and 3% NGS, and incubated for approximately 48-hrs at

4°C. The PER2 antibody has been previously tested and validated with blocking experiments (Amir, Lamont, Robinson, & Stewart, 2004). After the primary antibody incubation, sections were once again rinsed in cold TBS and then transferred to a secondary solution consisting of biotinylated anti-rabbit IgG made in goat (Vector Laboratories, Burlington, ON) diluted 1:200 in Triton-TBS and 3% NGS for one hour at 4°C. After incubation with the secondary antibody, sections were rinsed (3 x 10 min) with cold TBS and incubated in a tertiary solution (avidin biotin peroxidase complex in TBS) for 2hrs at 4°C (Vectastain Elite ABC Kit, Vector Laboratories). Finally, sections were rinsed in TBS, and then again in cold 50 mM Tris-HCl for 10 min. Sections were then incubated for 10 min in 0.05% 3,3'-diaminobenzidine (DAB) in Tris-HCl and further incubated for 10 min in a DAB/50 mM Tris-HCl with 0.01% H₂O₂ and 8% NiCl₂. Sections were rinsed a final time in cold TBS and wet-mounted onto gel-coated microscope slides, allowed to dry overnight, and then dehydrated through graded ethanol concentrations, soaked in Citrisolve (Fisher Scientific, Houston, TX) for a minimum of 30 min, and finally cover-slipped with Permount (Fisher).

Data Analysis

Brain sections were examined under a light microscope using a 20X objective (Leitz Laborlux S). Regions of interest were identified using Brain Maps: Structure of the rat brain 3rd edition (Swanson, 2004), except for the nucleus accumbens, where The Rat Brain 5th edition (Paxinos & Watson, 2005) was used. Given that the dorsal striatum (from now on referred to as the striatum only) is such a large structure, we determined that a simplified version of Willuhn et al.'s striatal subdivisions was the most appropriate

to use in our context, due the potential significance of the various afferent projections from different nuclei on the function of local clocks (Willuhn, Sun, & Steiner, 2003). We decided to examine four areas of the striatum based on distinct cortical afferents: a medial division, adjacent to the lateral ventricles, was recognized due to distinct afferents from both the ventral and dorsal anterior cingulate cortex. A dorsal division, located laterally just under the corpus callosum, was recognized due to afferents from the somatosensory cortex and medial agranular cortex (corticostriatal afferents are reviewed in Willuhn, Sun, & Steiner, 2003). Moreover, due to such a large rostral-caudal expansion of the striatum, these regions were further subdivided into anterior and posterior sections, with the joining of the anterior commissure as the boundary between the anterior from posterior portions, yielding a total of four striatal subdivisions (see Figures 17-20 for visual representations). Once identified, all regions were digitized using a Sony XC-77 Video Camera, a Scion LG-3 frame grabber, and NIH Image software (v1.63, <http://rsb.info.nih.gov/nih-image/>). Multiple bilateral images from these regions were captured using a 400X400 μm template. Cells immunopositive for PER2 were counted by an observer blind to group membership (in this case ZT) using Image SXM software (v1.9, SD Barrett, <http://www.ImageSXM.org.uk>). To determine immunopositive cells, particle analysis was set to recognize pixels between 9 and 99 and the threshold was manually set as consistently as possible for each brain region. An average of the five unilateral sections containing the highest number of labeled nuclei for each region was calculated for each rat. If a brain region has an n less than 84, it is due to tissue damage and an inability to count cells in that specific area.

All analyses and graphs were done using GraphPad Prism (v5.0, HJ Motulsky, www.graphpad.com/prism). Data points for each individual rat were plotted for each brain region with number of PER2-immunoreactive cells (PER-ir) on the Y-axis and ZT on the X-axis. Sine waves (least-squares regression) were then fit to each graph in order to better visualize time of peak and trough for each region:

$$\text{Equation: } Y = M + A \cdot \sin(F \cdot X + PS)$$

Where M stands for the mesor (i.e. average of the spread of the data from the mid-point of the curve), A stands for amplitude (calculated from the mesor), F stands for frequency (in radians), and PS stands for phase shift, which is the earliest time $Y = 0$ measured in X axis units.

First, outliers were found using the ROUT method with a False Discovery Rate of 1% and removed from all analyses (see Motulsky & Brown, 2006 for details of the procedure). The data were then fit using two sine waves (models): one where the frequency was constrained to exactly 24-hrs, and one where the frequency was free to vary up to 28-hrs (since circadian rhythms can vary from 24-hrs). Next, the effectiveness of each model was compared using the Akaike Information Criterion (AIC), which quantifies how well each model fit the data compared to each other (reviewed in Anderson, 2008). We next determined whether the difference in AIC between the models was meaningful based on the ratio of probability (i.e. Evidence Ratio). The magnitude of the Evidence Ratio indicates how much more likely one model is over the other (reviewed in Anderson, 2008). The guidelines in the Prism manual that state that an Evidence Ratio of 12 or less suggests no meaningful differences between the models were followed (Motulsky & Christopoulos, 2003). When possible, both models are graphed for each brain region, however, if no significant difference

was found between the two models, information from the 24-hr model was used for further analysis (e.g. amplitude values).

Regressions assume that the data come from a normal, i.e. Gaussian, distribution. To further assess the goodness of fit of the curves generated from the models, the D'Agostino-Pearson omnibus K^2 normality test (D'Agostino, 1986) and the Wald-Wolfowitz Runs test (Wald & Wolfowitz, 1940) were applied to the data. The normality test examines skewness and kurtosis in order to assess how far from Gaussian the data are. A data set fails the normality test when the p value is $\leq .05$, meaning that it deviates significantly from a normal distribution. The Runs test determines whether the fitted curve deviates systematically from the data (i.e. it looks for patterns in the residuals). A data set fails the Runs test when the p value is $\leq .05$, meaning that the data points are not randomly distributed along the curve. The statistics for these two tests will only be mentioned in the Results if they are significant (meaning the data set has failed the test).

In addition to the tests mentioned above, PER2 rhythm amplitudes generated by the sine-fitting model (measured in PER2-ir cells from peak to trough) between sub-regions of each broader anatomical area (for example, the DG, CA1, and CA3 of the hippocampus) were compared using 1-way analysis of variances (ANOVA). Significant effects were further analyzed with Bonferroni multiple comparison post-hocs. In order to compare the strength of the rhythm in each region, we derived a Rhythmicity Index (RI) value by dividing the peak to trough amplitude by the mesor (the average of the spread of the data). Rhythmicity Indices for each region were then normalized to the SCN, which was given a value of 1. The RI therefore takes into account the amplitude of the PER2 rhythm as well as the average PER2

expression, providing a more meaningful analysis of the rhythms, and allowing for comparisons of rhythmicity between regions with different levels of PER2 expression.

The data from the SCN were used as the standard for determining the rhythmicity criteria for other regions, given that the SCN has a high amplitude rhythm in PER2 expression. The fit (R^2 value) for the best sine wave model (determined by the Evidence Ratio) and the normalized amplitude (RI value) for PER2 in the SCN were used. Specifically, the criteria for rhythmicity were set as follows: a brain region was considered rhythmic if the R^2 value was 1/3rd or more of that of the SCN, and the RI value was 1/4th or more (i.e. 25%).

Finally, correlations were made comparing PER2 expression patterns (using individual data points from each rat) between sub-regions of each broader anatomical area (i.e. amygdala, cortex, etc.) and with the SCN, to examine the nature and strength of the relationships between these regions. Alpha level was set to .05 for all analyses.

RESULTS

All rats entrained to their LD cycle with the majority of the wheel-running activity (WRA) being confined to the night (or dark) portion of the cycle. Figure 2 shows representative single plotted actograms showing stable entrainment to the 24-hr day. Figure 3 shows the day/night distribution of WRA separated into the seven perfusion groups. As expected, the majority of the activity was restricted to the dark portion of the cycle for all groups (main effect of light/dark WRA, $F_{(1,77)}=59.94$, $p<.0001$). Although there were group differences in the LD distribution of WRA (interaction: $F_{(6,77)}=2.99$, $p<.05$), this effect was not reflected in a main effect of group ($F_{(6,77)}=2.75$, $p=.067$).

In addition to the SCN, PER2 expression was characterized in four major brain areas that play important roles in a wide range of behaviours: the amygdala, hippocampus, striatum, and cortex. In total, 22 forebrain regions were analyzed for PER2 expression every 30 minutes across the 24-hr day. Figure 4 shows a schematic sagittal view of the rat brain (adapted from Swanson, 2004) illustrating the regions examined and their respective location. Detailed results for each individual region are as follows.

Suprachiasmatic nucleus

As previously shown by our laboratory and others (Beaule, Houle, & Amir, 2003; Field et al., 2000; Yoo et al., 2004), we found that PER2 expression in the SCN followed a high amplitude (peak to trough value of 329.2) circadian rhythm with peak expression occurring in the early part of the dark phase (Fig. 5). The AIC computation and an Evidence Ratio of 31.56 revealed that the <28-hr model is approximately 32 times more

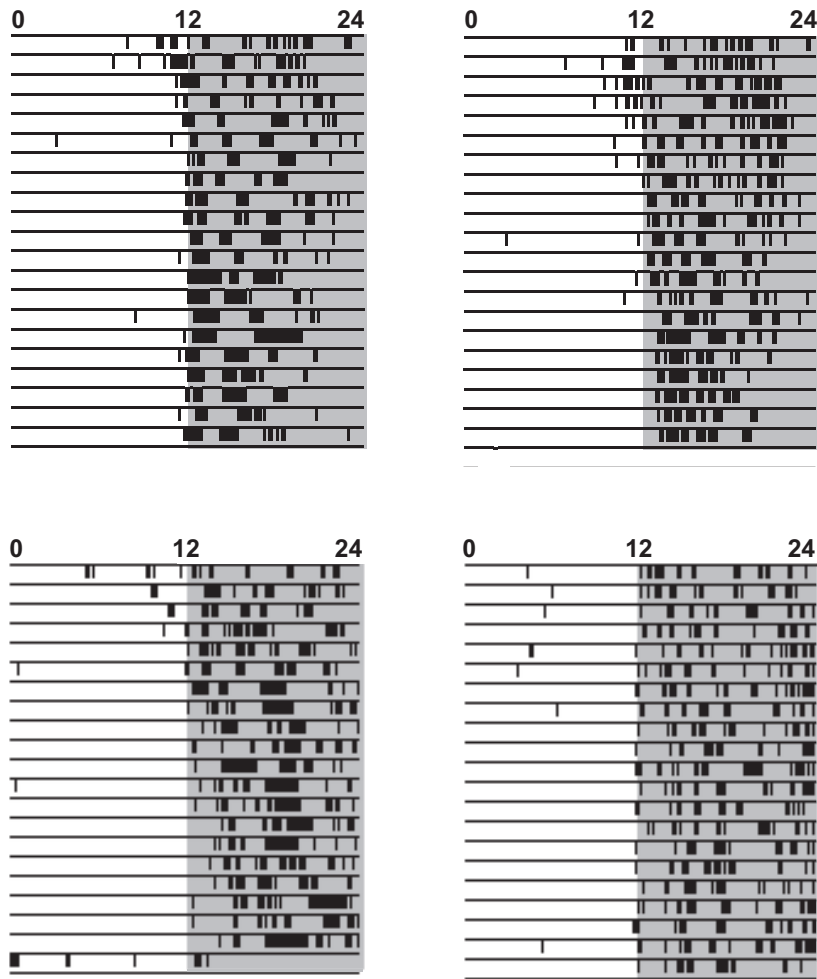


Figure 2. Wheel-running activity. Representative single-plotted actograms from 4 rats showing stable entrainment to the 24-hr LD cycle. White and grey backgrounds indicate lights on or off, respectively. Black vertical marks indicate periods of activity of at least 10 wheel revolutions/10 min. Successive days are plotted from top to bottom.

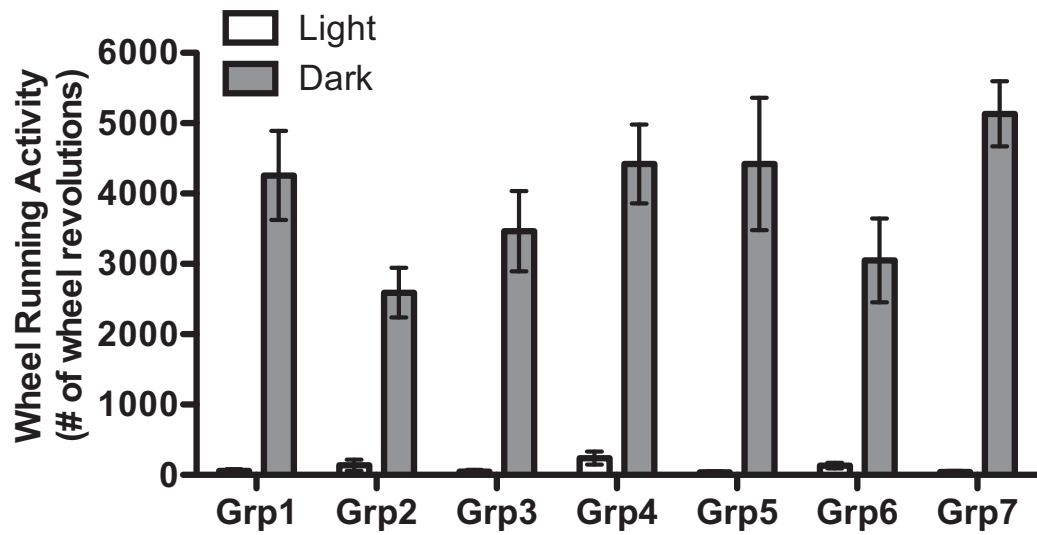


Figure 3. Individual differences in wheel-running activity. Average number of wheel revolutions (\pm SEM) for the light (ZT0-ZT12) and dark (ZT12-ZT24) periods of the last 7 days of activity for each group ($n= 12$ /group).



The master clock

- ★ SCN
core
shell

The amygdala

- BNSTov
- CEAI
- BLA
- MEA

The hippocampus

- ◇ DG
- ◇ CA1
- ◇ CA3

The striatum

- Ant Striatum m
- Ant Striatum d
- Post Striatum m
- Post Striatum d
- NAc core
- NAc shell

The cortex

- ▲ ACAv
- ▲ Alp
- ▲ EPd
- ▲ PIR2
- ▲ ENTI sup
- ▲ ENTI deep

Figure 4. Schematic diagram of the rat brain (sagittal view). Depiction of the five major brain areas (SCN:☆, Amygdala:■, Hippocampus:◇, Striatum:○, and Cortex:▲) that were analyzed for this study. In total, 22 different sub-regions were examined.

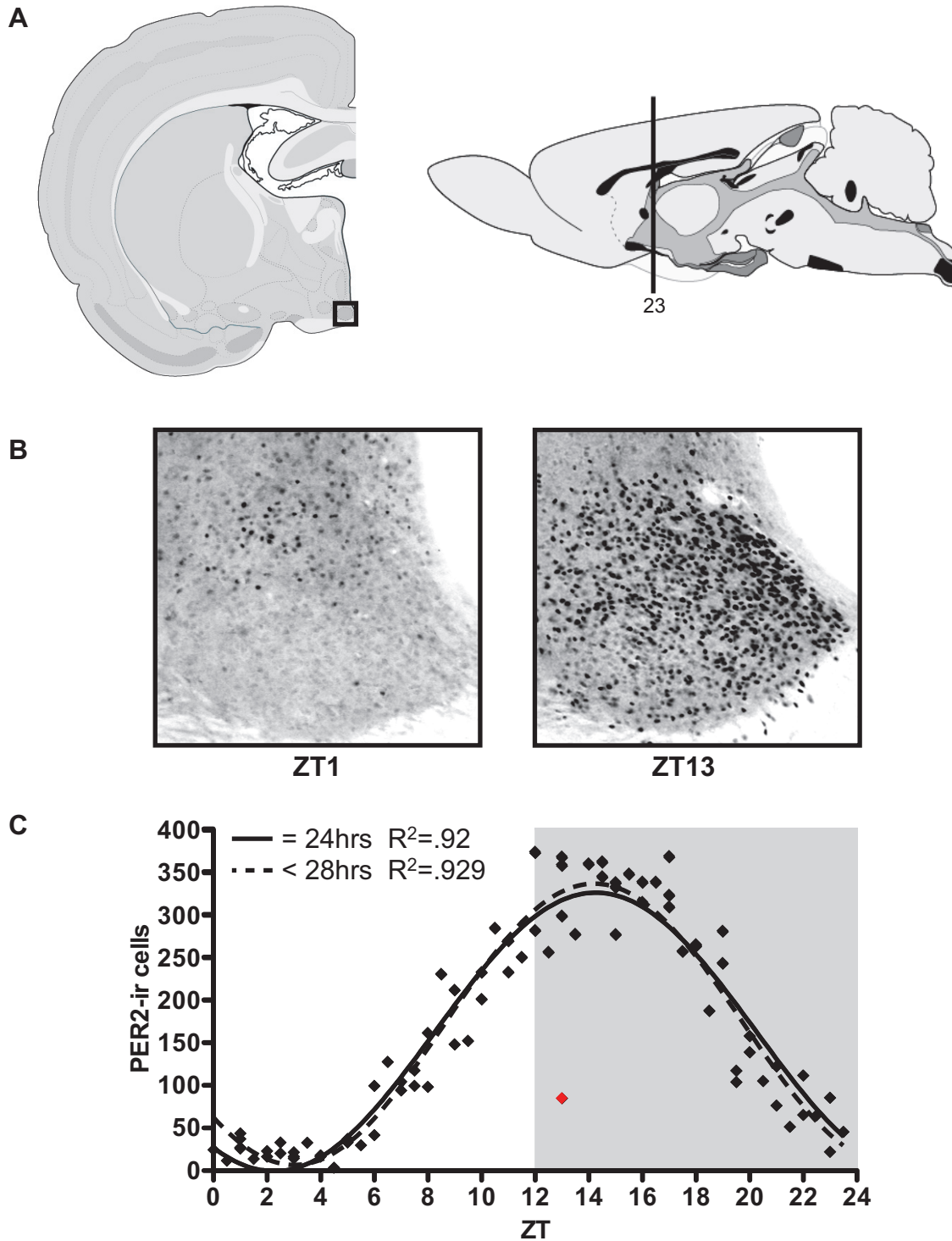


Figure 5. Suprachiasmatic Nucleus (SCN). A) Schematic diagrams of the SCN, coronal view (left) and sagittal view (right), number corresponds to level in the Swanson atlas. B) Representative photomicrographs (square in A) of PER2 expression at ZT1 and ZT13. C) Mean number of PER2-immunoreactive cells in the SCN of each individual rat (diamonds) across 48 *zeitgeber* times. White and grey backgrounds indicate lights on and off, respectively. R^2 = Goodness of fit value for given sine wave. $n= 81$ (1 outlier removed, red diamond).

likely to be correct than the 24-hr model (Fig. 5C). Interestingly, the <28-hr model fit a curve with a frequency (i.e. period) of 25.8-hrs for the SCN. The data also show that PER2 expression in the SCN peaks at around ZT14.5, which is slightly later than previously found when using fewer time-points (Amir, Lamont, Robinson, & Stewart, 2004; Beaulé, Houle, & Amir, 2003; Field et al., 2000). This can be further visualized by looking at Figure 6, which shows representative photomicrographs of PER2 expression every hour across the 24-hr day.

The best-fitted curve for the SCN has an R^2 value of .929, therefore, a brain region must have an R^2 value of at least .310 (1/3rd of that of the SCN) to meet the criteria for rhythmicity.

SCN subdivisions

As previously mentioned, the SCN can be subdivided into two anatomically and functionally different regions, the ventrolateral core and dorsomedial shell (Moore, Speh, & Leak, 2002; Van den Pol, 1980). PER2 expression patterns in the SCN were further explored by analyzing these two regions separately. The distinction between the two regions of the SCN can be seen at most ZT times (Figs. 6, 7A). Interestingly, the model that best fit the data differed between the core and shell. For the SCN core, the AIC computation and an Evidence Ratio of 4478.48 clearly suggest that the <28-hr model is the best fit for this SCN compartment (Fig. 7C). However, the <28-hr model reached the upper limit of the frequency constraint for the core and failed the Runs test ($p < .002$) (see Fig. A1). In summary, although the SCN core is visibly rhythmic, neither of the models fit the data perfectly.

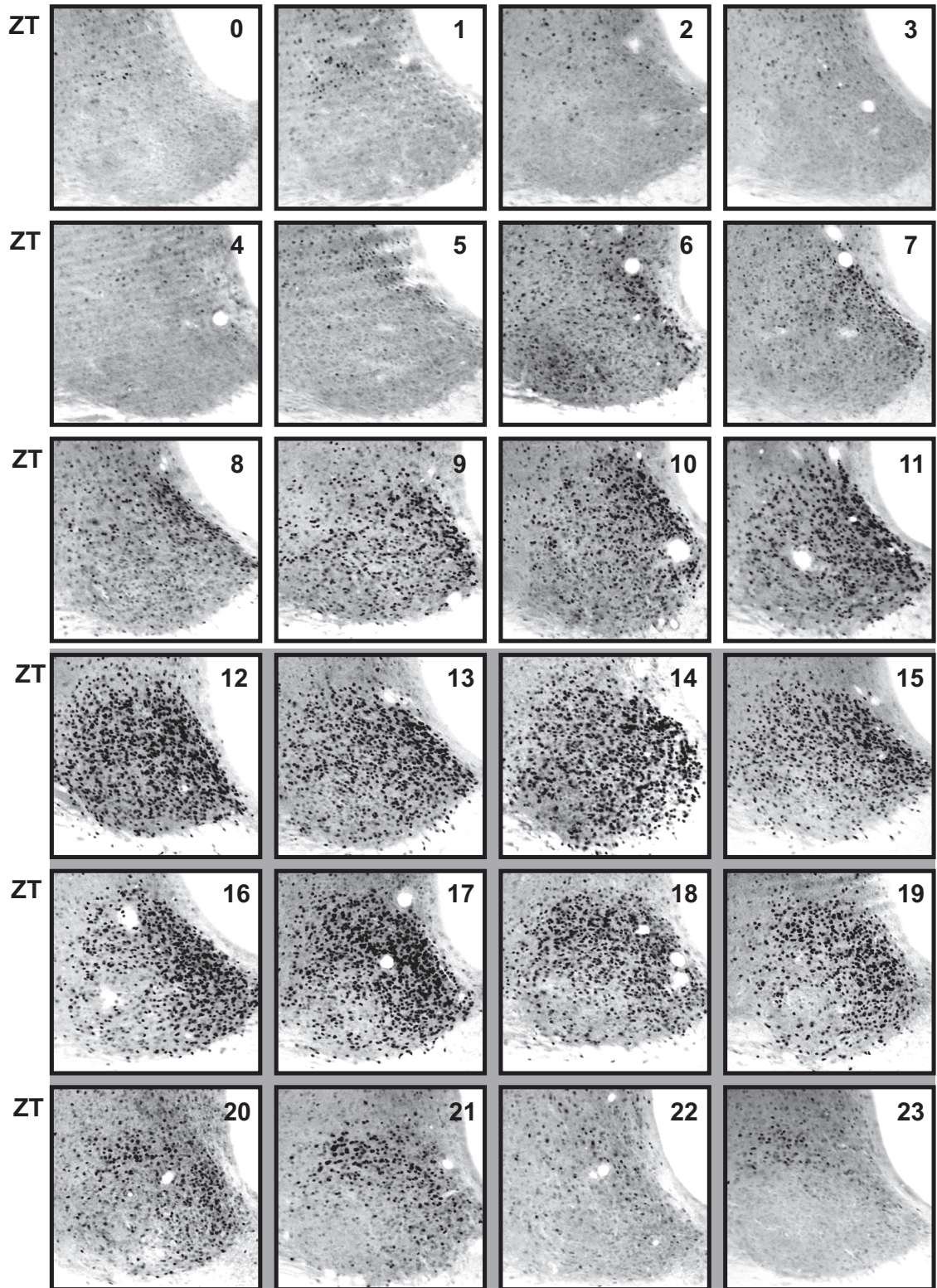


Figure 6. PERIOD2 in the SCN. Representative photomicrographs of PER2 expression in the SCN every hour across the 24-hr day. *Zeitgeber* time (ZT) 0 denotes lights on, ZT12 lights off.

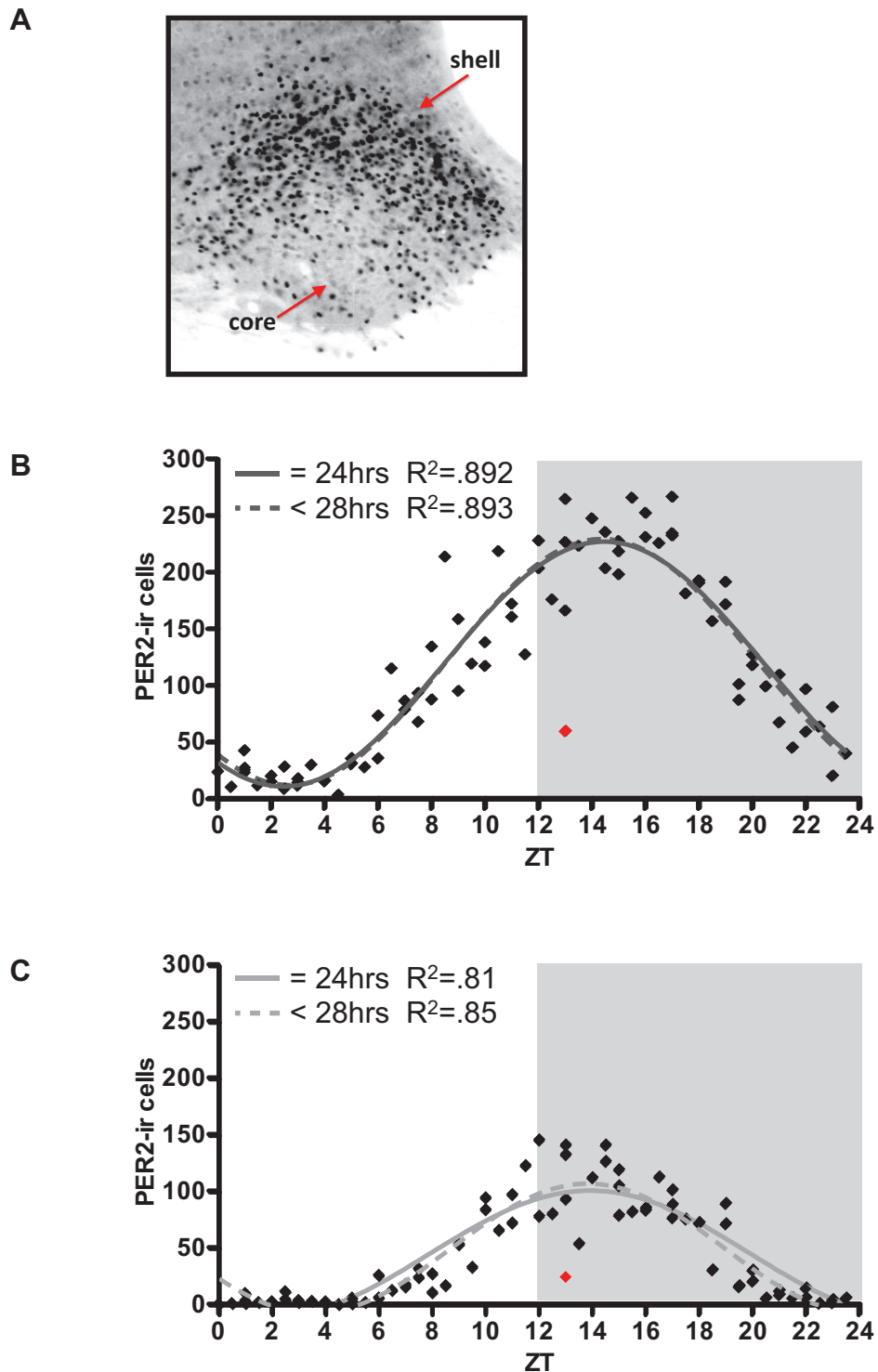


Figure 7. SCN core and shell. A) Representative photomicrograph of PER2 expression at ZT19. Arrows highlight the core and shell regions. Mean number of PER2-immunoreactive cells in the SCNsh (B) and SCNc (C) of each individual rat (diamonds) across 48 *zeitgeber* times. White and grey backgrounds indicate lights on and off, respectively. R^2 = Goodness of fit value for given sine wave. $n = 81$ (1 outlier removed, red diamond)

In contrast, there were no meaningful differences between the two models in their ability to provide a fit for the SCN shell (Evidence Ratio of 2.07, Fig. 7B). However, the <28-hr model fitted a curve with a period close to 24-hrs, 24.66-hrs. A summary of results from the AIC, normality test, and Runs test for the SCN (and all regions) can be found in Table 1.

Interestingly, the SCN core and shell also differed in time of peak PER2 expression, with the core peaking slightly earlier, a little before ZT14, and the shell peaking slightly after ZT14.5 (Fig. 8A). We found that the amplitude of the PER2 rhythm for the SCN core is much lower than that of the shell, with amplitude values (from peak to trough) of 107.7 and 216.8, respectively ($t_{(240)}=9.17, p<.001$, Fig. 8B). However, when normalized to take into account the spread of the data in each sub-region, the Rhythmicity Index (RI) revealed that individual rhythms in the core and shell are similar and are as strong as the rhythm in the whole SCN (RI values of 1.04 and .95, respectively, compared to the whole SCN (1)). Finally, PER2 expression between the core and shell of the SCN is highly correlated, with a Pearson r value of .85.

BNSTov and amygdala

Oval nucleus of the bed nucleus of the stria terminalis

Since the BNSTov is neurochemically and functionally similar to the CEA, and is considered part of the central extended amygdala (Alheid, 2003), we have chosen to group the BNSTov with the amygdala. As previously reported (Amir, Lamont, Robinson, & Stewart, 2004), the BNSTov showed a highly rhythmic pattern ($R^2 = .573$) of PER2 expression with an amplitude of 80.56 (Fig. 9). According to the AIC computation the

Table 1. Summary of statistical tests conducted on sine wave data. Values in bold are statistically significant ($p < .05$), except for AIC results which don't have a p value, here values in bold are deemed to be meaningfully different based on the Evidence Ratio.

Region	outliers	Akaike Information Criterion			D'Agostino-Pearson K ² omnibus test		Wald-Wolfowitz Runs Test	
		preferred model	difference in AICc	Evidence Ratio	K ²	p value	# of runs	p value
SCN	1	<28-hrs	6.90	31.56	0.10	0.95	38	0.29
SCNc	1	<28-hrs	16.81	4478.48	1.89	0.39	28	0.002
SCNsh	1	=24-hrs	-1.46	2.07	4.21	0.12	41	0.50
BNSTov	0	<28-hrs	0.55	1.31	3.24	0.20	45	0.73
CEAI	0	<28-hrs	2.78	4.02	4.81	0.09	45	0.72
BLA	0	=24-hrs	-2.26	3.10	1.37	0.51	43	0.60
MEApd	0	=24-hrs	-1.86	2.54	5.08	0.08	43	0.55
DG	6	<28-hrs	5.86	18.72	3.31	0.19	24	0.0002
CA1	0	=24-hrs	-1.95	2.65	1.87	0.39	40	0.39
CA3	2	=24-hrs	N/A	N/A	0.52	0.77	47	0.77
ASd	0	=24-hrs	N/A	N/A	0.70	0.70	31	0.006
ASm	0	=24-hrs	N/A	N/A	2.53	0.28	35	0.08
PSd	1	=24-hrs	N/A	N/A	1.37	0.51	33	0.03
PSm	0	=24-hrs	N/A	N/A	6.59	0.04	37	0.16
NAcc	0	<28-hrs	1.17	1.80	1.52	0.47	47	0.99
NAcsh	0	=24-hrs	N/A	N/A	6.59	0.04	31	0.08
EPd	0	=24-hrs	-0.32	1.17	1.12	0.57	35	0.05
PIR2	6	=24-hrs	N/A	N/A	2.64	0.27	25	0.0004
ACAv	0	<28-hrs	9.97	146.43	3.08	0.21	49	0.21
AIp	0	<28-hrs	2.81	4.08	3.04	0.22	37	0.13
<u>ENTIs</u>	0	=24-hrs	-2.0	2.71	1.81	0.40	46	0.92
<u>ENTId</u>	0	<28-hrs	0.82	1.51	3.69	0.16	42	0.79

Notes on following page.

Notes:

N/A: not applicable, for these regions the <28-hr model could not be fitted to the data.

Outliers were found using the ROUT method (which combines **R**obust regression with **O**utlier removal) with a False Discovery Rate of 1% (recommended by Prism) and removed from all analyses (Motulsky & Brown, 2006).

Akaike Information Criterion (AIC): The data were fit with two models, Model 1: frequency =24-hrs, Model 2: frequency is <28-hrs, and compared using the AIC. The AIC quantifies how well each model fit the data (based on goodness-of-fit, i.e. sum of squares, and the number of parameters in each model), and determines the preferred model (column 1 in AIC). The difference in AIC is what matters and tells us the likelihood that a model is correct (column 2, Prism calculates the corrected AIC (AICc) which corrects for low sample size), and with the Evidence Ratio (the probability that model 1 is correct over the probability that model 2 is correct, column 3), qualifies the difference between the models. We followed the guidelines in the Prism manual that state that an Evidence Ratio of 12 or less suggests no meaningful differences between the models (Motulsky & Christopoulos, 2003).

D'Agostino-Pearson omnibus K² test (i.e. normality test): This test determines the skewness and kurtosis for a given data set and quantifies how far from Gaussian the distribution is (in terms of asymmetry and shape) and calculates how far each of these values differs from the value expected with a Gaussian distribution. A data set **fails** the normality test when the **p value is ≤ 0.05** , meaning that it deviates significantly from a normal distribution.

Wald-Wolfowitz Runs Test (i.e. Runs test): This test determines whether the fitted curve deviates systematically from the data (i.e. it looks for patterns in the residuals). A run is a consecutive series of data points whose residuals are either all positive or all negative (a small number of runs would indicate patterns in the residuals). A data set **fails** the Runs test when the **p value is ≤ 0.05** , meaning that the data points are not randomly distributed along the curve.

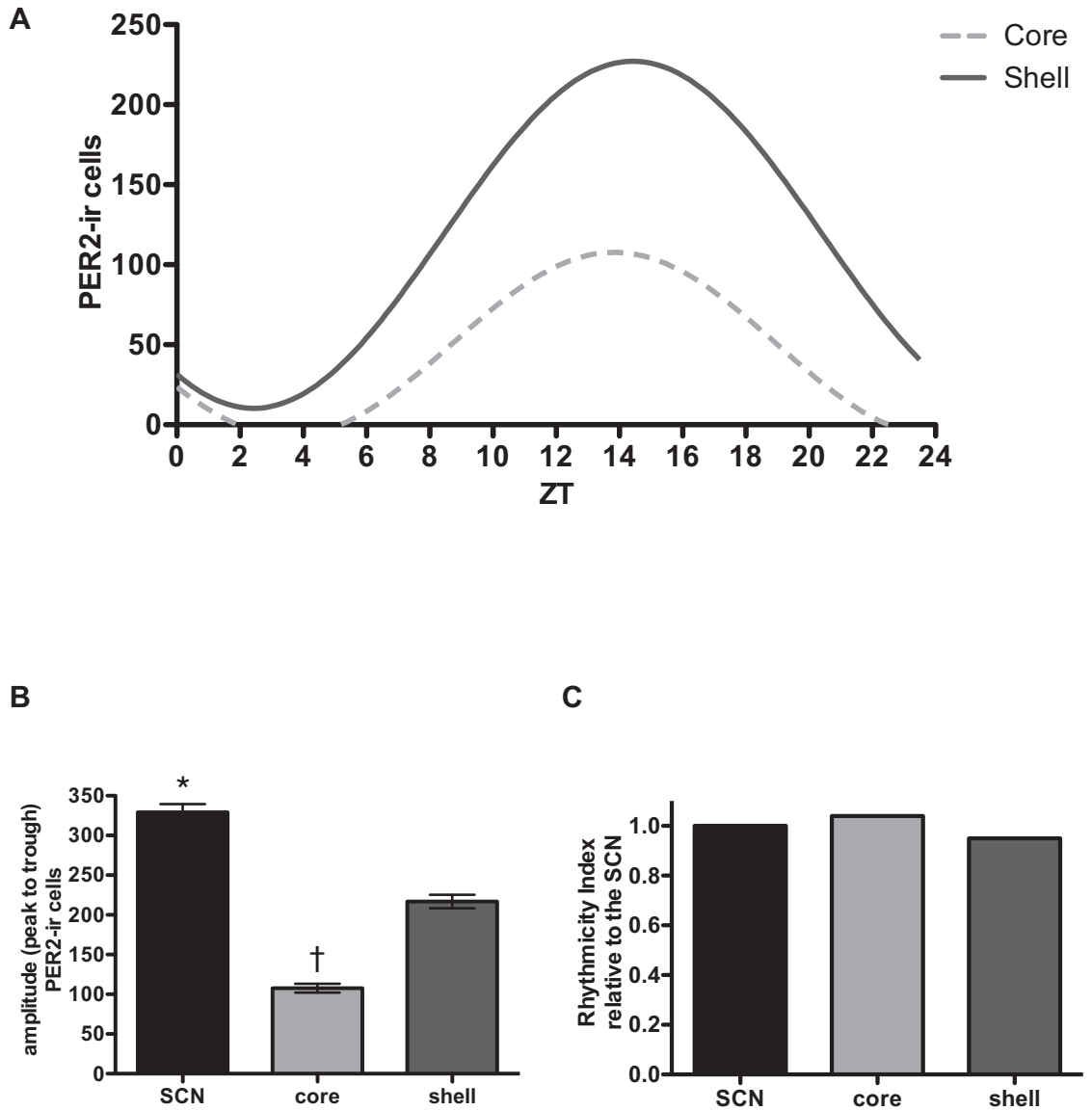


Figure 8. Suprachiasmatic Nucleus. A) Sine-fitted PER2 expression patterns in the SCN core and shell across 48 *zeitgeber* times. Solid line: 24-hr fit, dotted line: <28-hr fit. B) Amplitudes (mean number \pm SEM of PER2 immunoreactive cells) measured from peak to trough, in the core and shell compared to the whole SCN, Symbols indicate statistical significance ($p < .001$) as follows: *: whole SCN compared to both subdivisions, †: core compared to shell. C) Rhythmicity index values for the SCN core and shell normalized to the whole SCN.

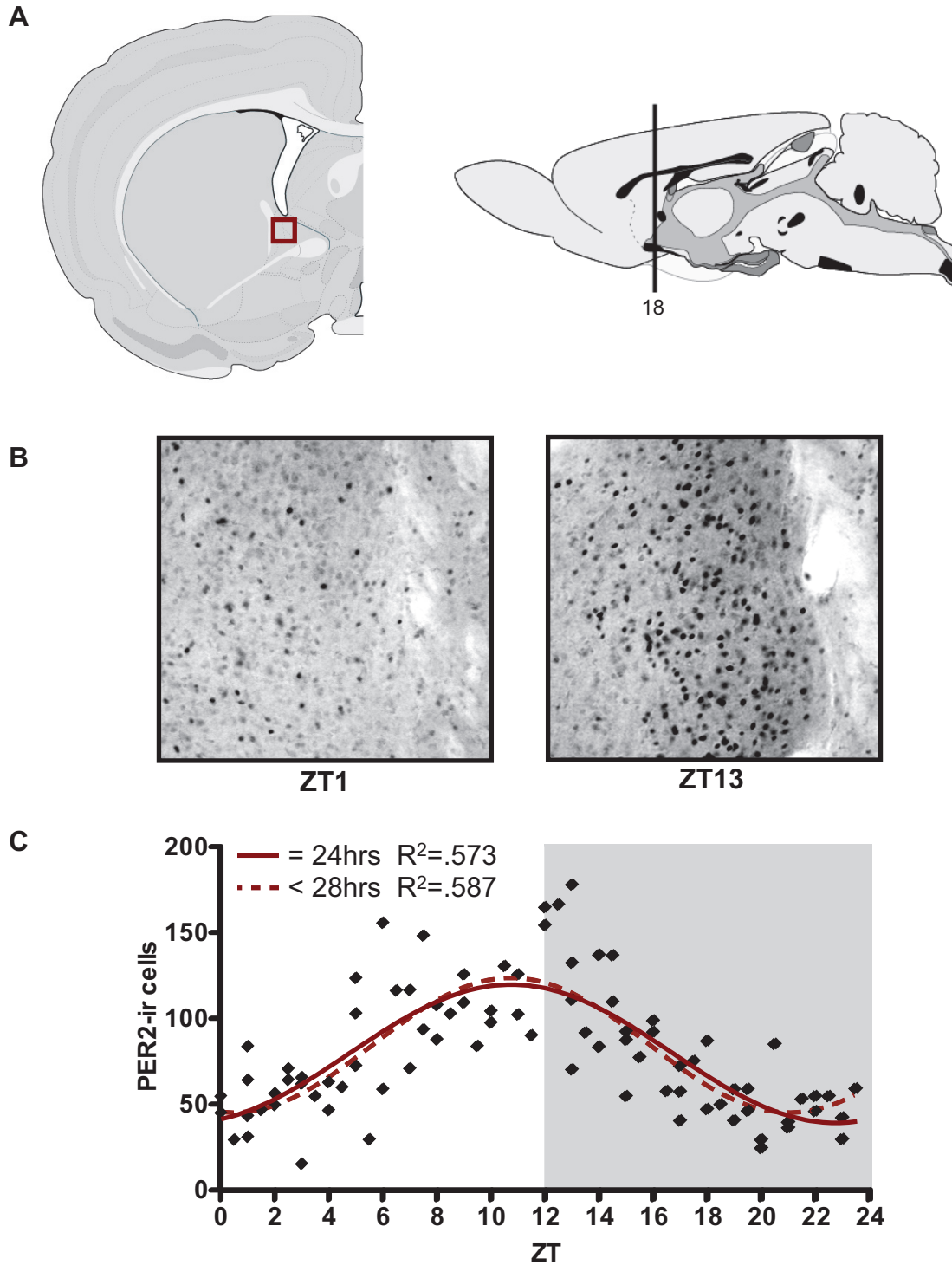


Figure 9. Oval Nucleus of the Bed Nucleus of the Stria Terminalis (BNSTov). A) Schematic diagrams of the BNSTov, coronal view (left) and sagittal view (right), number corresponds to level in the Swanson atlas. B) Representative photomicrographs (square in A) of PER2 expression at ZT1 and ZT13. C) Mean number of PER2-immunoreactive cells in the BNSTov of each individual rat (black diamonds) across 48 *zeitgeber* times. White and grey backgrounds indicate lights on and off, respectively. R^2 = Goodness of fit value for given sine wave. $n= 84$

<28-hr model best fit the data for this region, however, an Evidence Ratio of 1.31 revealed that the difference between the two models is insignificant (Fig. 9C). We found that PER2 expression peaks at approximately ZT11 in the BNSTov, which is slightly earlier than previously reported when using fewer time-points. Importantly, these results indicate that PER2 expression in the BNSTov is not in perfect phase with the SCN, as previously thought.

Central amygdala, lateral part

The CEAl also showed highly rhythmic PER2 expression ($R^2 = .564$) across the 24-hr day with an amplitude of 115.14 (Fig. 10). Like the BNSTov, the AIC computation suggested that the <28-hr model best fit the data for this region, but an Evidence Ratio of 4.02 indicated that the difference between the two models is insignificant (Fig. 10C). Importantly, as previously reported (Lamont, Robinson, Stewart, & Amir, 2005), PER2 expression in the CEAl is in phase with that of the BNSTov, showing peak expression at ZT11.

Basolateral amygdala

As previously reported (Lamont, Robinson, Stewart, & Amir, 2005), PER2 expression in the BLA is highly rhythmic with an amplitude of 64.36 (Fig. 11). There were no meaningful differences between the 24-hr and <28-hr model for the BLA data (Evidence Ratio 3.1), as can be seen by the visual representations of the sine waves along with the identical R^2 values of .606 (Fig. 11C). The <28-hr model fit a curve with a period of 23.9-hrs for the BLA, supporting the quality of the fit obtained with the 24-hr

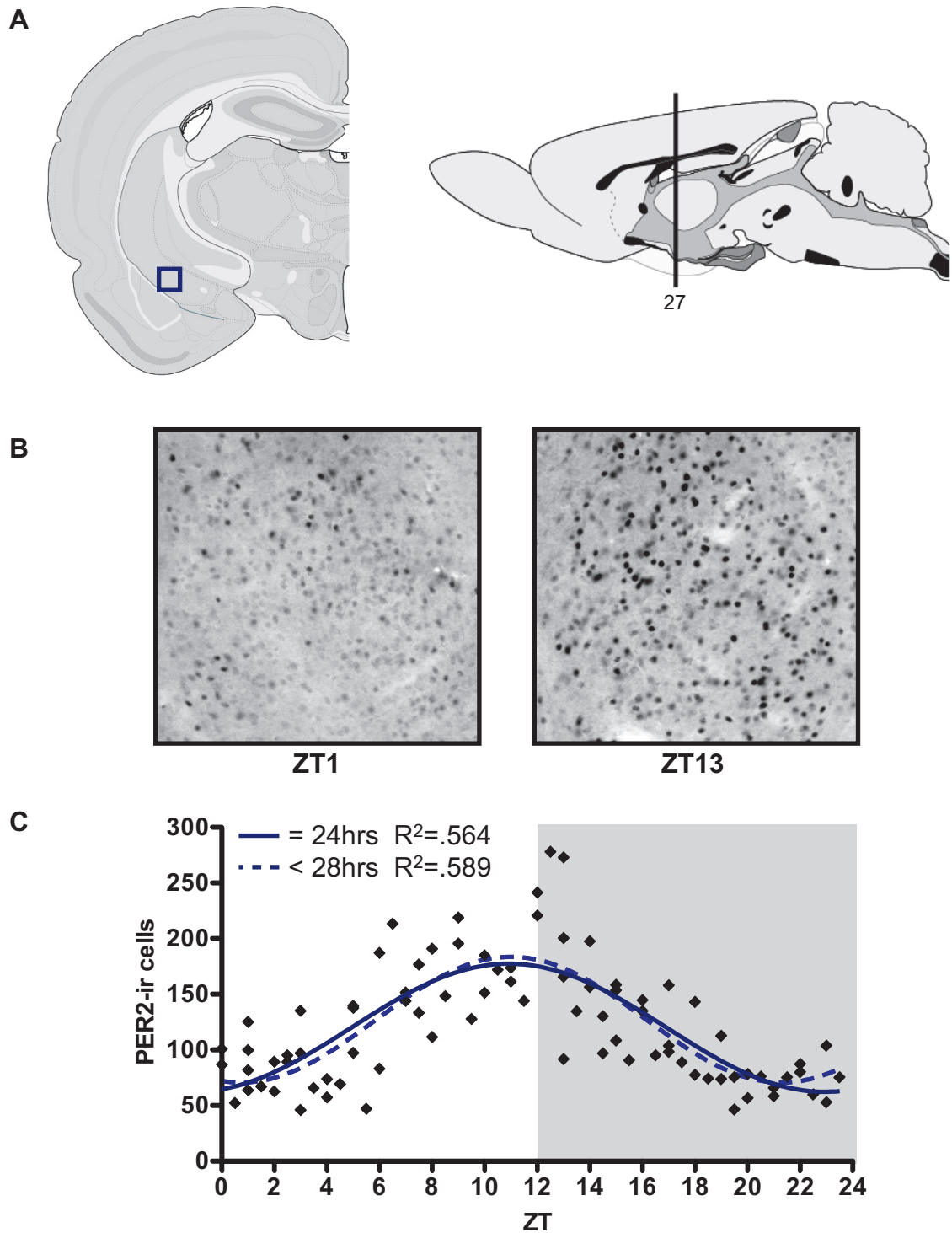


Figure 10. Central Nucleus of the amygdala, lateral (CEAl). A) Schematic diagrams of the CEAl, coronal view (left) and sagittal view (right), number corresponds to level in the Swanson atlas. B) Representative photomicrographs (square in A) of PER2 expression at ZT1 and ZT13. C) Mean number of PER2-immunoreactive cells in the CEAl of each individual rat (black diamonds) across 48 *zeitgeber* times. White and grey backgrounds indicate lights on and off, respectively. R^2 = Goodness of fit value for given sine wave. $n = 84$

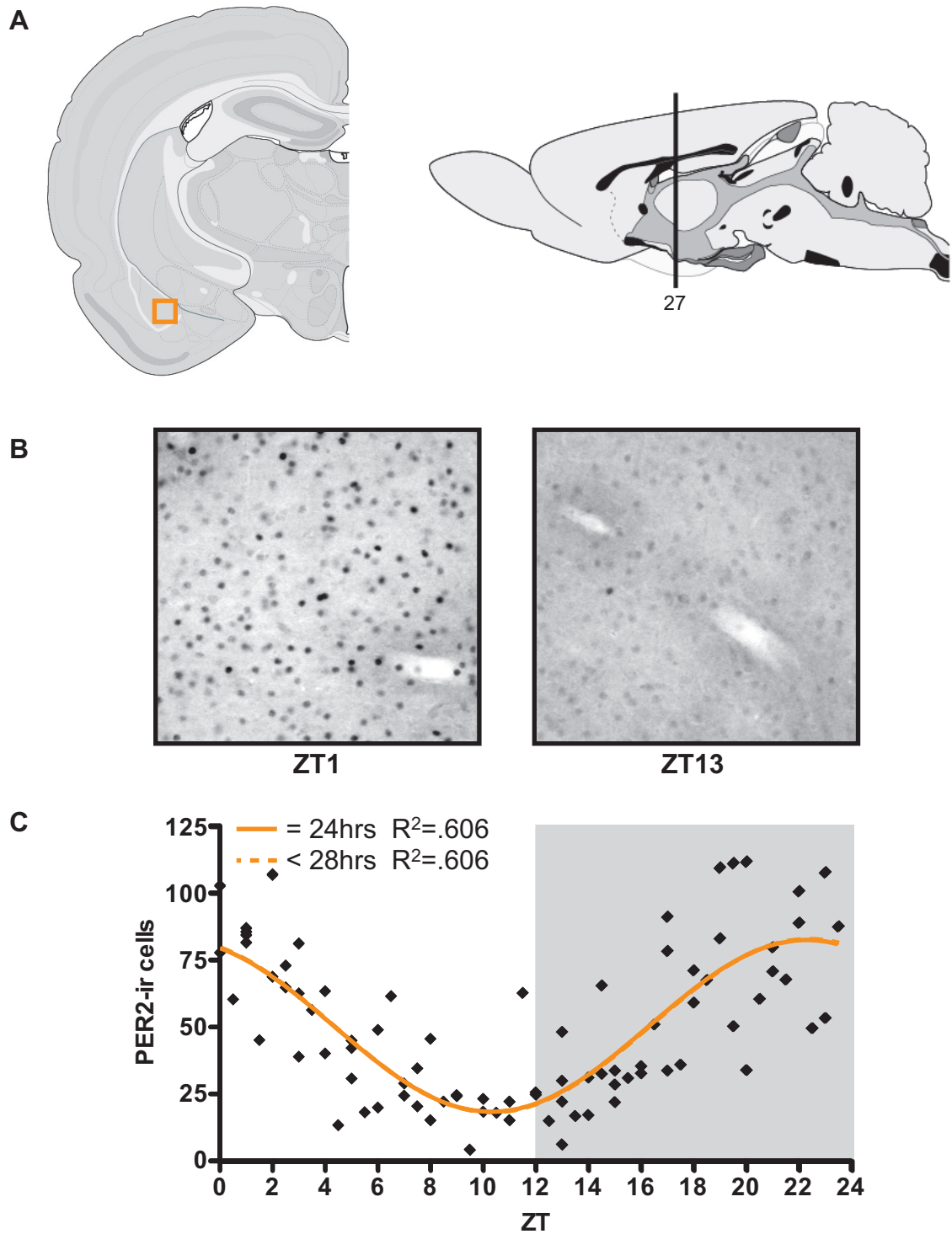


Figure 11. Basolateral Amygdala (BLA). A) Schematic diagrams of the BLA, coronal view (left) and sagittal view (right), number corresponds to level in the Swanson atlas. B) Representative photomicrographs (square in A) of PER2 expression at ZT1 and ZT13. C) Mean number of PER2-immunoreactive cells in the BLA of each individual rat (black diamonds) across 48 *zeitgeber* times. White and grey backgrounds indicate lights on and off, respectively. R^2 = Goodness of fit value for given sine wave. $n= 84$

model. Interestingly, peak PER2 expression in the BLA also occurs earlier than previously found (Lamont, Robinson, Stewart, & Amir, 2005), with expression peaking at the end of the dark phase, at around ZT22.5. Importantly, the rhythm in PER2 expression in the BLA remained in anti-phase with that of the BNSTov and CEAl, as previously reported by our laboratory.

Medial amygdala, posteriodorsal part

As can be seen in Figures 12B and 12C, PER2 expression in the MEApd is evenly distributed throughout the 24-hr day. No significant differences were found between the 24-hr and <28-hr model for this region (Evidence Ratio of 2.54). Although PER2 is expressed in the MEApd, suggesting the presence of a circadian clock, the extremely low amplitude of 16.74 and an R^2 of .141 led us to conclude that this region is arrhythmic under normal lighting conditions.

In summary, there are phase differences in PER2 expression in the different sub-regions of the BNSTov/amygdala. Specifically, PER2 expression in the BNSTov and CEAl is in phase with each other, while the BLA is in anti-phase with these regions, and the MEApd is arrhythmic (Fig. 13A). Notably, none of the rhythms in these regions are in phase (or anti-phase) with the PER2 rhythm of the SCN, which peaks at approximately ZT14.5.

There are also differences in amplitude between the SCN, BNSTov, and amygdala ($F_{(4,412)}=208.6, p<.0001$, Fig. 13B). Specifically, the amplitude in the CEAl is significantly higher than in all other sub-regions of the amygdala (BNSTov: $t_{(414)}=2.95$,

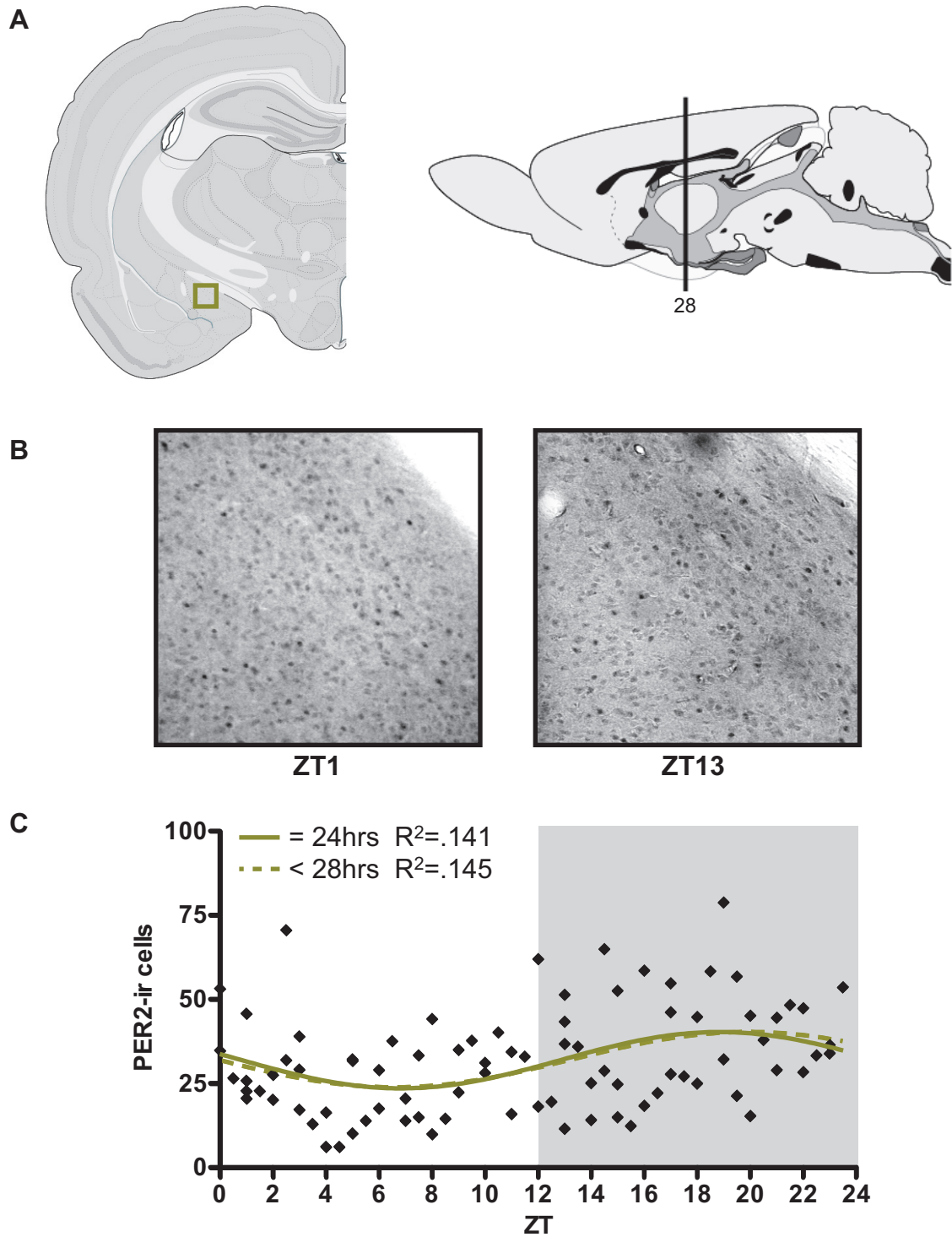


Figure 12. Medial Amygdala, posteriodorsal (MEApd). A) Schematic diagrams of the MEdApd, coronal view (left) and sagittal view (right), number corresponds to level in the Swanson atlas. B) Representative photomicrographs (square in A) of PER2 expression at ZT1 and ZT13. C) Mean number of PER2-immunoreactive cells in the MEdApd of each individual rat (black diamonds) across 48 *zeitgeber* times. White and grey backgrounds indicate lights on and off, respectively. R^2 = Goodness of fit value for given sine wave. $n= 84$

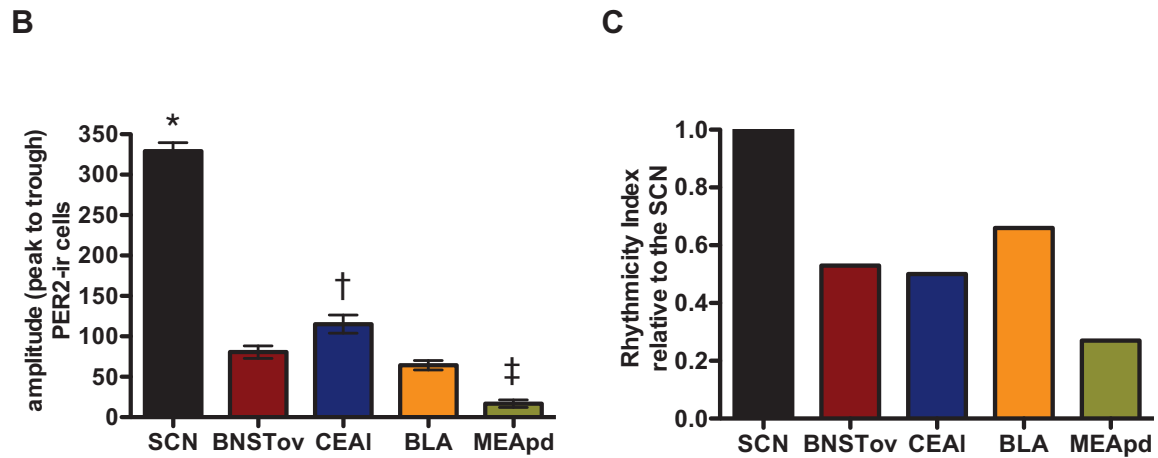
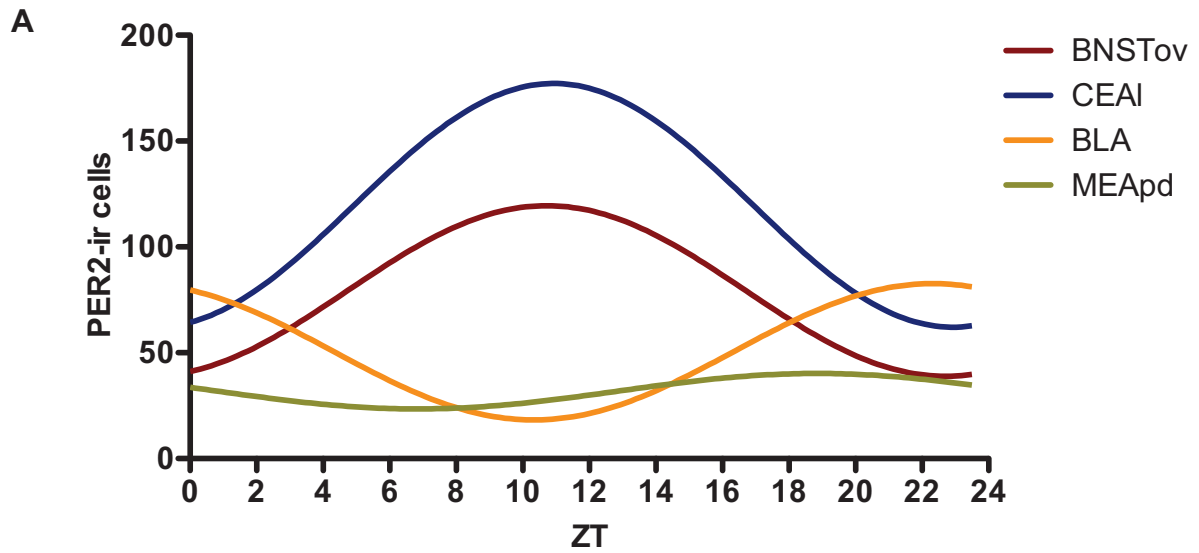


Figure 13. Amygdala. A) Sine-fitted PER2 expression patterns in all 4 regions of the amygdala across 48 *zeitgeber* times. B) Amplitudes (mean number \pm SEM of PER2 immunoreactive cells) measured from peak to trough, in each region of the amygdala, compared to the SCN. Symbols indicate statistical significance ($p < .05$) as follows: *: SCN compared to all other regions, †: CEAI compared to all other regions, ‡: MEApd compared to all other regions. C) Rhythmicity index values for the 4 regions of the amygdala normalized to the SCN.

$p < .05$, BLA: $t_{(414)} = 4.32$, $p < .001$, MEApd: $t_{(414)} = 8.38$, $p < .001$), whereas the amplitude in the MEApd is lower than in all other regions (BNSTov: $t_{(414)} = 5.44$, $p < .001$, BLA: $t_{(414)} = 4.06$, $p < .001$). Finally, the PER2 amplitude in the SCN is significantly higher than in all the BNST/amygdalar sub-regions. However, when normalized to take into account the spread of the data for each region relative to the SCN, the BNSTov, CEAI, and BLA show rhythms that are at least 50% as rhythmic as the SCN (RI values of .51, .50, .66, respectively, Fig. 13C). We found that the MEApd has an RI value of .27 relative to the SCN. Although this is slightly more (2%) than the RI cutoff for rhythmicity, given the low R^2 value for this region (less than half of 1/3rd of the SCN) it was determined to be arrhythmic.

Correlations of PER2 expression across the 24-hr day between the three rhythmic BNST/amygdala regions and the SCN revealed statistically significant moderate relationships (see Table 2). Notably, a very high correlation of .88 was found between the BNSTov and CEAI, consistent with the anatomical evidence that these two regions are highly interconnected and functionally related.

Table 2. Correlations of PER2 expression in the amygdala. Pearson r values comparing regions of the BNST/amygdala and the master SCN clock across the 24-hr day. The MEApd has been omitted since it is arrhythmic. Values in bold are statistically significant ($p < .05$).

Region	BNSTov	CEAI	BLA
SCN	0.45	0.49	-0.34
BNSTov		0.88	-0.49
CEAI			-0.45

Hippocampus

Dentate gyrus

As previously reported (Lamont, Robinson, Stewart, & Amir, 2005), the DG showed a highly rhythmic PER2 expression pattern ($R^2 = .843$) with an amplitude of 77.39 (Fig. 14). According to the AIC computation and an Evidence Ratio of 18.72, the <28-hr model best fit the data for the DG (Fig. 14C). Here, the <28-hr model fit a curve with a period of 20.4-hrs but also failed the Runs test ($p < .001$) (see Fig. A2), indicating that neither model fit the data perfectly. The PER2 peak in the DG occurs at approximately ZT23.5, only slightly earlier than previously found. Importantly, the time of peak PER2 expression in the DG is 1-hr later than in the BLA, two regions we previously thought to be in perfect phase.

CA1

We found that the CA1 exhibits a weak rhythm in PER2 expression (R^2 value of .392) with relatively low amplitude of 31.68 (Fig. 15). No meaningful differences were found between the two models for this region (Evidence Ratio of 2.65) (Fig. 15C). Notably, the peak of PER2 expression in the CA1 occurs at approximately ZT21.5, which is 2-hrs earlier than the peak found in the DG.

CA3

Compared to the CA1, the CA3 displays a highly rhythmic pattern in PER2 expression ($R^2 = .725$, Fig. 16). Here, the <28-hr model could not be fitted to the data; Prism labeled the curve as ‘ambiguous’, meaning that it could not fit all parameters

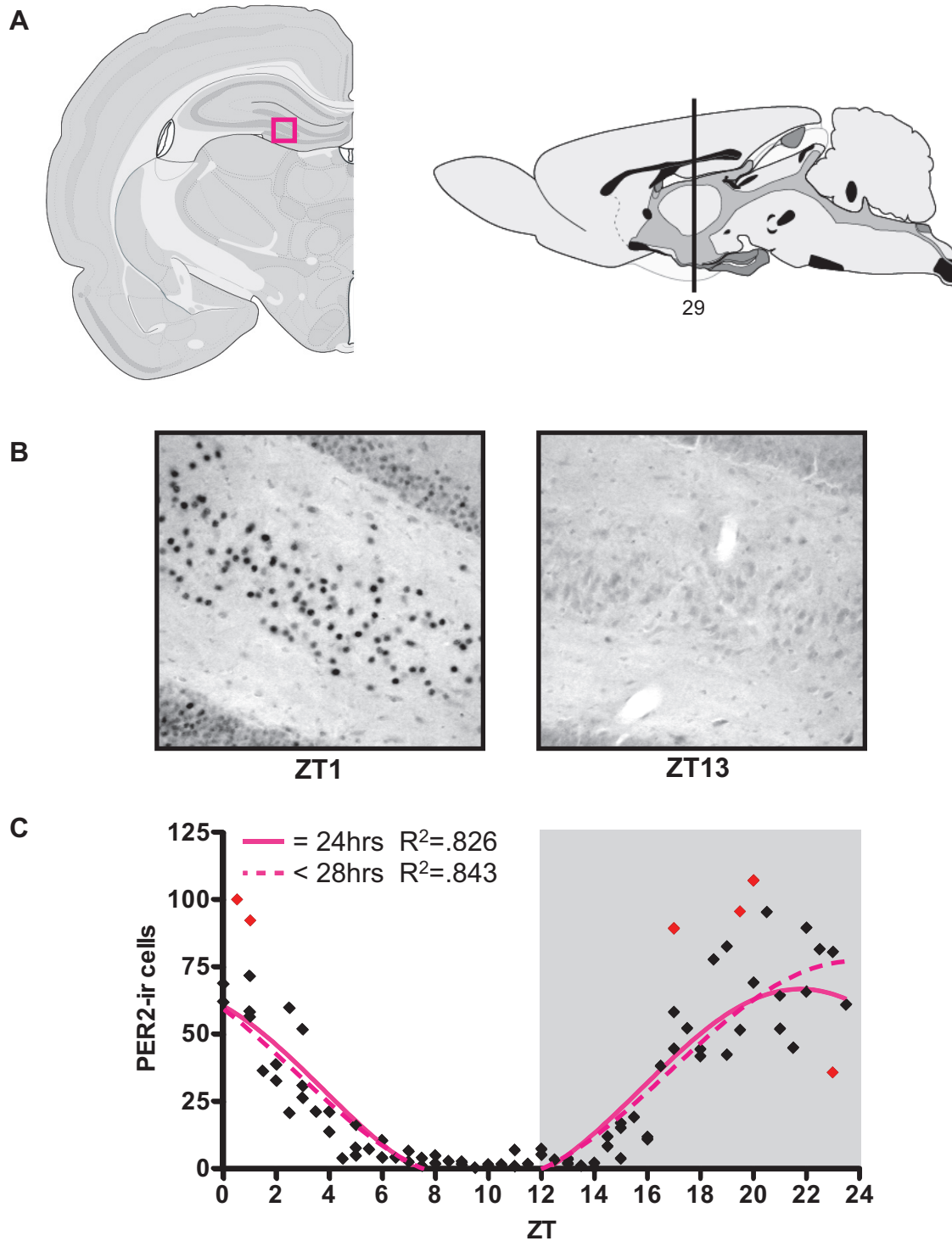


Figure 14. Dentate Gyrus (DG). A) Schematic diagrams of the DG, coronal view (left) and sagittal view (right), number corresponds to level in the Swanson atlas. B) Representative photomicrographs (square in A) of PER2 expression at ZT1 and ZT13. C) Mean number of PER2-immunoreactive cells in the DG of each individual rat (diamonds) across 48 *zeitgeber* times. White and grey backgrounds indicate lights on and off, respectively. R^2 = Goodness of fit value for given sine wave. $n= 78$ (6 outliers removed, red diamonds)

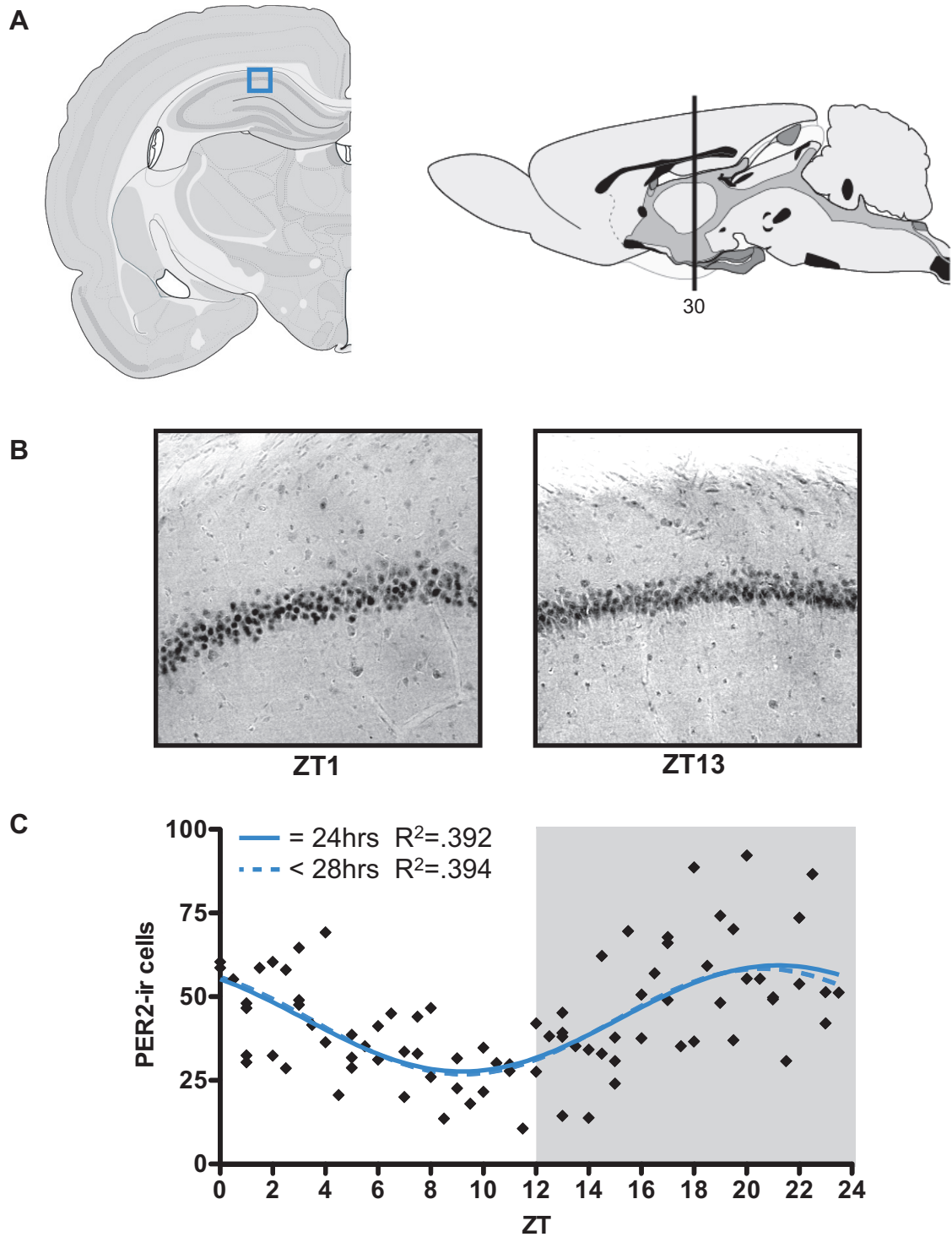


Figure 15. CA1. A) Schematic diagrams of the CA1, coronal view (left) and sagittal view (right), number corresponds to level in the Swanson atlas. B) Representative photomicrographs (square in A) of PER2 expression at ZT1 and ZT13. C) Mean number of PER2-immunoreactive cells in the CA1 of each individual rat (black diamonds) across 48 *zeitgeber* times. White and grey backgrounds indicate lights on and off, respectively. R^2 = Goodness of fit value for given sine wave. $n= 84$

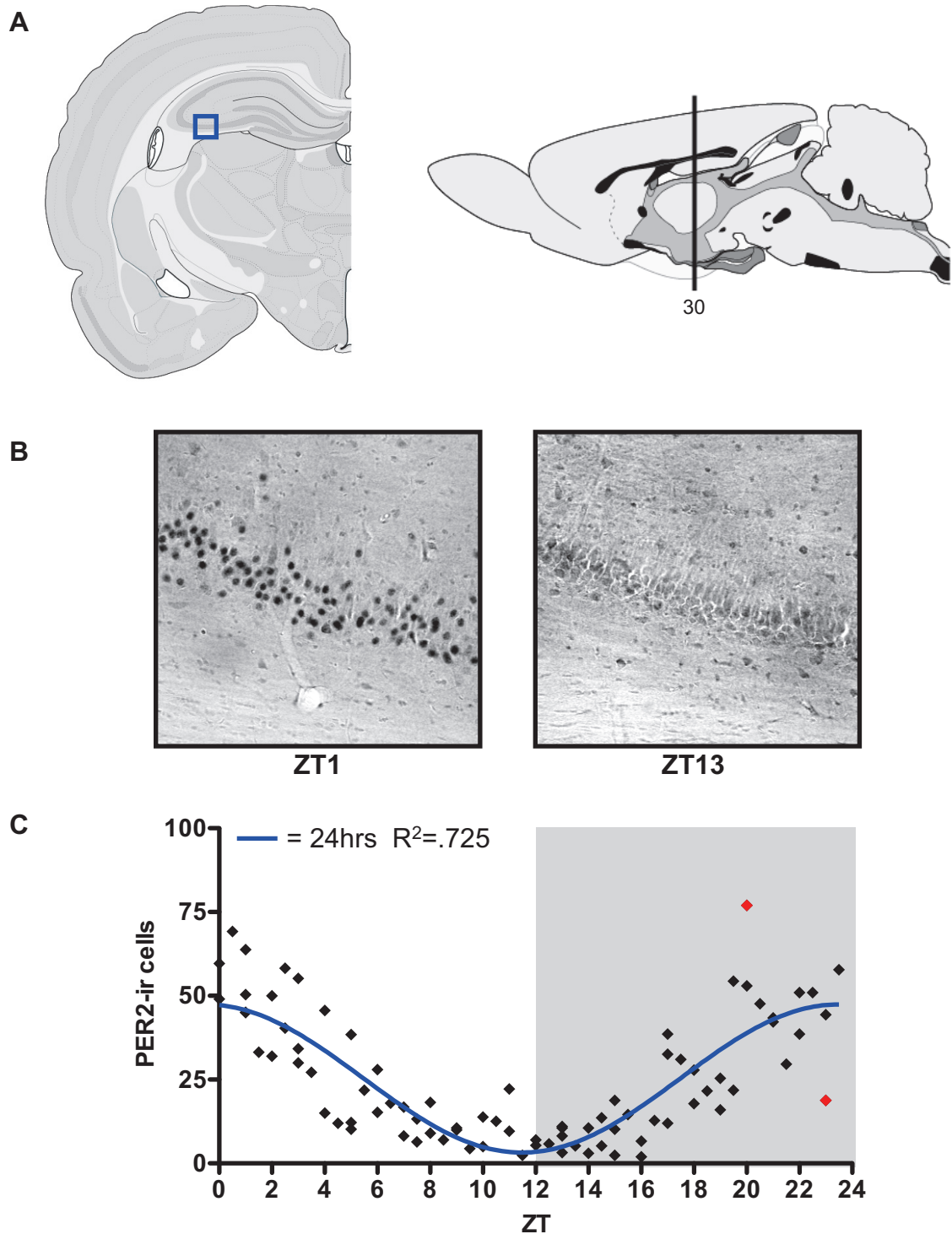


Figure 16. CA3. A) Schematic diagrams of the CA3, coronal view (left) and sagittal view (right), number corresponds to level in the Swanson atlas. B) Representative photomicrographs (square in A) of PER2 expression at ZT1 and ZT13. C) Mean number of PER2-immunoreactive cells in the CA3 of each individual rat (diamonds) across 48 *zeitgeber* times. White and grey backgrounds indicate lights on and off, respectively. R^2 = Goodness of fit value for given sine wave. $n= 82$ (2 outliers removed, red diamonds)

appropriately for this model. Therefore, the AIC could not be calculated for this region and thus the 24-hr model was used. We found that the CA3 has an amplitude of 44.2 and PER2 expression in this region peaks in phase with the DG, at around ZT23.5.

In summary, the three sub-regions of the hippocampus differ slightly in PER2 phase (Fig. 17A). Specifically, PER2 expression in the CA1 peaks 2-hrs earlier than in the DG and CA3 (which are in phase regarding peak expression but differ by 2-hrs for the trough of PER2 expression). Notably, none of the rhythms in these regions are in phase (or anti-phase) with the PER2 rhythm of the SCN.

Amplitude levels in these regions and the SCN also differ ($F_{(3,321)}=451.0, p<.0001$, Fig. 17B). Specifically, the amplitude in the DG is significantly higher than in the CA1 ($t_{(322)}=4.87, p<.001$) and CA3 ($t_{(322)}=3.52, p<.01$), and the PER2 amplitude in the SCN is significantly higher than in all three hippocampal regions. Interestingly, calculation of the RI showed that the rhythm in the DG is as strong as the rhythm in the SCN (RI value of 1.04) (Fig. 17C). Furthermore, the CA3 also has a very strong rhythm with an RI value of .91. The CA1, on the other hand, has a relatively weak rhythm when compared to the SCN (RI value of .38).

Correlations of PER2 expression between these hippocampal regions and the SCN revealed differences in the strength of the relationship between these regions. For all results consult Table 3. Notably, the SCN has a low negative correlation of -.28 with the DG and an even lower non-significant correlation with the CA1 ($r=-.07$). However, the SCN is highly correlated with the CA3 ($r=-.61$). Finally, the DG and CA3, which are in

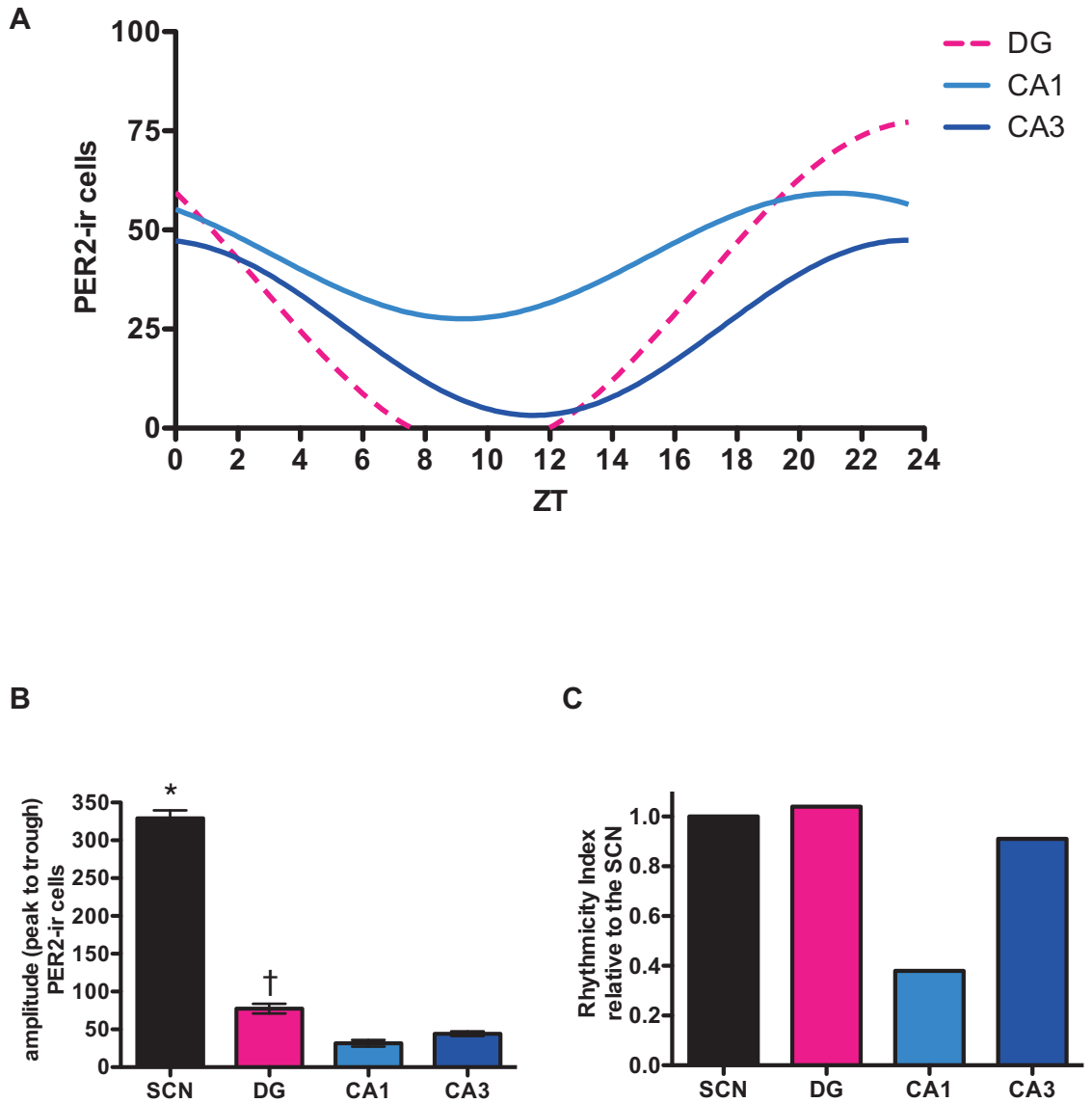


Figure 17. Hippocampus. A) Sine-fitted PER2 expression patterns in all 3 regions of the hippocampus across 48 *zeitgeber* times. Solid line: 24-hr fit, dotted line: <28-hr fit. B) Amplitudes (mean number \pm SEM of PER2 immunoreactive cells) measured from peak to trough, in each region of the hippocampus, compared to the SCN. Symbols indicate statistical significance ($p < .01$) as follows: *: SCN compared to all other regions, †: DG compared to all other regions. C) Rhythmicity index values for the 3 regions of the hippocampus normalized to the SCN.

phase for peak PER2 expression and have similar amplitudes, are also highly correlated ($r = .75$).

Table 3. Correlations of PER2 expression in the hippocampus. Pearson r values comparing regions of the hippocampus and the master SCN clock across the 24-hr day. Values in bold are statistically significant ($p < .05$).

Region	DG	CA1	CA3
SCN	-0.28	-0.07	-0.61
DG		0.59	0.75
CA1			0.54

Striatum

Anterior striatum, dorsal and medial

Both the dorsal and medial anterior striatum exhibit rhythmic patterns of PER2 expression ($R^2 = .64$ and $.542$, respectively; Fig. 18 & 19). The <28 -hr model could not be fitted to the data for either region (Prism labeled the curves as ‘ambiguous’), thus the 24-hr model was used for each region (Fig. 18C & 19C, respectively). The dorsal subdivision, however, failed the Runs test ($p < .01$) indicating that the fit is not perfect (see Fig. A3). We found that the dorsal and medial striatum have similar amplitudes (76.54 and 79.44, respectively) and are in phase, with peak PER2 expression occurring at around ZT23.5 for each region.

Posterior striatum, dorsal and medial

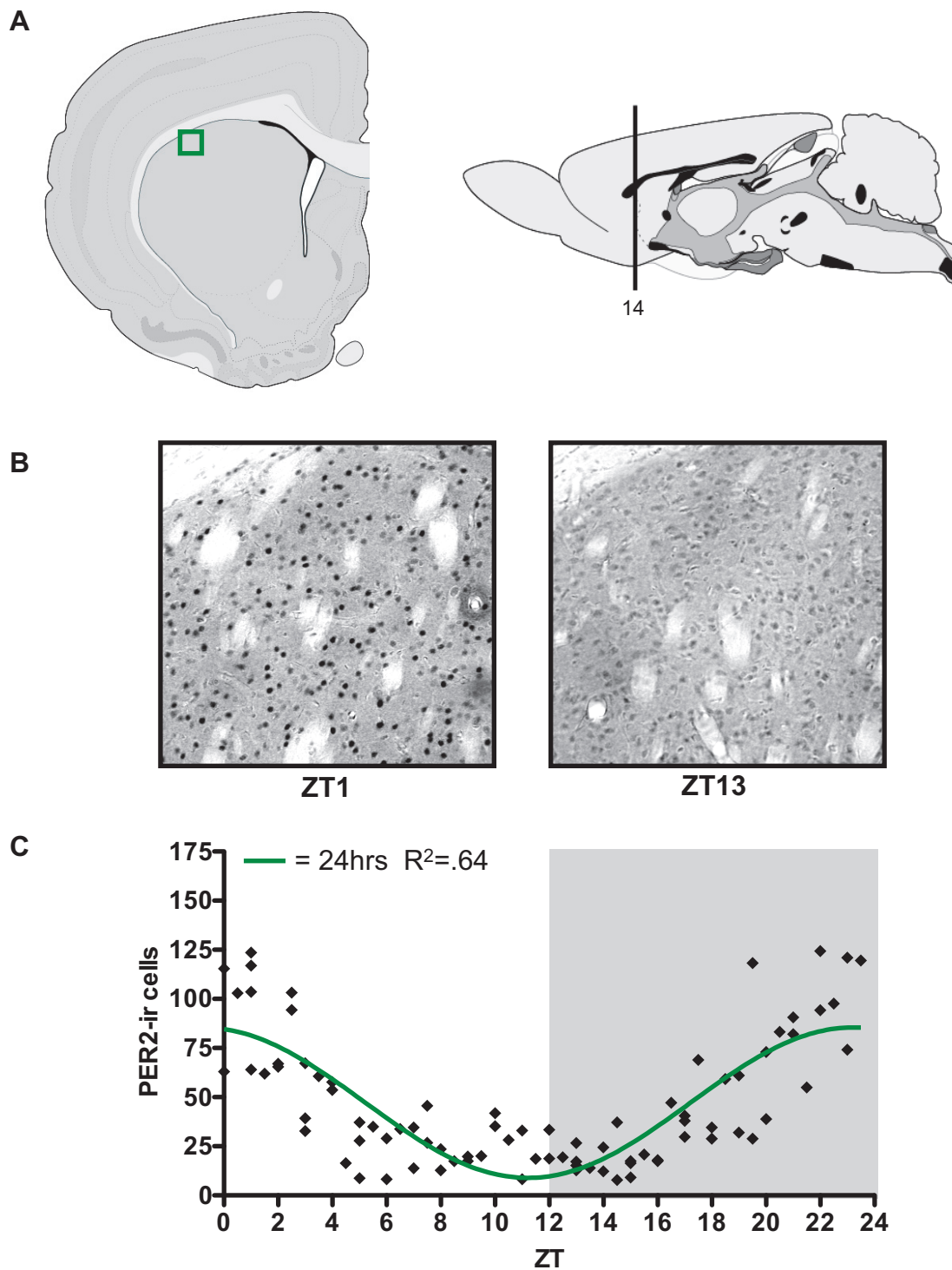


Figure 18. Anterior striatum, dorsal (ASd). A) Schematic diagrams of the ASd, coronal view (left) and sagittal view (right), number corresponds to level in the Swanson atlas. B) Representative photomicrographs (square in A) of PER2 expression at ZT1 and ZT13. C) Mean number of PER2-immunoreactive cells in the ASd of each individual rat (black diamonds) across 48 *zeitgeber* times. White and grey backgrounds indicate lights on and off, respectively. R^2 = Goodness of fit value for sine wave. $n= 84$

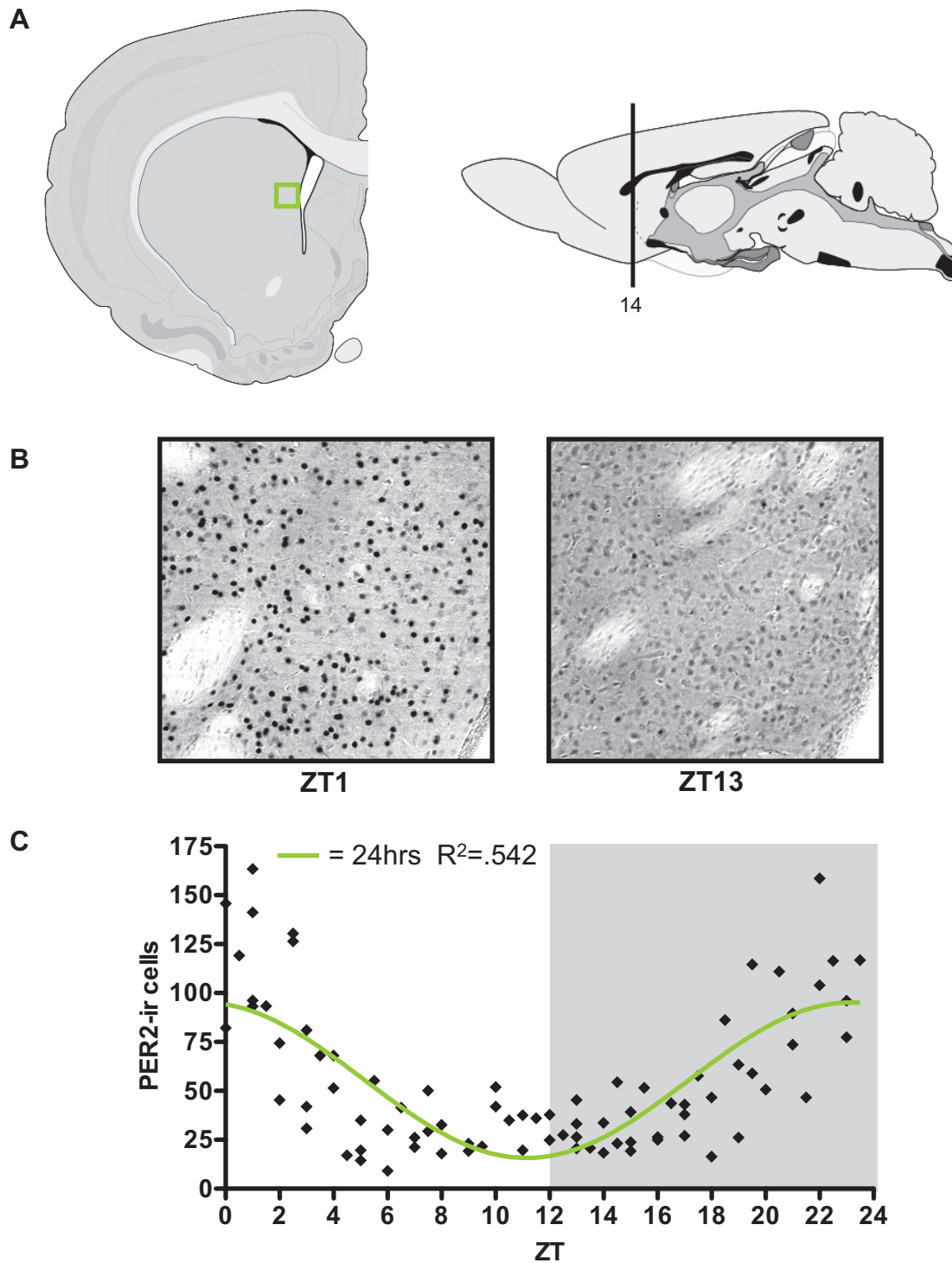


Figure 19. Anterior striatum, medial (ASm). A) Schematic diagrams of the ASm, coronal view (left) and sagittal view (right), number corresponds to level in the Swanson atlas. B) Representative photomicrographs (square in A) of PER2 expression at ZT1 and ZT13. C) Mean number of PER2-immunoreactive cells in the ASm of each individual rat (black diamonds) across 48 *zeitgeber* times. White and grey backgrounds indicate lights on and off, respectively. R²= Goodness of fit value for sine wave. *n*= 82

Both the dorsal and medial posterior striatum also exhibit rhythmic patterns of PER2 expression ($R^2 = .49$ and $.492$, respectively; Fig. 20 & 21). Similar to the anterior striatum, the <28-hr model could not be fitted to the data for either posterior region, thus the 24-hr model was used (Fig. 20C & 21C, respectively). However, the 24-hr model does not fit the data perfectly, as indicated by the dorsal part failing the Runs Test ($p < .05$) (see Fig. A4), and the medial part failing the normality test ($K^2 = 6.56$, $p < .05$). The posterior dorsal striatum has a slightly lower amplitude compared to the medial striatum (54.28 vs. 79.58), however this difference is not statistically significant ($t_{(558)} = 2.03$, $p > .05$). Importantly, we found that the two subdivisions of the posterior striatum are in phase with each other as well as with the two subdivisions of the anterior striatum, with peak PER2 expression occurring at around ZT23.5.

Nucleus accumbens, core and shell

The NAc is part of the ventral striatum. The core and shell of the NAc show strikingly different patterns of PER2 expression. The core (NAcc) shows a highly rhythmic pattern of PER2 expression ($R^2 = .69$; Fig. 22) with an amplitude of 176.78 (2nd highest after the SCN). According to the AIC computation, the <28-hr model best fit the data for this region, but an Evidence Ratio of 1.8 indicates that the difference between the two models is insignificant (Fig. 22C). We found that peak PER2 occurs at approximately ZT22.5, 1-hr earlier than the four sub-regions of the dorsal striatum.

As can be seen by the spread of data points in Figure 23C, PER2 expression in the shell (NAcsh) is evenly distributed throughout the 24-hr day. The <28-hr could not be fitted to the data in this region and the 24-hr model failed the normality test ($K^2 = 6.59$,

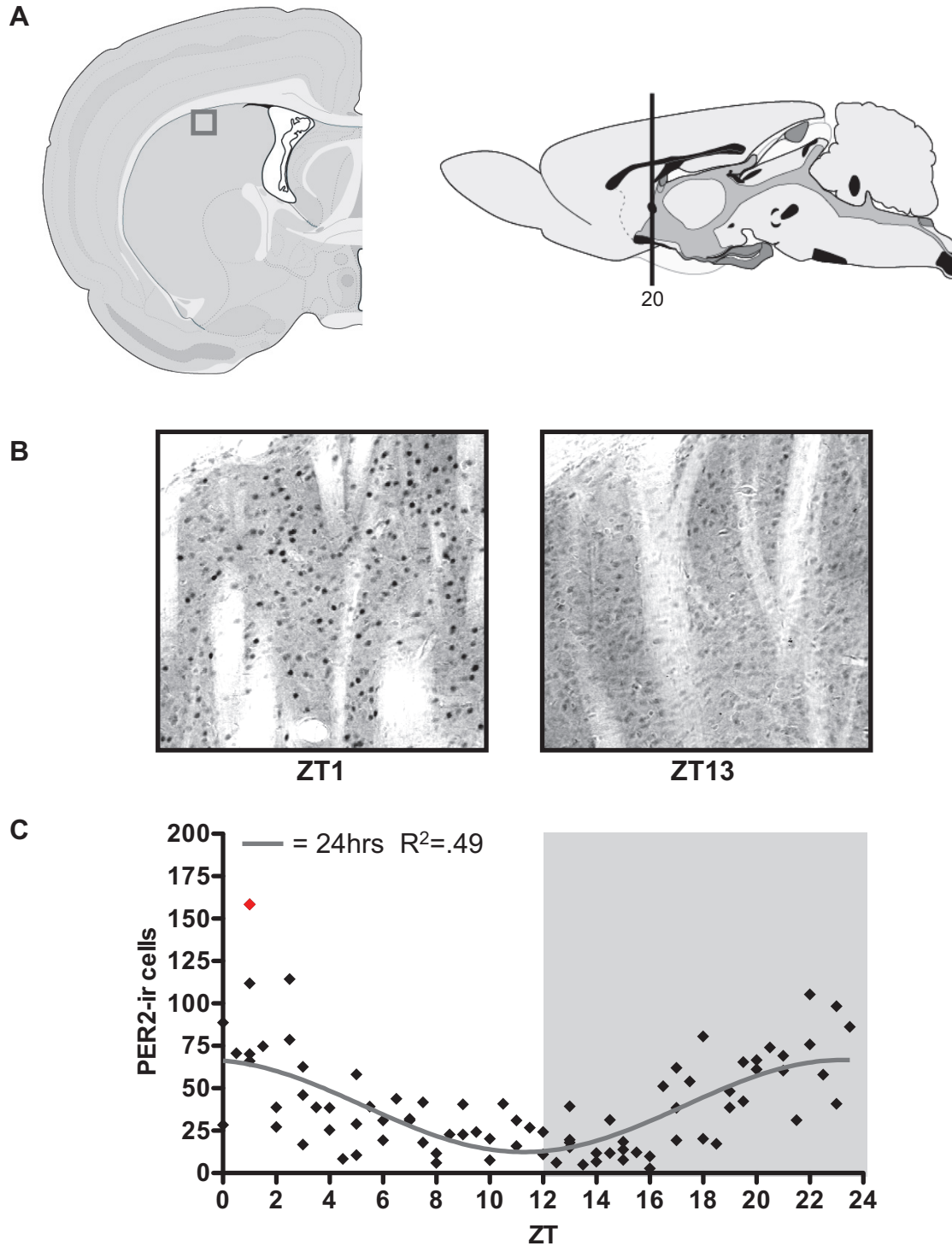


Figure 20. Posterior striatum, dorsal (PSd). A) Schematic diagrams of the PSd, coronal view (left) and sagittal view (right), number corresponds to level in the Swanson atlas. B) Representative photomicrographs (square in A) of PER2 expression at ZT1 and ZT13. C) Mean number of PER2-immunoreactive cells in the PSd of each individual rat (diamonds) across 48 *zeitgeber* times. White and grey backgrounds indicate lights on and off, respectively. R^2 = Goodness of fit value for sine wave. $n= 83$ (1 outlier removed, red diamond)

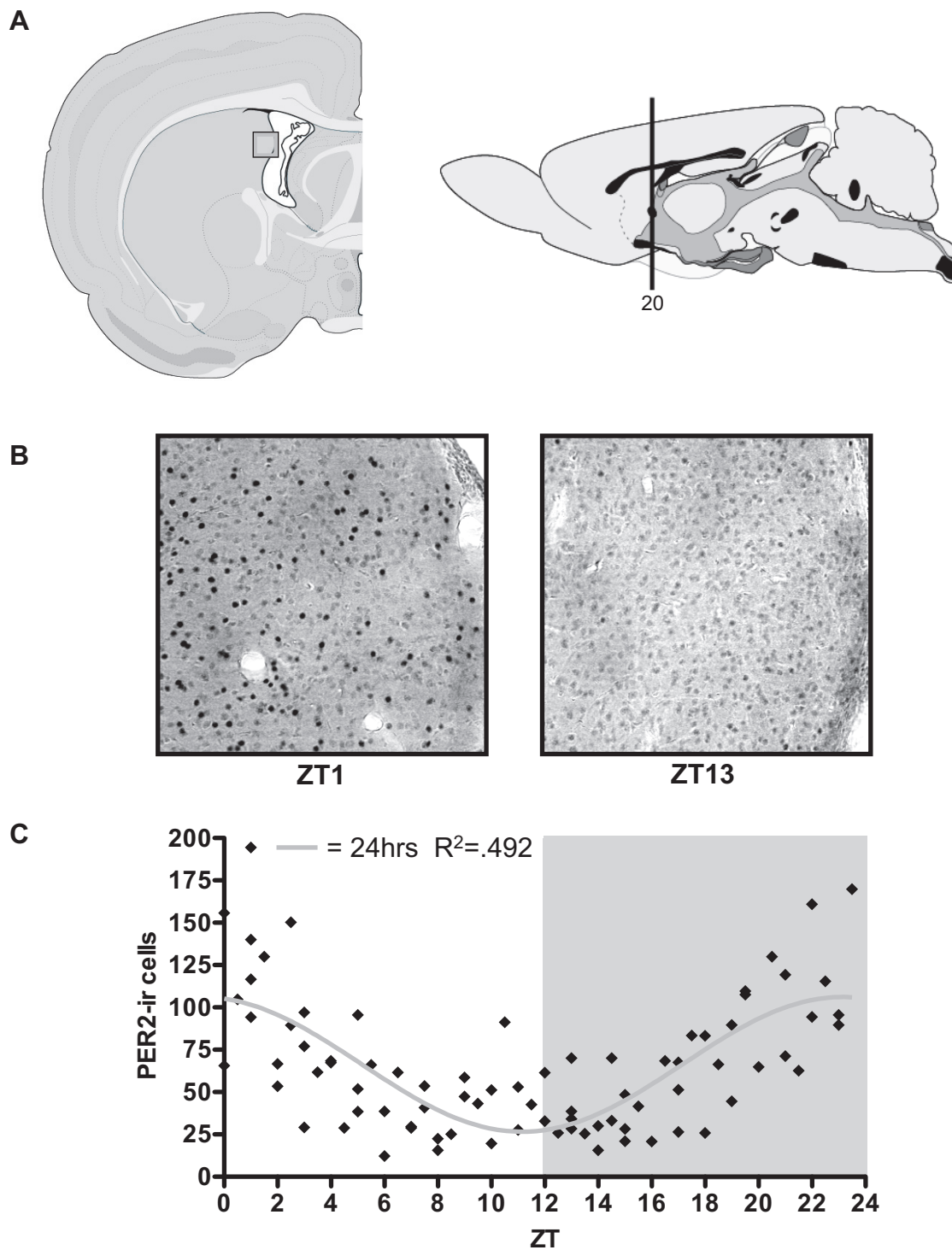


Figure 21. Posterior striatum, medial (PSm). A) Schematic diagrams of the PSm, coronal view (left) and sagittal view (right), number corresponds to level in the Swanson atlas. B) Representative photomicrographs (square in A) of PER2 expression at ZT1 and ZT13. C) Mean number of PER2-immunoreactive cells in the PSm of each individual rat (black diamonds) across 48 *zeitgeber* times. White and grey backgrounds indicate lights on and off, respectively. R^2 = Goodness of fit value for sine wave. $n= 82$

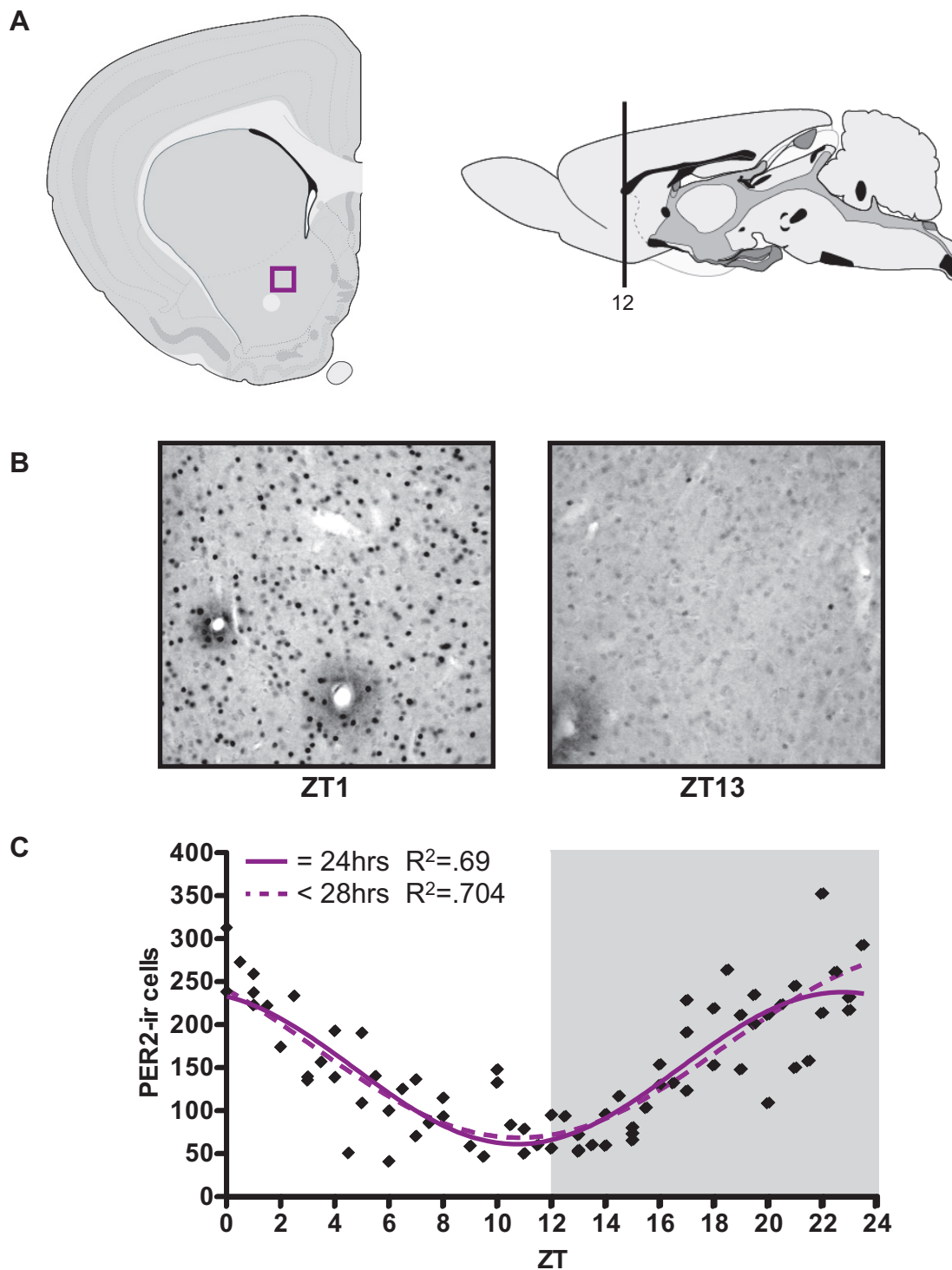


Figure 22. Nucleus Accumbens, core (NAcc). A) Schematic diagrams of the NAcc, coronal view (left) and sagittal view (right), number corresponds to level in the Swanson atlas. B) Representative photomicrographs (square in A) of PER2 expression at ZT1 and ZT13. C) Mean number of PER2-immunoreactive cells in the NAcc of each individual rat (black diamonds) across 48 *zeitgeber* times. White and grey backgrounds indicate lights on and off, respectively. R^2 = Goodness of fit value for given sine wave. $n= 74$

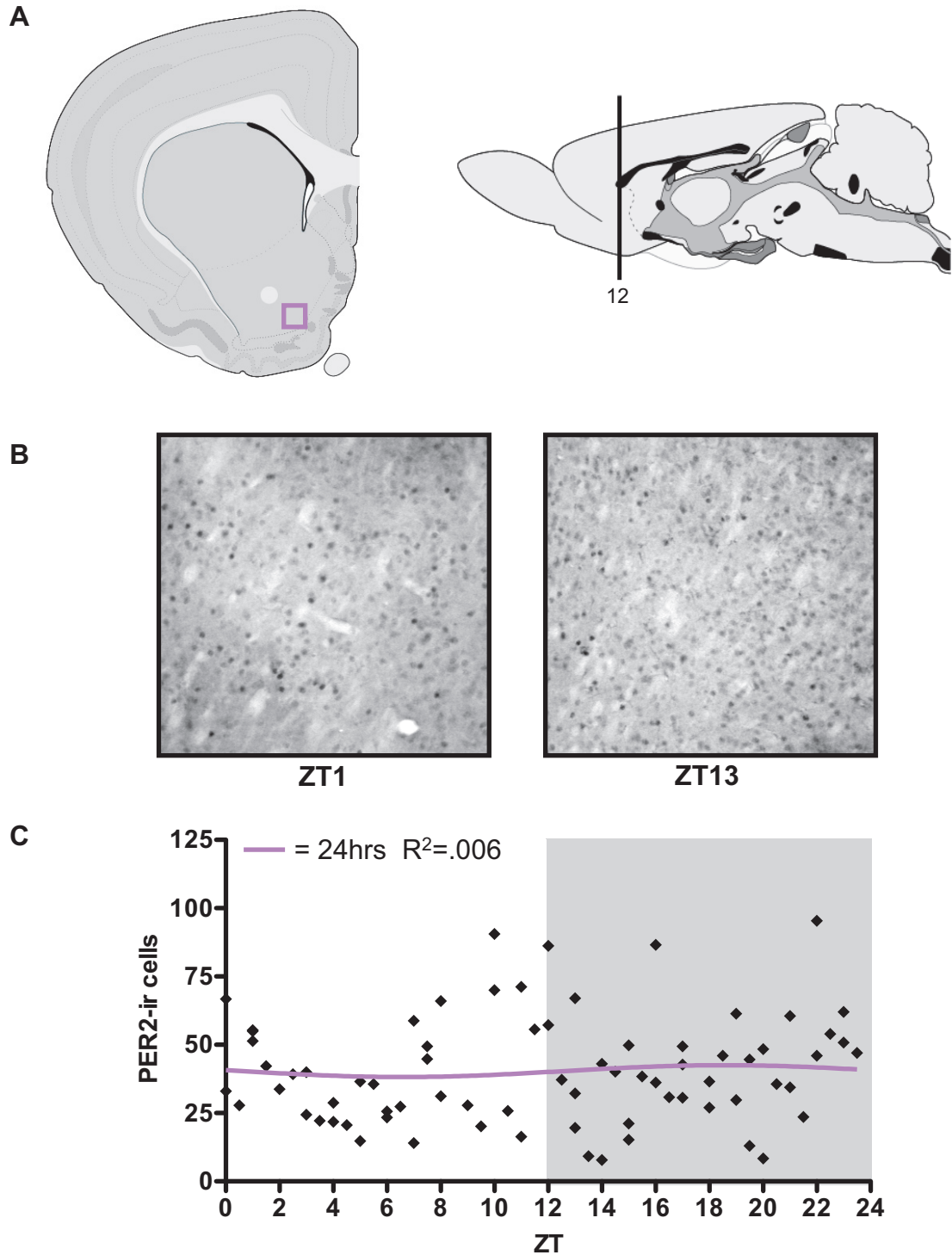


Figure 23. Nucleus Accumbens, shell (NAcsh). A) Schematic diagrams of the NAcsh, coronal view (left) and sagittal view (right), number corresponds to level in the Swanson atlas. B) Representative photomicrographs (square in A) of PER2 expression at ZT1 and ZT13. C) Mean number of PER2-immunoreactive cells in the NAcsh of each individual rat (black diamonds) across 48 *zeitgeber* times. White and grey backgrounds indicate lights on and off, respectively. R^2 = Goodness of fit value for sine wave. $n=74$

$p < .05$). Although PER2 is expressed in the NAcsh, suggesting the presence of a circadian clock, the extremely low amplitude of 4.33 and an R^2 of .006 does not meet the criteria for rhythmicity outlined earlier, and so it was determined that this region is not rhythmic under normal lighting conditions.

In summary, PER2 expression patterns in the four sub-regions of the dorsal striatum are similar to one another, with identical peak PER2 times and comparable amplitudes. Notably, none of the rhythms in these regions are in anti-phase with the rhythm of the SCN. Moreover, the dorsal and ventral striatum differ slightly in phase (Fig. 24A) as well as differ greatly in amplitude levels (SCN included: $F_{(6,554)}=144$, $p < .0001$, Fig. 24B). Specifically, the amplitude in the NAcc is higher than in all other striatal regions (ASd: $t_{(558)}=7.84$, $p < .001$, ASm: $t_{(558)}=7.57$, $p < .001$, PSd: $t_{(558)}=9.58$, $p < .001$, PSm: $t_{(558)}=7.56$, $p < .001$, NAcsh: $t_{(558)}=13.1$, $p < .001$), whereas the amplitude in the NAcsh is lower than in all other striatal regions (ASd: $t_{(558)}=5.65$, $p < .001$, ASm: $t_{(558)}=5.84$, $p < .001$, PSd: $t_{(558)}=3.91$, $p < .01$, PSm: $t_{(558)}=5.85$, $p < .001$). Furthermore, the PER2 amplitude in the SCN is significantly higher than in all the striatal sub-regions. However, when the RI values are compared, all regions of the striatum, except for the NAcsh, show strong rhythms with values ranging from .62 to .84 (Fig. 24C). The NAcsh shell, which we determined to be arrhythmic, has an RI value of .06 relative to the SCN.

Correlations of PER2 expression across the 24-hr day between the five rhythmic regions of the striatum and the SCN reveal statistically significant moderate to high relationships between these regions (see Table 4). Notably, the SCN is moderately negatively correlated with all sub-regions of the striatum, while the sub-regions of the

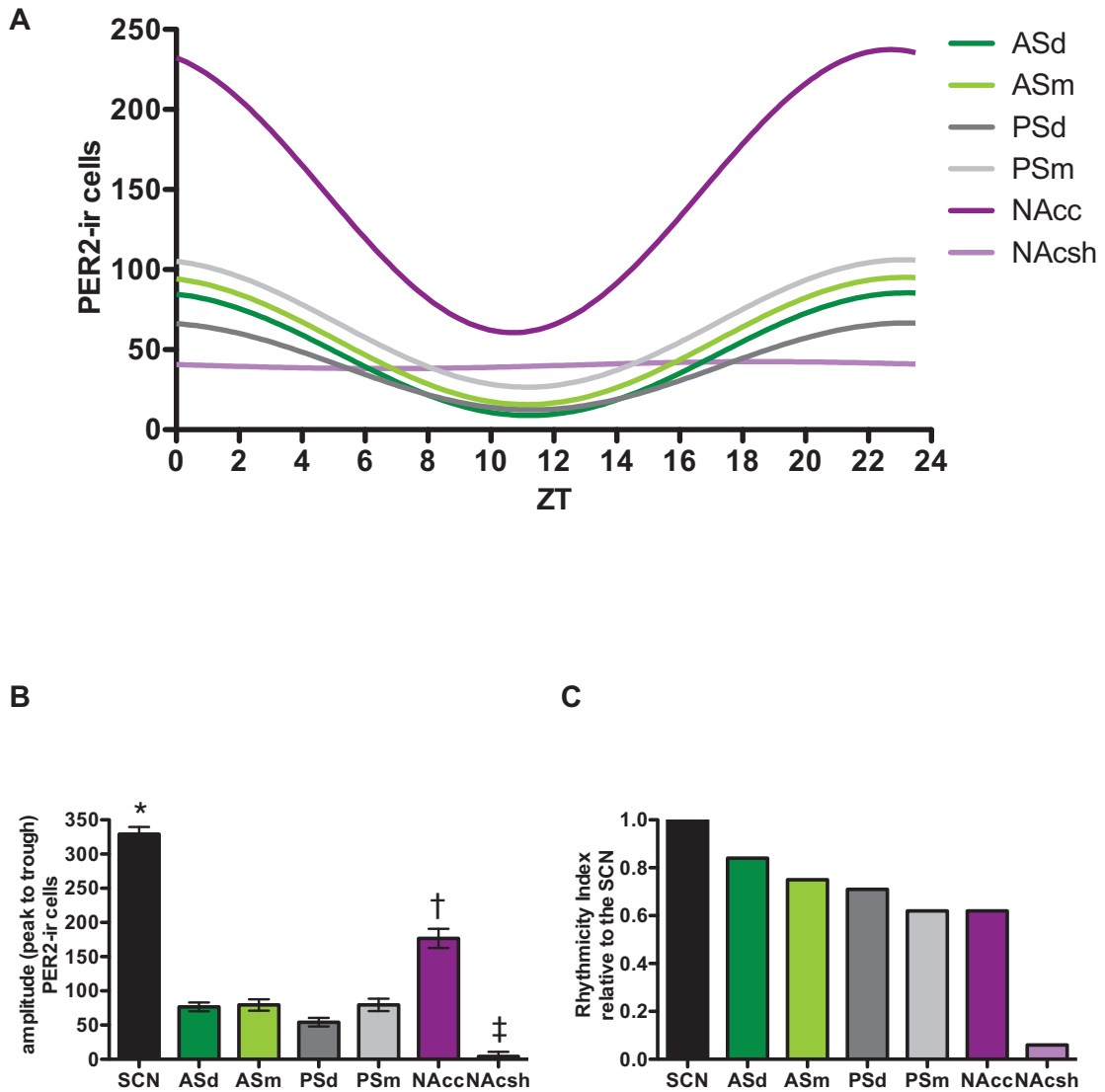


Figure 24. Striatum. A) Sine-fitted PER2 expression patterns in all 6 regions of the striatum across 48 *zeitgeber* times. B) Amplitudes (mean number \pm SEM of PER2 immunoreactive cells) measured from peak to trough, in each region of the striatum, compared to the SCN. Symbols indicate statistical significance ($p < .01$) as follows: *: SCN compared to all other regions, †: NAcc compared to all other regions, ‡: NAcsh compared to all other regions. C) Rhythmicity index values for the 6 regions of the striatum normalized to the SCN.

striatum are highly correlated with each other, with Pearson r values ranging from .70 to .91.

Table 4. Correlations of PER2 expression in the striatum. Pearson r values comparing regions of the striatum and the master SCN clock across the 24-hr day. The NAcsh has been omitted since it is arrhythmic. Values in bold are statistically significant ($p < .05$).

Region	ASd	ASm	PSd	PSm	NAcc
SCN	-0.52	-0.47	-0.44	-0.45	-0.41
ASd		0.91	0.83	0.83	0.84
ASm			0.81	0.88	0.82
PSd				0.89	0.70
PSm					0.76

Cortex

Endopiriform cortex, dorsal

As shown in Fig. 25, the EPd showed a clear rhythmic pattern of PER2 expression ($R^2 = .76$). No meaningful differences were found between the 24-hr and <28-hr model (Evidence Ratio of 1.17), however, the 24-hr model failed the Runs Test ($p = .05$) (see Fig. A5), indicating that it does not fit the data perfectly. We found that the EPd has an amplitude of 76.22 and peak PER2 expression occurs at approximately ZT21.

Piriform cortex, pyramidal layer II

The PIR2 showed a rhythmic pattern of PER2 expression ($R^2 = .736$) with a low amplitude of 28.06 (Fig. 26). The <28-hr model could not be fitted to the data for this

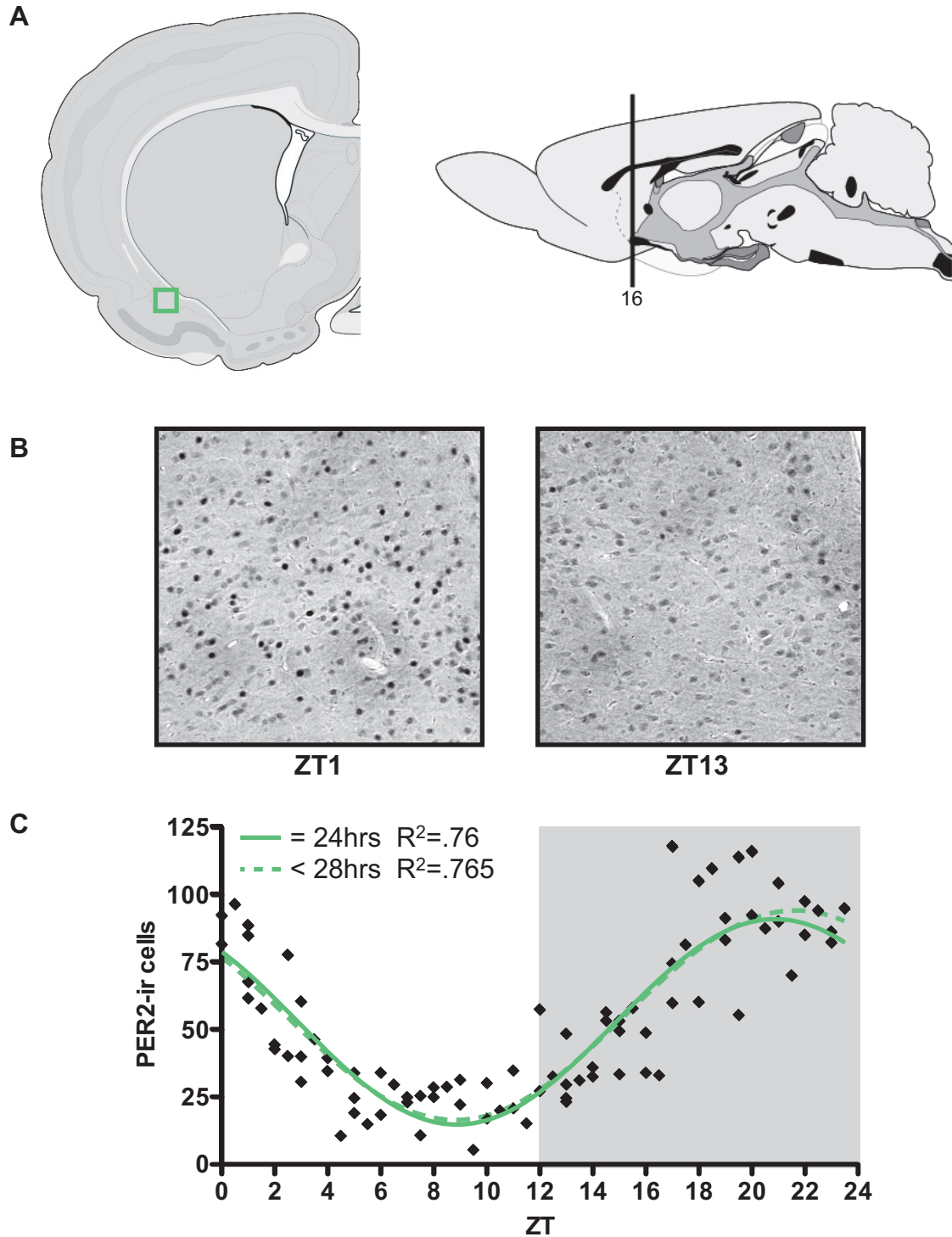


Figure 25. Endopiriform cortex, dorsal (EPd). A) Schematic diagrams of the EPd, coronal view (left) and sagittal view (right), number corresponds to level in the Swanson atlas. B) Representative photomicrographs (square in A) of PER2 expression at ZT1 and ZT13. C) Mean number of PER2-immunoreactive cells in the EPd of each individual rat (black diamonds) across 48 *zeitgeber* times. White and grey backgrounds indicate lights on and off, respectively. R^2 = Goodness of fit value for given sine wave. $n= 84$

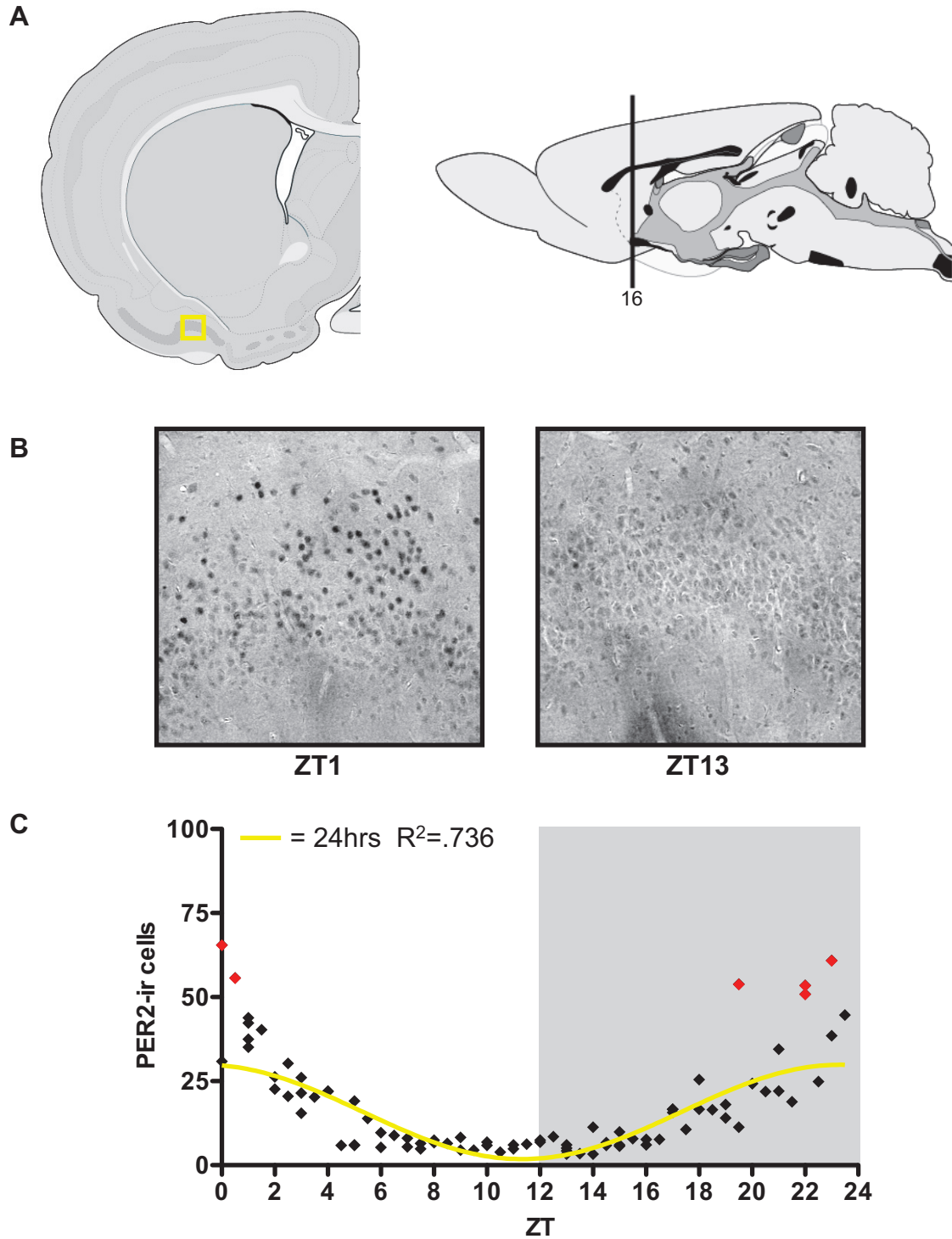


Figure 26. Piriform cortex, pyramidal layer (PIR2). A) Schematic diagrams of the PIR2, coronal (left) and sagittal view (right), number corresponds to level in the Swanson atlas. B) Representative photomicrographs (square in A) of PER2 expression at ZT1 and ZT13. C) Mean number of PER2-immunoreactive cells in the PIR2 of each individual rat (diamonds) across 48 *zeitgeber* times. White and grey backgrounds indicate lights on and off, respectively. R^2 = Goodness of fit value for sine wave. $n=78$ (6 outliers removed, red diamonds)

region (Prism labeled the curves as ‘ambiguous’), thus the 24-hr model was used (Fig. 26C). However, the Runs Test indicates that the 24-hr model does not fit the data perfectly ($p < .001$, see Fig. A6). We found that peak PER2 expression in the PIR2 occurs at approximately ZT23.5, 2.5-hrs later than in the EPd.

Anterior cingulate area, ventral

We found that the ACAv exhibits a rhythmic pattern of PER2 expression ($R^2 = .427$) with an amplitude of 83.84 (Fig. 27). According to the AIC computation and an Evidence Ratio of 146.43, the <28-hr model best fit the data for this region (Fig. 27C). Interestingly, the <28-hr model reached the upper limit of the frequency constraint for the ACAv, indicating that the curve fit the data with a period of 28-hrs. Peak PER2 expression in this region occurs at approximately ZT17.

Agranular insular cortex, posterior

The AIp also shows a rhythmic pattern of PER2 expression ($R^2 = .74$) across the 24-hr day (Fig. 28). Although the AIC computation suggests that the <28-hr best fit the data for this region, an Evidence Ratio of 4.08 indicates that the difference between the two models is insignificant (Fig. 28C). We found that the AIp has an amplitude of 116.74 and peak PER2 expression occurs at approximately ZT21.

Entorhinal cortex, lateral, superficial (I-III) and deep (IV-VI) layers

The superficial and deep layers of the ENTl show similar patterns of PER2 expression across the 24-hr day (Fig. 29 & 30, respectively). However, the deep layers

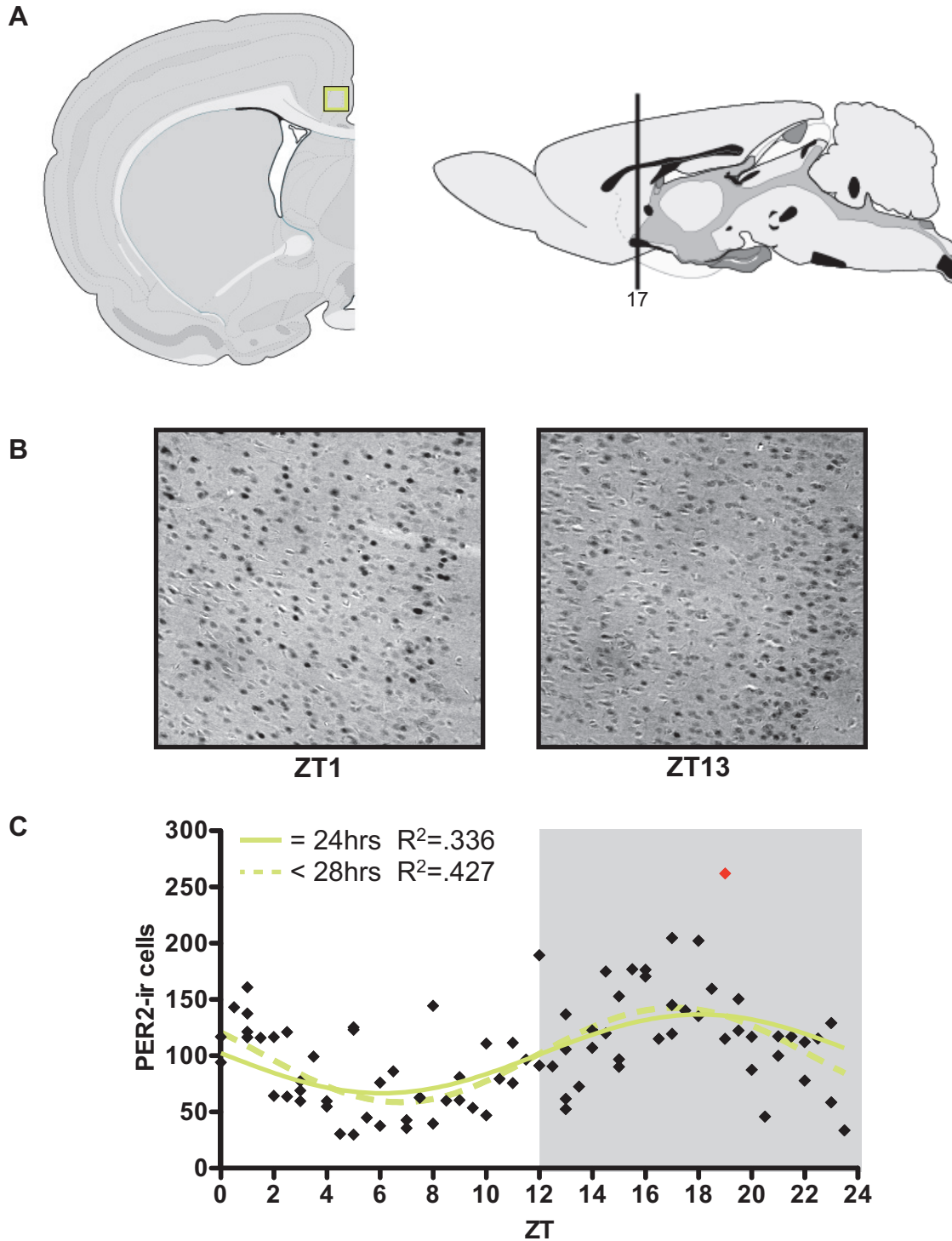


Figure 27. Anterior Cingulate Area, ventral (ACAv). A) Schematic diagrams of the ACAv, coronal view (left) and sagittal view (right), number corresponds to level in the Swanson atlas. B) Representative photomicrographs (square in A) of PER2 expression at ZT1 and ZT13. C) Mean number of PER2-immunoreactive cells in the ACAv of each individual rat (black diamonds) across 48 *zeitgeber* times. White and grey backgrounds indicate lights on and off, respectively. R^2 = Goodness of fit value for given sine wave. $n = 83$ (1 outlier removed, red diamond)

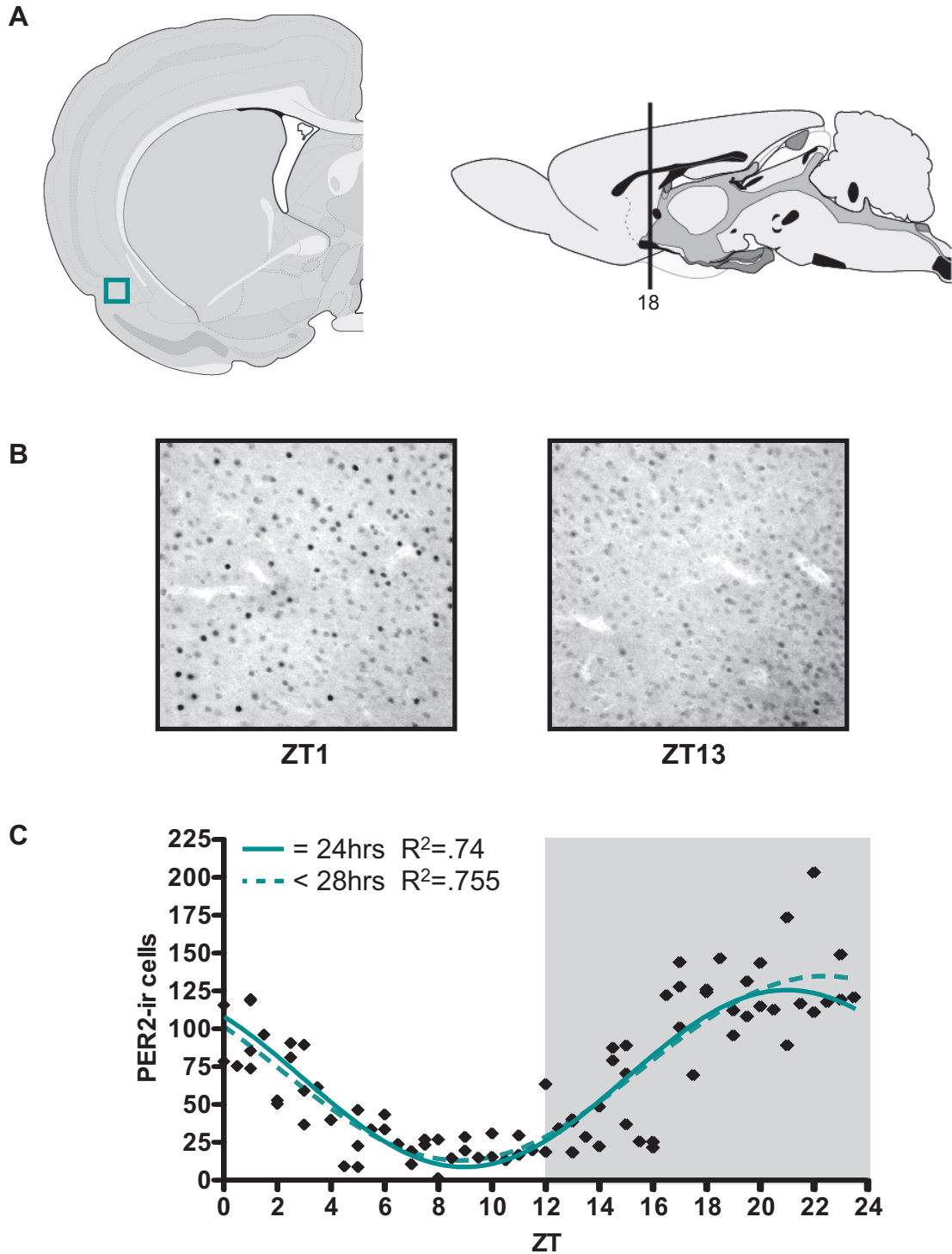


Figure 28. Agranular Insular cortex, posterior (AIP). A) Schematic diagrams of the AIP, coronal view (left) and sagittal view (right), number corresponds to level in the Swanson atlas. B) Representative photomicrographs (square in A) of PER2 expression at ZT1 and ZT13. C) Mean number of PER2-immunoreactive cells in the AIP of each individual rat (black diamonds) across 48 *zeitgeber* times. White and grey backgrounds indicate lights on and off, respectively. R²= Goodness of fit value for given sine wave. *n*= 84

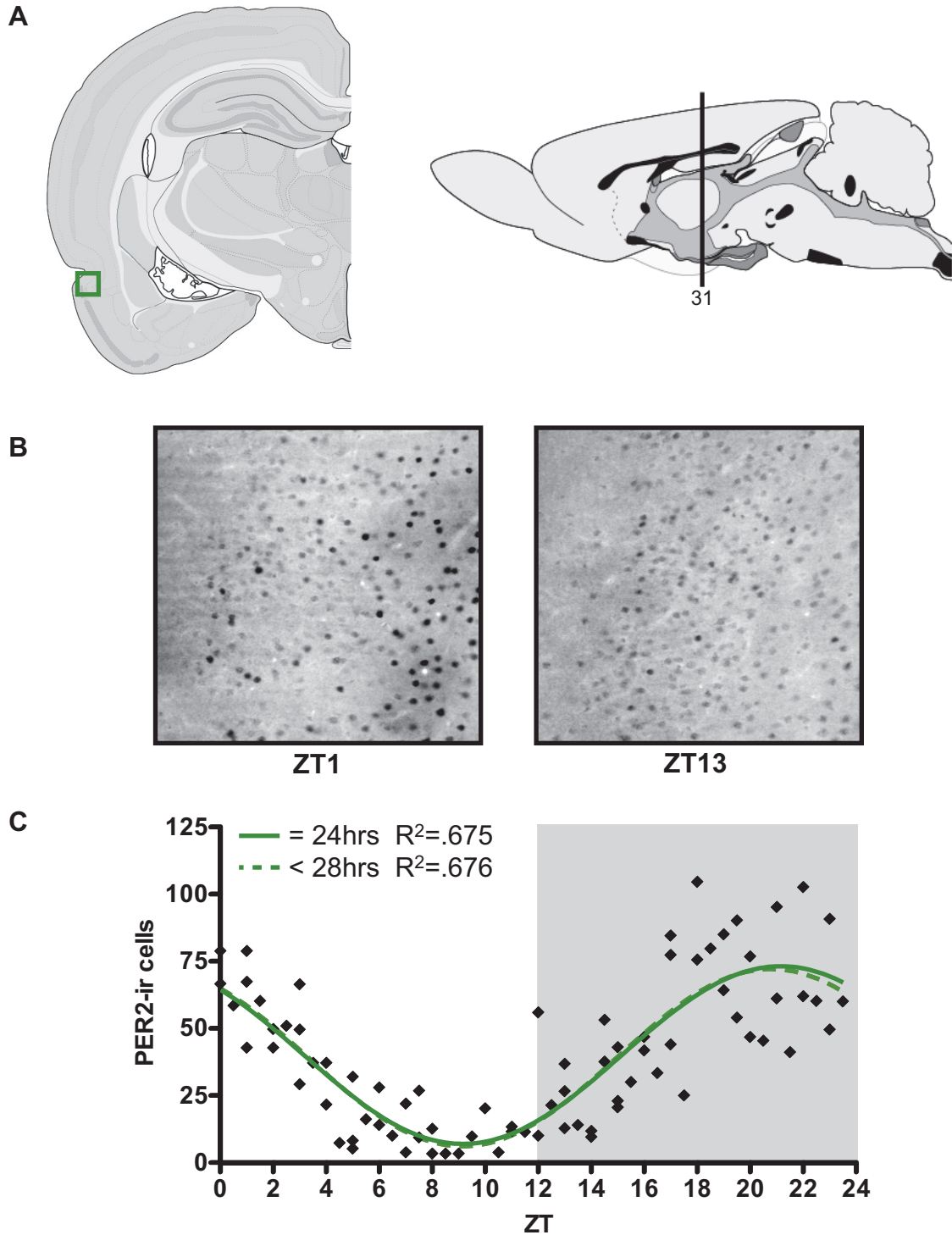


Figure 29. Entorhinal cortex, lateral, superficial layers (ENTIs). A) Schematic diagrams of the ENT1 sup, coronal view (left) and sagittal view (right), number corresponds to level in the Swanson atlas. B) Representative photomicrographs (square in A) of PER2 expression at ZT1 and ZT13. C) Mean number of PER2-immunoreactive cells in the ENT1 sup of each individual rat (black diamonds) across 48 *zeitgeber* times. White and grey backgrounds indicate lights on and off, respectively. R²= Goodness of fit value for given sine wave. *n*= 79

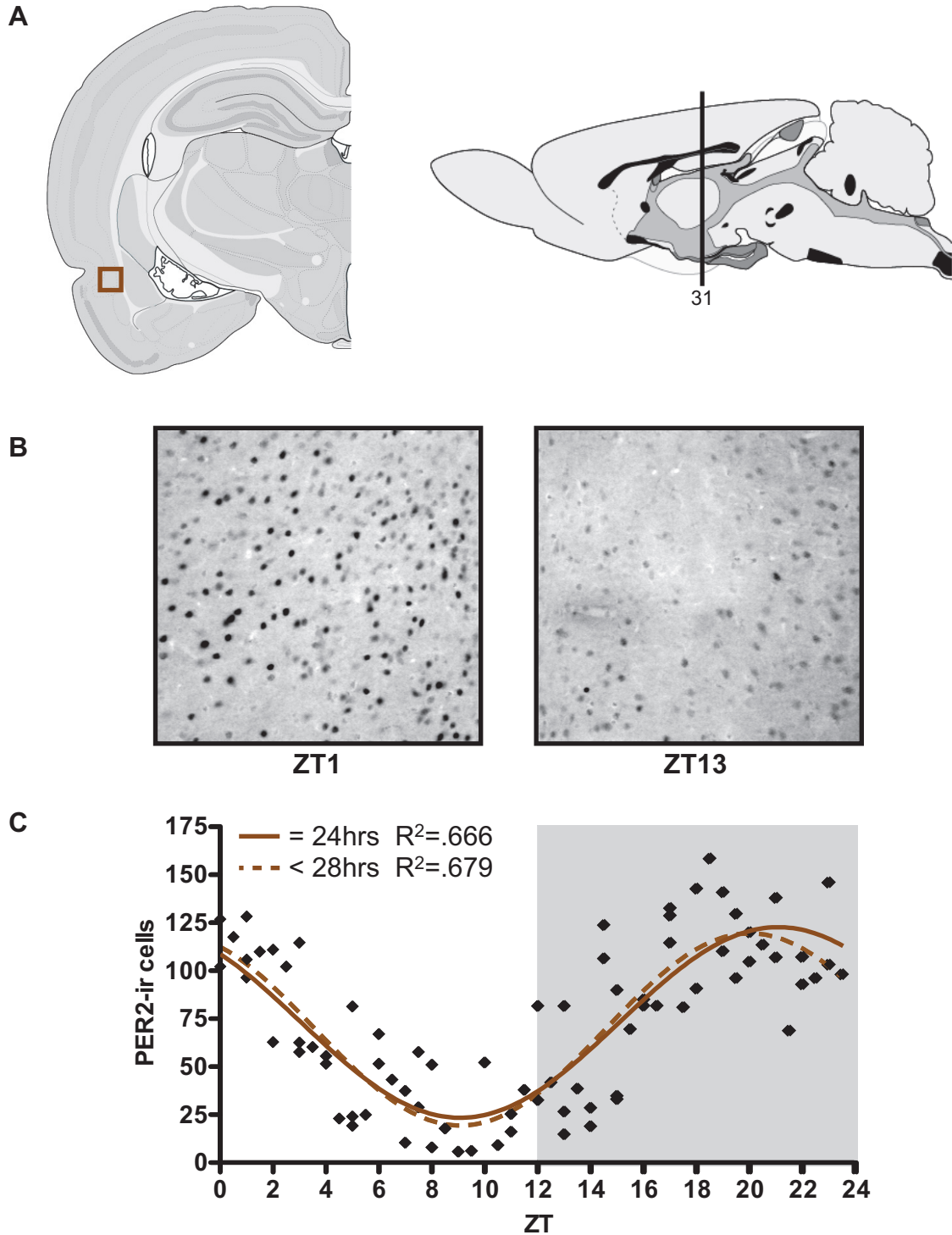


Figure 30. Entorhinal cortex, lateral, deep layers (ENTId). A) Schematic diagrams of the ENTId deep, coronal view (left) and sagittal view (right), number corresponds to level in the Swanson atlas. B) Representative photomicrographs (square in A) of PER2 expression at ZT1 and ZT13. C) Mean number of PER2-immunoreactive cells in the ENTId deep of each individual rat (black diamonds) across 48 *zeitgeber* times. White and grey backgrounds indicate lights on and off, respectively. R^2 = Goodness of fit value for given sine wave. $n= 79$

have a higher amplitude (99.2 vs. 66.14, non-significant difference) and higher overall levels of PER2 compared to the superficial layers. No meaningful differences were found between the 24-hr and <28-hr models for the ENTIs (Evidence Ratio of 2.71), as can be seen by the visual representation of the sine waves and the almost identical R^2 values of .675 and .676, respectively (Fig. 29C). Peak PER2 expression in this region occurs at approximately ZT21.5. These data originate solely from layers II and III of the ENTl, as there were no detectable PER2 labeled cells in layer I (see Fig. 29B).

According to the AIC computation, the <28-hr model best fit the data for the ENTld but an Evidence Ratio of 1.51 indicates that this difference is insignificant (Fig. 30C). Peak PER2 expression in this region of the ENTl occurs at approximately ZT21, in phase with two other regions of the cortex, the AIp and EPd.

In summary, certain sub-regions of the cortex mentioned above differ in phase. Specifically, PER2 expression in the ENTIs peaks half an hour later than in the ENTld, EPd, and AIP (which are in phase), expression in the PIR2 peaks almost 3-hrs later, and the rhythm of PER2 expression in the ACAv peaks 4-hrs earlier than in the ENTld/EPd/AIp cluster (Fig. 31A). Once again, none of the rhythms in these regions are in phase (or anti-phase) with the rhythm in the SCN.

Most of the cortical regions differ in amplitude levels (SCN included: $F_{(6,561)}=164.5, p<.0001$). Specifically, the amplitude in the PIR2 is significantly lower than in all other cortical regions (EPd: $t_{(565)}=4.43, p<.001$, ACAv: $t_{(565)}=5.12, p<.001$, AIp: $t_{(565)}=8.12, p<.001$, ENTIs: $t_{(565)}=3.45, p<.05$, ENTld: $t_{(565)}=6.45, p<.001$), and the amplitude in the AIp is higher than in the EPd ($t_{(565)}=3.8, p<.01$), ACAv ($t_{(565)}=3.07,$

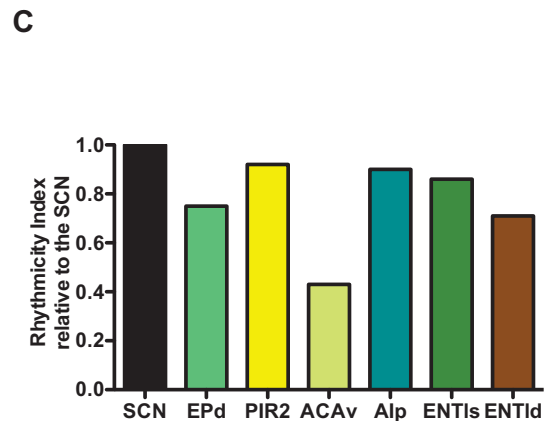
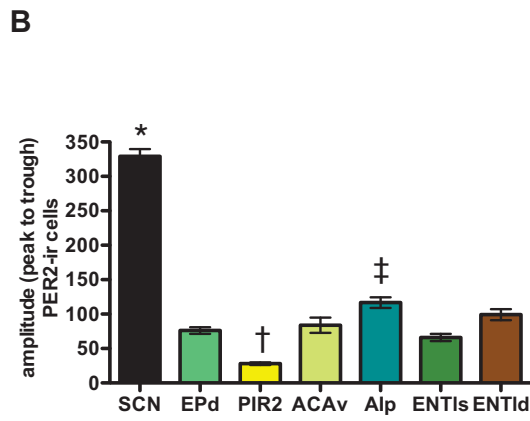
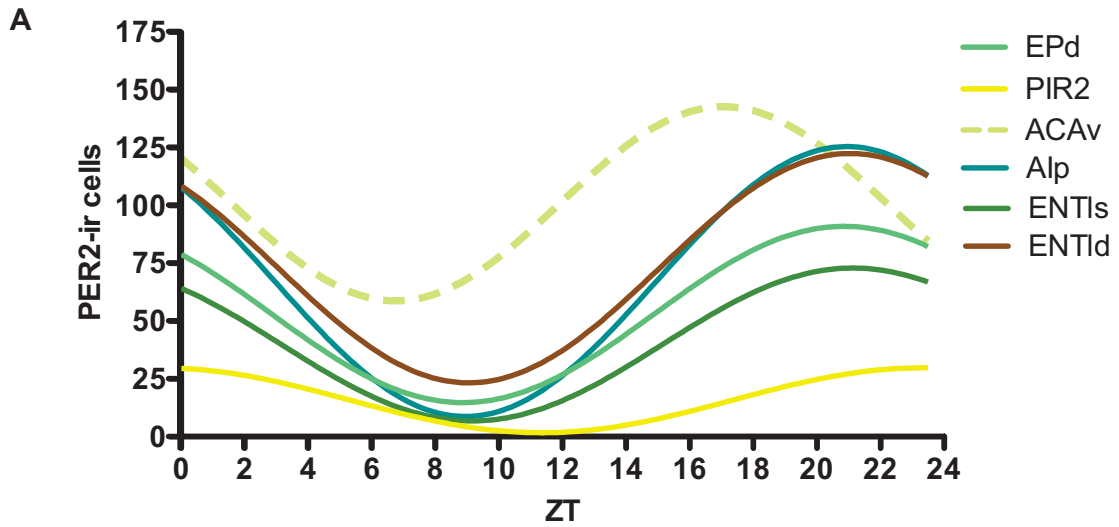


Figure 31. Cortex. A) Sine-fitted PER2 expression patterns in all 6 regions of the cortex across 48 *zeitgeber* times. Solid line: 24-hr fit, dotted line: <28-hr fit. B) Amplitudes (mean number \pm SEM of PER2 immunoreactive cells) measured from peak to trough, in each region of the cortex, compared to the SCN. Symbols indicate statistical significance ($p < .05$) as follows: *: SCN compared to all other regions, †: PIR2 compared to all other regions, ‡: Alp compared to EPd, ACAv, and ENTIs. C) Rhythmicity index values for the 6 regions of the cortex normalized to the SCN.

$p < .05$), and ENTls ($t_{(565)} = 4.67$, $p < .001$) (Fig. 31B). Finally, the amplitude in the SCN is significantly higher than in all the cortical regions. However, when RI values for these regions are normalized to the SCN, it becomes evident that most of the sub-regions of the cortex show strong rhythms (Fig. 31C). Specifically, the EPd has a rhythm that is 75% as rhythmic as the SCN, while surprisingly, the cortical region with the lowest amplitude, the PIR2, has a very strong rhythm comparable to that of the SCN (RI value of .92). The ACAv has the weakest rhythm out of the cortical regions with a rhythm that is just under half as rhythmic as that of the SCN (RI value of .43), while the AIp is 90% as rhythmic as the SCN. Finally, the two regions of the ENTl cortex show differences in rhythmicity levels with the ENTls having a slightly stronger rhythm than the ENTld (RI values of .86 and .70, respectively).

Correlations of PER2 expression across the 24-hr day between the six regions of the cortex and the SCN reveal differences in the strength of the relationships between these regions (see Table 5). Notably, the SCN is only significantly correlated with two sub-regions of the cortex, the ACAv (.42) and PIR2 (-.56). Not surprisingly, the three regions that are in perfect phase, the EPd, AIp, and ENTld, are all highly correlated with each other, with Pearson r values ranging from .84 to .86.

Table 5. Correlations of PER2 expression in the cortex. Pearson r values comparing regions of the cortex and the master SCN clock across the 24-hr day. Values in bold are statistically significant ($p < .05$).

Region	ACA _v	AI _p	EP _d	PIR ₂	ENT _{ls}	ENT _{ld}
SCN	0.42	-0.11	-0.07	-0.56	-0.07	-0.06
ACA _v		0.37	0.45	0.11	0.47	0.53

Region	ACAv	AIp	EPd	PIR2	ENTIs	ENTId
AIp			0.86	0.67	0.88	0.84
EPd				0.67	0.86	0.84
PIR2					0.68	0.64
ENTIs						0.91

Summary of results

It is clear that the previous notion of simply two phase patterns in PER2 expression (i.e. peaking at either the beginning of the dark or light portion of the cycle) is not supported by the present findings. The high temporal resolution analysis used in this thesis revealed complex patterns of PER2 expression between brain regions (Fig. 32A). In addition, two arrhythmic regions were also identified: the MEApd and NAcsh. Except for the BNSTov and CEAl, PER2 expression in all regions peaked during the dark phase (between ZT12-ZT24). Regions can be grouped into four “clusters” based on time of peak PER2 expression, with a cluster being defined as multiple regions peaking within 30 min of each other: the BNSTov and CEAl form the only cluster peaking during the light phase at ZT11, four regions of the cortex (the AIp, EPd, ENTl deep and superficial) and the CA3 of the hippocampus form a cluster around ZT21-ZT21.5, the BLA and NAc core form a cluster at ZT22.5, and the four sub-regions of the dorsal striatum along with the DG, CA3, and PIR2 form a final cluster at ZT23.5. The rhythms of PER2 expression in the SCN and ACAv stand on their own, peaking several hours apart from all other regions (Fig. 32B).

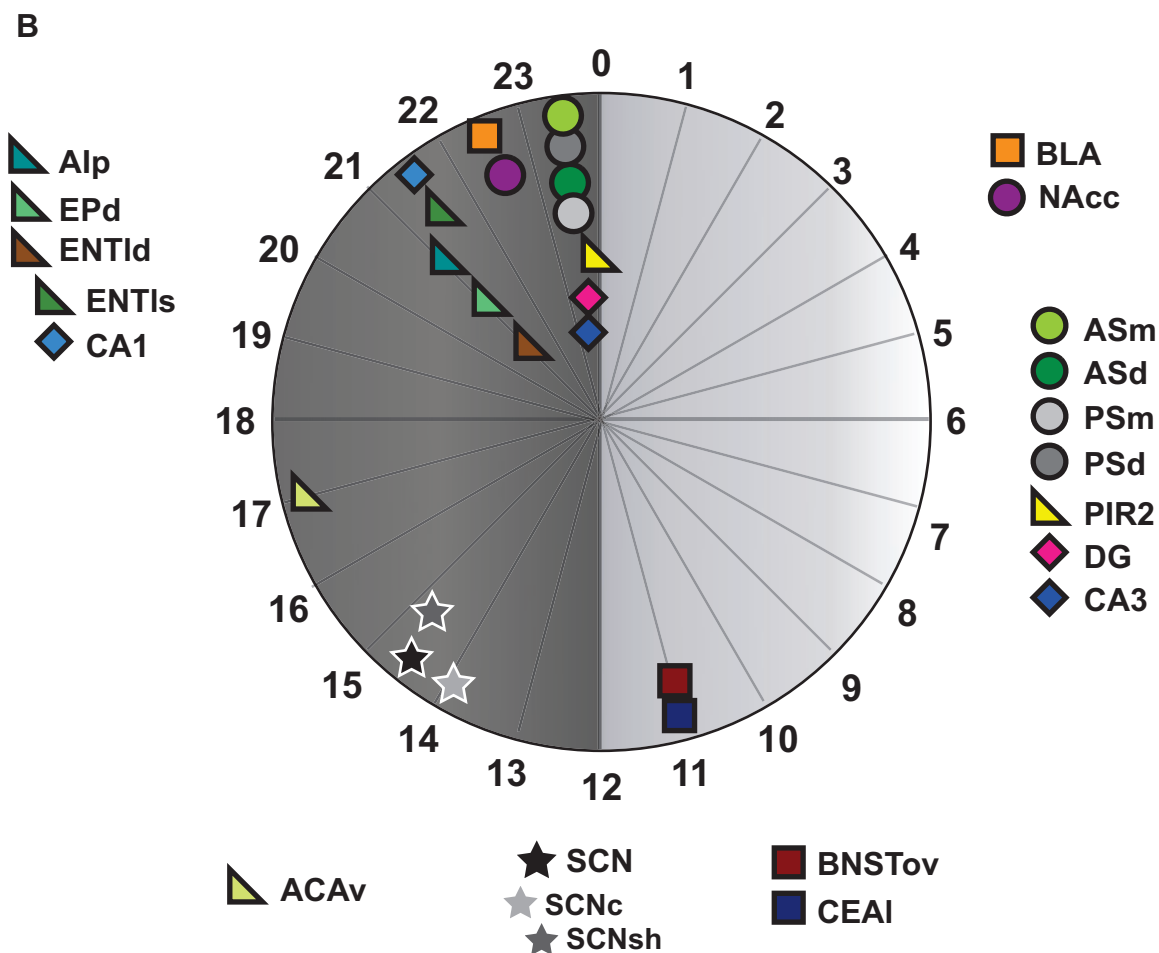
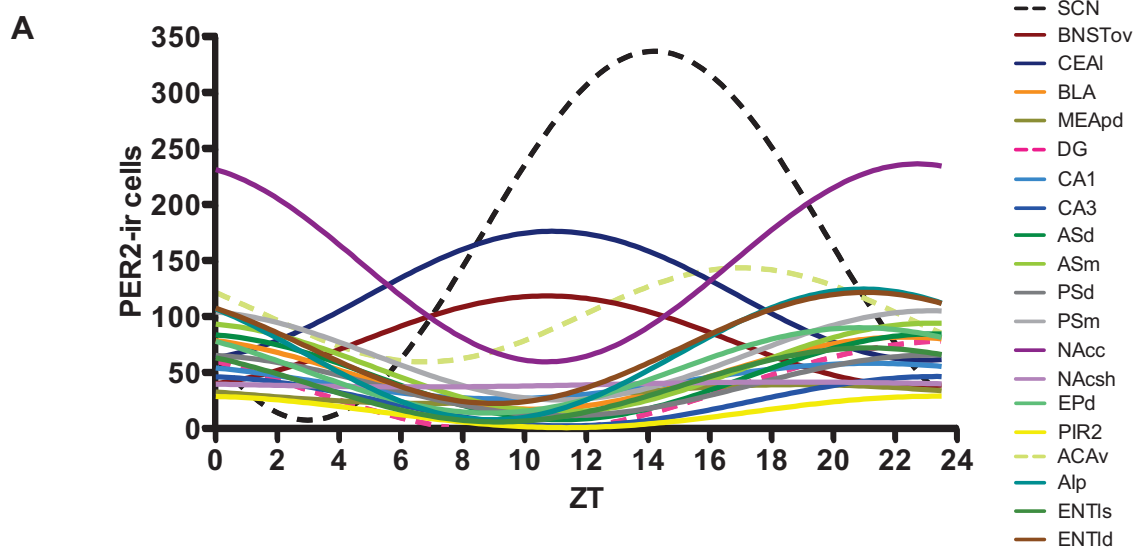


Figure 32. Summary: Comparing phase between all regions. A) Sine-fitted PER2 expression patterns in all 22 regions analyzed across 48 *zeitgeber* times. B) 24-hr circular diagram

Fi

displaying peak PER2 expression in all 20 rhythmic regions. Numbers around the 'clock' are in ZT time. ☆: SCN, □: amygdala, ◇: hippocampus, ○: striatum, ▲: cortex.

While the SCN undoubtedly has the highest amplitude (Fig. 33A), the RI revealed that most of the regions analyzed have strong PER2 rhythms regardless of having low absolute amplitude levels (Fig. 33B). Moreover, it was found that the CA1 of the hippocampus has the weakest rhythm among the rhythmic regions while the DG of the hippocampus has the strongest rhythm, relative to the SCN.

In conclusion, we found that 20/22 brain regions analyzed display rhythms in PER2 expression, with a clustered distribution of phases mostly during the night period, and surprisingly, with none of the rhythms in any regions being in phase with the SCN.

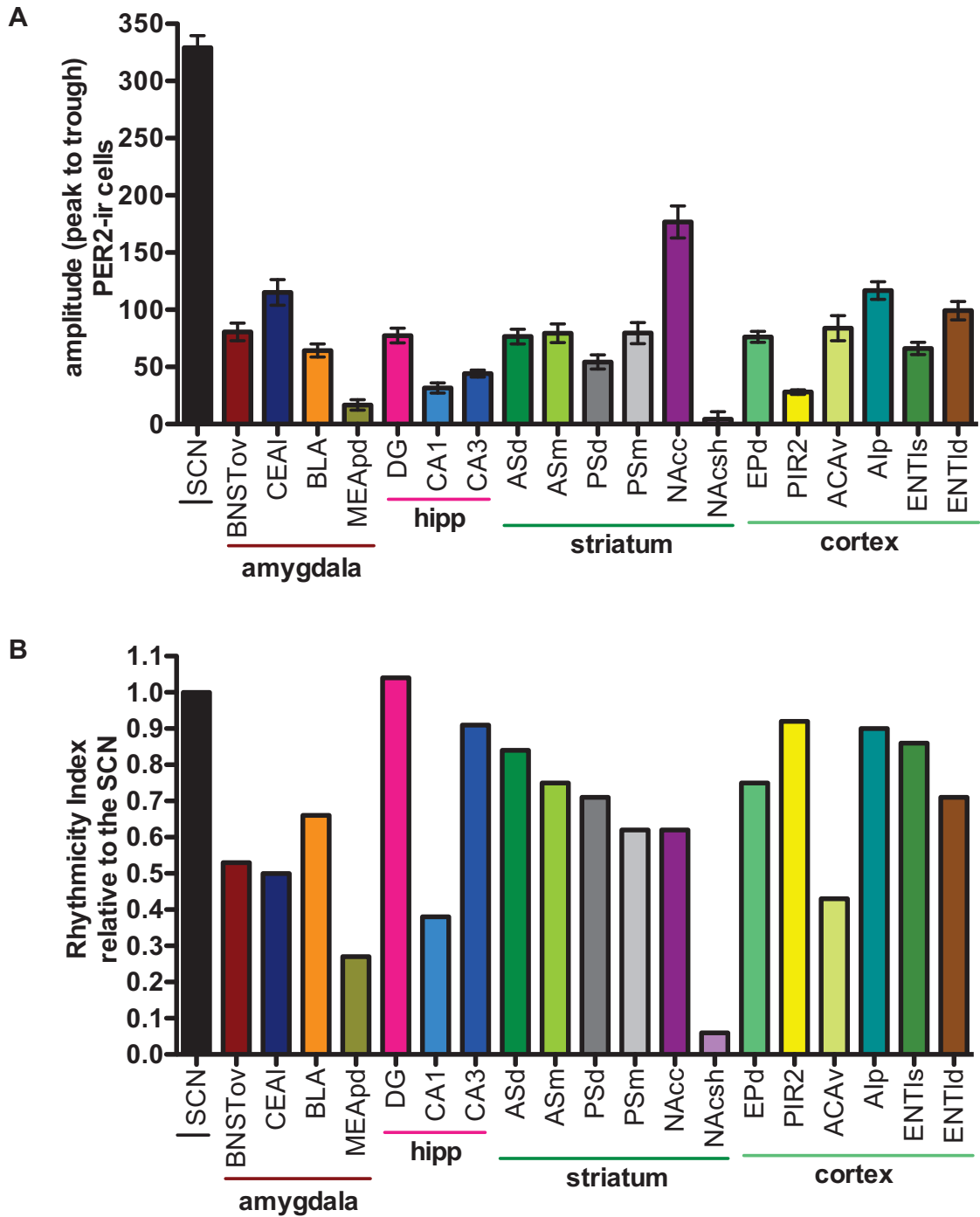


Figure 33. Summary: Comparing amplitude and strength of rhythms between all regions. A) Amplitudes (mean number \pm SEM of PER2 immunoreactive cells) measured from peak to trough, in all brain regions. B) Rhythmicity Index for each brain region normalized to the SCN.

CHAPTER 2: *Period2*, *Bmal1*, and *Dbp* mRNA

METHODS

Subjects from this experiment were the same as those used in Chapter 1, therefore, animal housing and tissue preparation are the same as described previously.

Procedure

Brains sections from 74 of the 84 rats were used for the quantitative real-time polymerase chain reaction (qRT-PCR) analysis. Messenger RNA (mRNA) expression of two core clock genes (*Per2*, *Bmal1*) and one clock-controlled gene (*Dbp*) were compared between three brain regions: the SCN, CEAL, and DG. *Per2* and *Bmal1* were chosen so that a clock gene from both the negative and positive arms of the molecular loop could be examined, while *Dbp* was chosen as it provides information about rhythms driven by the clock, while not being part of the core molecular loop. The CEAL and DG were selected because of their antiphase PER2 expression patterns.

RNA extraction

Free-floating sections from the 2nd set of brain slices were rinsed (6 x 5 min) in cold TBS to remove the Watson's Cryoprotectant solution. The three regions of interest (the SCN, CEAL, and DG) were bilaterally dissected from the relevant 50µm thick sections under a dissecting microscope using sterile plastic Petri dishes (filled with cold TBS) and a scalpel. All instruments were pre-cleaned with RNaseZap solution (#AM9780, Ambion) to neutralize RNase, and a new Petri dish, scalpel blade, and gloves were used for each individual brain to avoid contamination. Total RNA was isolated from

each of the regions using the RecoverAll™ Total Nucleic Acid Isolation kit (#AM1975, Ambion) following modified manufacturer's instructions. Briefly, the dissected tissues were dehydrated with two washes in 100% ethanol. The pellet was then air dried at room temperature for 30 min then re-suspended in 150µl of digestion buffer with 4µl protease and incubated at 50°C for 15 min and then 80°C for 30 min. RNA was isolated by capture on a glass-fiber filter and purified from residual cellular fragments and proteins by subsequent 100% ethanol and isolation additive washes and centrifugation steps (10,000g for 30 sec). Then, 60µl of DNase mix was added to the filter and incubated at room temperature for 30 min and washed out with a series of ethanol washes and centrifugation steps (10,000g for 30-60 sec) in order to purify the RNA from DNA residuals. Finally, the purified RNA was eluted in 60 µl of elution solution at room temperature for 1 min and centrifuged at 10,000g for 1 min. Three µl from each sample were taken for RNA quantification and the rest was frozen at -80°C.

The RNA integrity profile (RIN) of each sample and its concentration was assessed using the Experion RNA StdSens Analysis kit (Bio-Rad, Hercules, CA). The Nanodrop2100c spectrophotometer (Thermo Fisher Scientific, Wilmington, DE) was used to measure the absorbance ratios at 260/280nm and 260/230nm to assess DNA and protein contamination, respectively.

RNA purification

If the absorbance ratio at 260/280nm was below 1.7, indicating probable DNA contamination, RNA samples were treated with the TURBO DNA-free kit (#AM1907, Ambion) following manufacturer's instructions. The RNA samples were then re-frozen at -80C until reverse-transcribed.

cDNA reverse transcription

Total RNA ($\leq 1\mu\text{g}$) from each brain region of each rat was reverse transcribed to single stranded cDNA using the High-Capacity cDNA Reverse Transcription kit with RNase inhibitor (#4374966, Applied Biosystems, Foster City, CA) according to manufacturer's instructions. Briefly, the reaction was carried out in a $40\mu\text{l}$ volume, consisting of $20\mu\text{l}$ of RNA and $20\mu\text{l}$ of 2XRT master mix containing $4\mu\text{l}$ reverse transcription (RT) buffer, $1.6\mu\text{l}$ of 100mM deoxyribonucleotide triphosphate (dNTP) mixture, $4\mu\text{l}$ of 10X random primers, $2\mu\text{l}$ of MultiScribe™ RT enzyme (50U/ μl), and $2\mu\text{l}$ of RNase inhibitor. For each brain region, two negative controls were also included: one without the reverse transcriptase enzyme (No Reverse Transcriptase, NRT) to control for any potential genomic DNA contamination, and one without any RNA to assess purity of reagents. Reverse transcription was carried out on the $40\mu\text{l}$ samples using the CFX96 Real-Time PCR C-1000™ Thermo Cycler (Bio-Rad) with the following reaction conditions: 10 min at 25°C , 120 min at 37°C , and 5 min at 85°C (enzyme inactivation and denaturation). Once reverse-transcription was complete, samples were stored at -20°C .

Quantitative Real-Time PCR

For each of the brain structures, mRNA levels for the three target genes (*Per2*, *Bmal1*, and *Dbp*) were determined using qRT-PCR with custom-designed PerfectProbe Gene Detection kits (PrimerDesign, Southampton, UK). Primers/probe sequences and amplicon lengths of the genes of interest are listed in Table 6. The relative quantity of mRNA for each gene of interest was measured relative to four housekeeping genes

(HKGs): *B2M* (beta-2-microglobulin), *Hmbs* (hydroxymethyl-bilane synthase), *Top1* (topoisomerase (DNA) 1), and *Ywhaz* (tyrosine 3-monooxygenase/tryptophan 5-monooxygenase activation protein, zeta polypeptide), which were measured using prevalidated PerfectProbe kits (HKG sequences not available, PrimerDesign).

Housekeeping genes encode proteins that provide essential functions for cell survival, and, in theory, remain stable across different tissues and manipulations. However, it has been recognized that HKGs can vary across different conditions and cell types (Deindl, Boengler, van Royen, & Schaper, 2002; Dheda et al., 2005), and so must be pre-tested for any given study (Radonic et al., 2004). Furthermore, the use of at least three HKGs has been proposed for optimal normalization of qRT-PCR data (Vandesompele et al., 2002).

The four HK genes used in this thesis remained stable across the SCN, CEAI, and DG during pre-testing and therefore were deemed to be satisfactory internal controls. A fifth and commonly used HKG, *Gapdh* (glyceraldehyde-3-phosphate dehydrogenase), was also tested but its expression varied and so was eliminated from the study. Quantitative real-time PCR was performed on the CFX96 Real Time PCR Detection System (Bio-Rad) with the following parameters: Initialization 95°C for 30 sec, followed by 50 cycles of Denaturation 95°C for 10 sec, Annealation 50°C for 20 sec, and Extension (and data collection) 62°C for 30 sec. Amplifications were performed in 20µl volume reactions containing 5µl of cDNA (optimally 25ng), 10µl of TaqMan Fast Universal Master Mix (#4367846, Applied Biosystems), and 5µl of PerfectProbe primers/probe mix (PrimerDesign) according to manufacturer's instructions. Samples with a CT (threshold cycle) value of 35 or less were deemed usable.

Table 6. Primer/ Probe sequences and Amplicon length of target clock genes.

Target Gene	Sense Primer Sequence, 5':	Antisense Primer Sequence, 5':	Probe Sequence, 5':	Length (bp)
<i>Per2</i>	TTC CAC CAG CAA CCC CAA A 3'	CAG GAG TTA TTT CAG AGG CAA GT 3'	CTT CCC CAG CCA GCC TCA CTT TCC Ggg aag 3'	93
<i>Bmall</i> (<i>Arntl</i>)	ACC AGG GTT TGA AGT TAG AGT C 3'	AAG TCA CTG ATT GTG GAG GAA AT 3'	CCA TTC TCT GGT CCG CCA TTG GAA GGg aat gg 3'	88
<i>Dbp</i>	ACC CAC TCG CCC AGA CTA TA 3'	AGC AAG CCT CCA GTA TCA GAA 3'	CTT CAA ATC CTA CGA GCA CTG CGG GGG ttg aag 3'	125

For each sample type, a 4-fold serial dilution (100-0.39 ng) standard curve was used to determine amplification efficiency of the target genes and the working cDNA concentration, with samples run in duplicate. The qRT-PCR reactions were carried out on 96-well plates. During cDNA synthesis, a negative control (NRT) with all synthesis reagents, but without RNA, was made and run once for every brain region and gene. A no template control (NTC), with water in place of cDNA, was also run for every gene on every plate to rule out contamination. In addition, two positive controls were used in order to validate the efficiency and repetitive nature of the primer/probe assays. Specifically, a commercial brain sample (with validated high RIN quality) was run once for every brain region and gene, and two of the pooled cDNA dilutions taken for the standard curve were run across all plates. All cDNA samples were run in triplicate.

Data analysis

The $2^{-\Delta\Delta CT}$ method (Livak & Schmittgen, 2001) was applied in order to quantify the relative mRNA levels of *Per2*, *Bmall*, and *Dbp* for each rat and brain region. First,

the target gene expression levels in each rat and brain region were normalized to a combination of the ≥ 2 most stable HKGs as determined by geNorm software (<http://medgen.ugent.be/~jvdesomp/genorm>). Then, the relative values were re-normalized with respect to the highest expression value within each of the seven groups described earlier.

As in the previous chapter, 24-hr and <28-hr sine waves were fitted to each data set along with the previously mentioned tests. Correlations were also made between the expression patterns in the three clock genes in each brain region and between brain regions for the same clock gene. Alpha level was set to .05 for all analyses.

RESULTS

For the three brain regions and three genes examined, no outliers were found and all data sets passed the Runs test, indicating that the data do not deviate systematically from the fitted curves. However, compared to the PER2 protein data, the distribution of individual points for the mRNA is noisier, as can be seen by smaller R^2 values associated with the sine fitted curves. Because of this, the criteria for rhythmicity are slightly more lenient for the mRNA data to avoid falsely determining a region as being arrhythmic. For each clock gene data set, the two other regions must have an R^2 value that is at least 1/4th that of the SCN to be considered rhythmic. Since the amplitudes are already normalized, Rhythmicity Indices were not calculated for these data.

Suprachiasmatic nucleus

The SCN showed a highly rhythmic pattern in *Per2* expression with a relative amplitude of .61 (measured from peak to trough in relative mRNA levels). There were no meaningful differences between the 24-hr and <28-hr model for the *Per2* data (Evidence Ratio of 3.12). This is confirmed visually by representations of the sine waves with identical R^2 values of .496 (Fig. 34A). We found that the peak of *Per2* expression in the SCN occurs at approximately ZT9.5, which is within the time range previously reported (Bae et al., 2001; Reppert & Weaver, 2001).

Bmal1 expression in the SCN also showed a rhythmic pattern of expression, although with the lowest R^2 value out of the SCN clock genes (.297), with a relative amplitude of .37 (Fig. 34B). Here, the AIC computation indicated that the <28-hr best fit the data, however, the difference between the two models is not significant (Evidence Ratio of 4.05). Peak *Bmal1* expression in the SCN occurs at around ZT17.5.

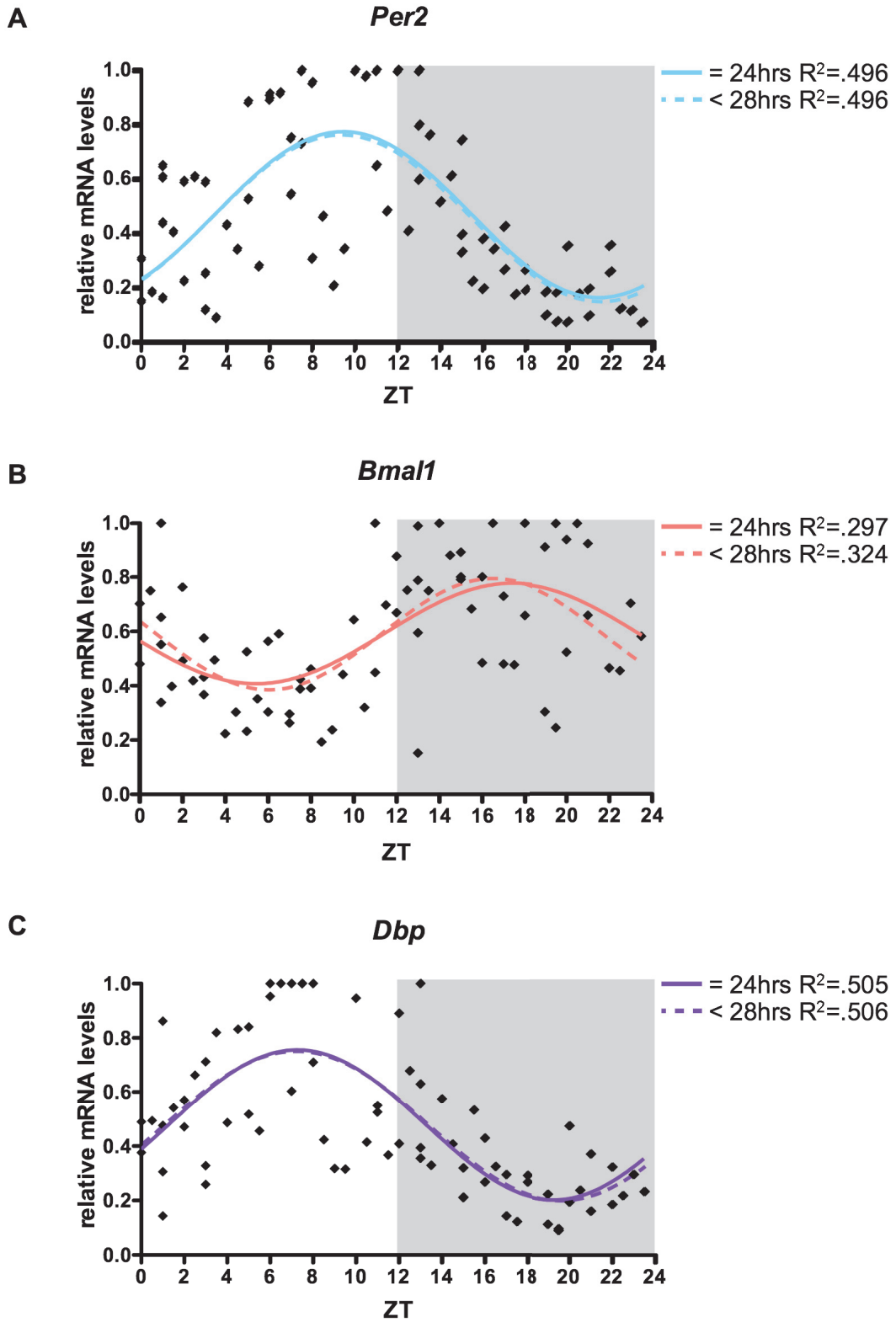


Figure 34. Suprachiasmatic Nucleus (SCN). Relative mRNA levels of A) *Per2* B) *Bmal1* and C) *Dbp* in the SCN of each individual rat (black diamonds) across 48 *zeitgeber* times. White and grey backgrounds indicate lights on and off, respectively. R^2 = Goodness of fit value for given sine wave. $n= 73$ for each graph

We found that the clock-controlled gene, *Dbp*, is highly rhythmic in the SCN with a relative amplitude of .55. There were no meaningful differences between the 24-hr and <28-hr models for the *Dbp* data (Evidence Ratio of 2.91). This is confirmed by visual representations of the sine waves along with the almost identical R^2 values of .505 and .506, respectively (Fig. 34C). Peak *Dbp* expression in the SCN occurs at around ZT7.5.

Naturally, phase differences were found between the three genes examined in the SCN (Fig. 35A). Specifically, *Per2* and *Dbp* follow similar patterns but with a 2-hr difference in time of peak expression (peaks at ZT9.5 and ZT7.5, respectively). In contrast, *Per2* and *Dbp* peak 16 and 14-hrs later, respectively, than *Bmal1* expression (ZT17.5). Correlations in the SCN between the three genes across the 24-hr day revealed a statistically significant moderate relationship between *Per2* and *Dbp* only ($r = .59$, see Table 7A).

Given the R^2 values for the three genes in the SCN, the rhythmicity criteria for the CEAl and DG (1/4th that of the SCN) are as follows: for *Per2* these regions must have an R^2 value of at least .124, for *Bmal1* an R^2 value of at least .074, and for *Dbp* an R^2 value of at least .126.

Central amygdala, lateral part

Per2 expression in the CEAl showed a low relative amplitude (.24) rhythm with peak expression at around ZT9 (Fig. 36A). There were no meaningful differences between the 24-hr and <28-hr model for the *Per2* data (Evidence Ratio 3.16), as can be seen by the visual representations of the sine waves and identical R^2 values of .153 (Fig. 36A).

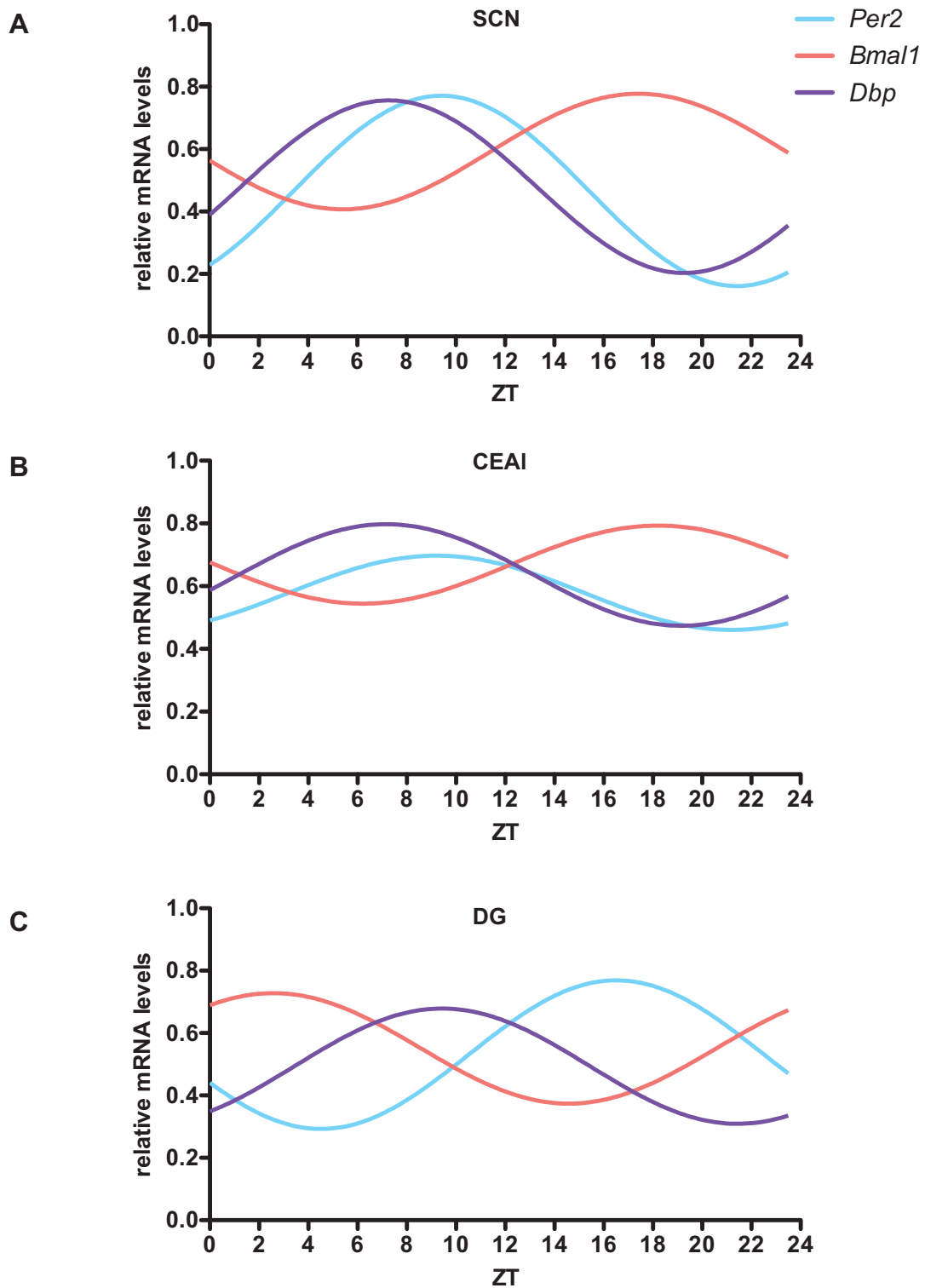


Figure 35. Summary: Comparing phase between all regions and genes. Sine fitted *Per2*, *Bmal1*, and *Dbp* expression patterns in the SCN (A), CEAI (B), and DG (C) across 48 *zeitgeber* times.

Table 7. Correlations between *Per2*, *Bmal1*, and *Dbp* expression. Pearson r values comparing clock genes in the SCN (A), CEAl (B), and DG (C) across the 24-hr day. Values in bold are statistically significant ($p < .05$).

A) SCN

clock gene	<i>Bmal1</i>	<i>Dbp</i>
<i>Per2</i>	-0.08	0.59
<i>Bmal1</i>		-0.20

B) CEAl

clock gene	<i>Bmal1</i>	<i>Dbp</i>
<i>Per2</i>	0.17	0.40
<i>Bmal1</i>		-0.19

C) DG

clock gene	<i>Bmal1</i>	<i>Dbp</i>
<i>Per2</i>	-0.20	0.20
<i>Bmal1</i>		0.13

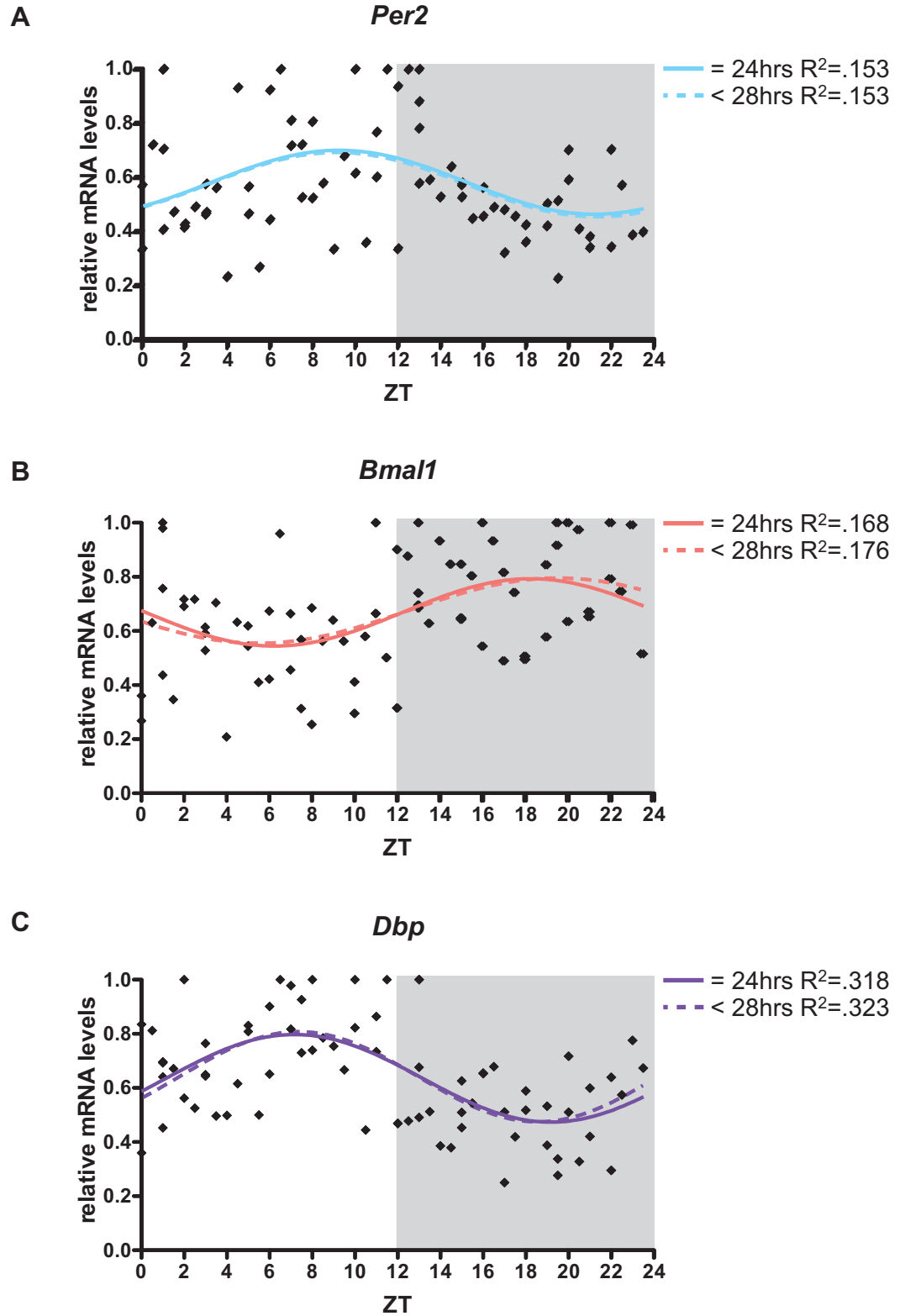


Figure 36. Central amygdala, lateral (CEAI). Relative mRNA levels of A) *Per2* B) *Bmal1* and C) *Dbp* in the CEAI of each individual rat (black diamonds) across 48 *zeitgeber* times. White and grey backgrounds indicate lights on and off, respectively. R^2 = Goodness of fit value for given sine wave. $n= 74$ for each graph

Bmal1 expression in the CEAl also showed a low relative amplitude (.25) rhythm with peak expression occurring at around ZT18 ($R^2=.168$, Fig. 36B). No meaningful differences were found between the two models for this region (Evidence Ratio of 2.15).

Dbp expression in the CEAl, on the other hand, showed a stronger rhythmic pattern (R^2 value of .318) with a relative amplitude of .32 (Fig. 36C). No meaningful differences were found between the two models for this region (Evidence Ratio of 2.38). We found that peak *Dbp* expression in the CEAl occurs at approximately ZT7.

Both *Per2* and *Bmal1* rhythms in the CEAl were weaker (lower R^2 values) than in the SCN and DG. Similar phase differences as in the SCN were found between the three genes examined in the CEAl (Fig. 35B). Specifically, *Per2* and *Dbp* follow similar patterns but, again, with a 2-hr difference in time of peak expression (ZT9 and ZT7, respectively), while these two genes follow *Bmal1* peak expression (ZT18) by 15 and 13-hrs, respectively. Correlations in the CEAl between the three genes across the 24-hr day also revealed a statistically significant moderate relationship between *Per2* and *Dbp* only ($r=.40$, see Table 7B).

Dentate gyrus

The DG showed a highly rhythmic pattern in *Per2* expression ($R^2=.408$) with a relative amplitude of .48 (Fig. 37A). No meaningful differences were found between the two models for this region (Evidence Ratio of 1.78), however, both models failed the normality test (24-hr model: $K^2=6.36$, $p<.05$), indicating that neither model fit the data perfectly. We found that peak *Per2* expression in the DG occurs at approximately

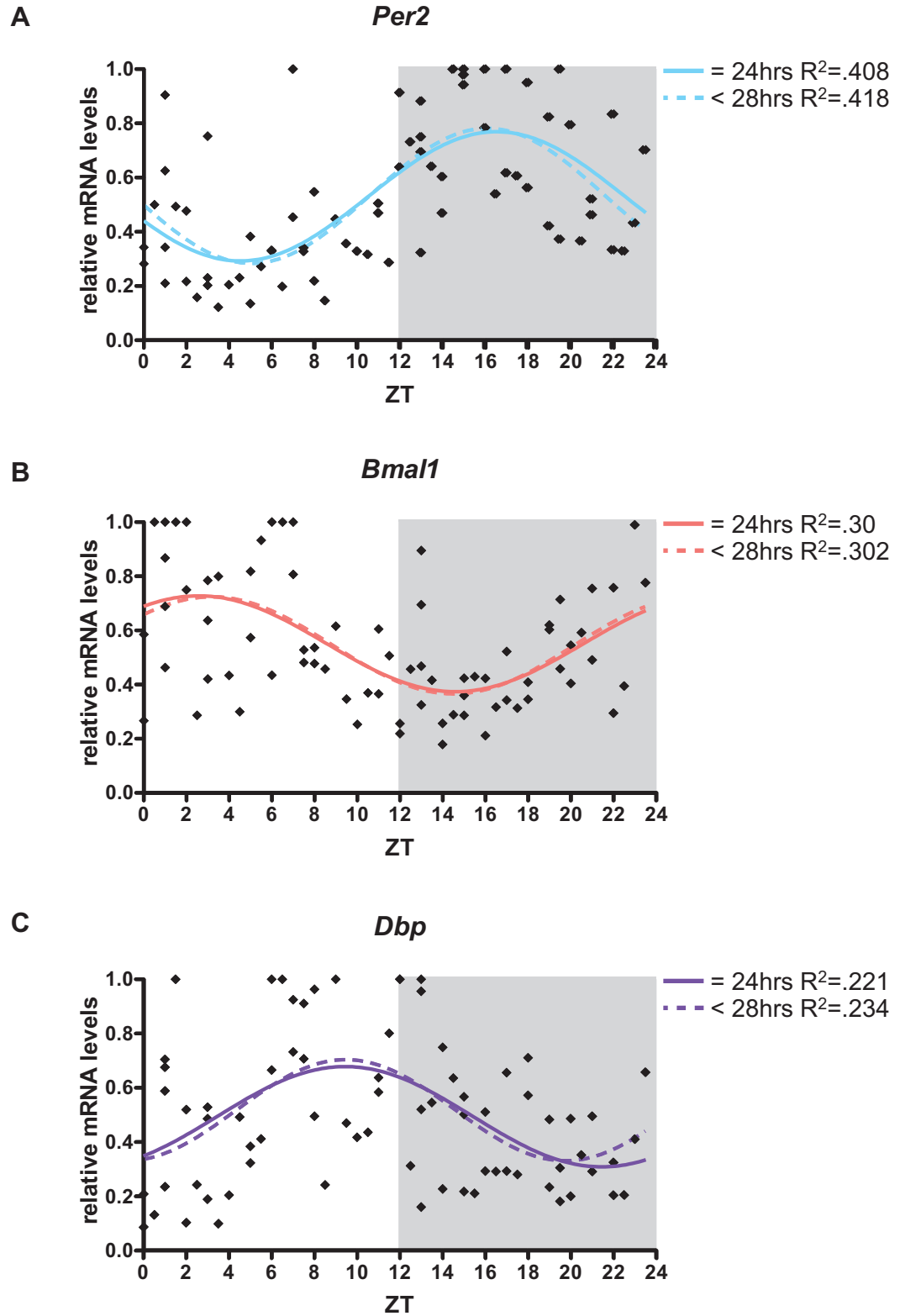


Figure 37. Dentate gyrus (DG). Relative mRNA levels of A) *Per2* B) *Bmal1* and C) *Dbp* in the DG of each individual rat (black diamonds) across 48 *zeitgeber* times. White and grey backgrounds indicate lights on and off, respectively. R^2 = Goodness of fit value for given sine wave. $n= 74$, except for *Per2* where $n=73$

ZT16.5. One sample in this data set had a CT value of over 35 with high variability between the triplicates and so was excluded from the analysis.

Bmal1 expression in the DG also showed a rhythmic pattern of expression with a relative amplitude of .35 (Fig. 37B). No meaningful differences were found between the 24-hr and <28-hr models for this region (Evidence Ratio of 2.8), as can be seen by the visual representations of the sine waves and the almost identical R^2 values of .30 and .302, respectively (Fig. 36B). Peak *Bmal1* expression in the DG occurs at approximately ZT2.5.

Dbp expression in the DG also showed a rhythmic pattern of expression ($R^2 = .221$) with a relative amplitude of .37 (Fig. 37C). No meaningful differences were found between the two models for this region (Evidence Ratio of 1.74). We found that peak *Dbp* expression in the DG occurs at approximately ZT9.5.

In the DG, we found that each gene examined has a different phase. Specifically, peak *Per2* expression (ZT16.5) follows *Bmal1* peak expression (ZT2.5) by 14-hrs, while peak *Dbp* expression (ZT9.5) follows *Bmal1* by 7-hrs (Fig. 35C). Correlations in the DG between the three genes across the 24-hr day revealed no statistically significant relationships (see Table 7C).

Summary of results

Per2

There are phase differences in *Per2* expression in the three brain regions analyzed. Specifically, unlike PER2 protein, *Per2* gene expression in the SCN and CEAL are almost in phase with only a half hour difference in time of peak expression, while the

DG peaks approximately 7-hrs later (Fig. 38A, 42A). Importantly, when comparing PER2 protein to *Per2* mRNA for each of these three regions, we found that in the SCN, protein expression peaks 5-hrs after mRNA (Fig. 39A), in the CEAl, PER2 protein peaks only 2-hrs after *Per2* mRNA (Fig. 39B), and in the DG PER2 protein peaks 7-hrs after *Per2* mRNA (Fig. 39C).

Relative *Per2* mRNA amplitude levels also differ in these regions ($F_{(2,218)}=7.4$, $p<.001$, Fig. 38B). Specifically, Bonferroni post-hoc tests showed that the amplitude in the CEAl is significantly lower than in both the SCN ($t_{(218)}=3.79$, $p<.001$) and DG ($t_{(218)}=2.44$, $p<.05$). Finally, correlations of *Per2* expression across the 24-hr day between the SCN, CEAl, and DG revealed differences in the strength of the relationships between these regions (see Table 8A). Specifically, a moderate statistically significant relationship of .40 was found between the SCN and CEAl only.

Bmal1

Phase differences in *Bmal1* expression between the three regions examined were also found. Specifically, similar to the results obtained for *Per2*, *Bmal1* rhythms in the SCN and CEAl are almost in phase, with only a half hour difference in time of peak expression, while the DG peaks about 15-hrs earlier (Fig. 40A, 42B). Relative *Bmal1* mRNA amplitude levels did not differ significantly in these regions ($F_{(2,218)}=.993$, $p=.372$, Fig. 40B). Finally, correlations of *Bmal1* expression across the 24-hr day between the SCN, CEAl, and DG revealed differences in the strength of the relationships between these regions (see Table 8B). Specifically, a small to moderate statistically significant correlation of .30 was found between the SCN and CEAl only.

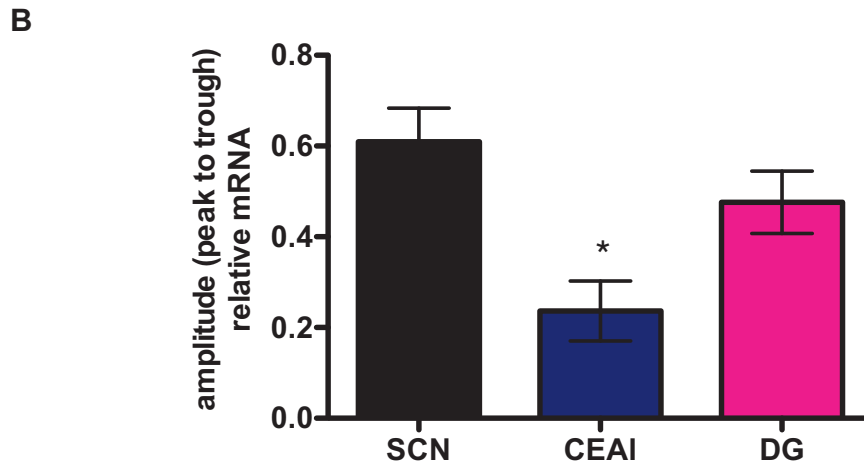
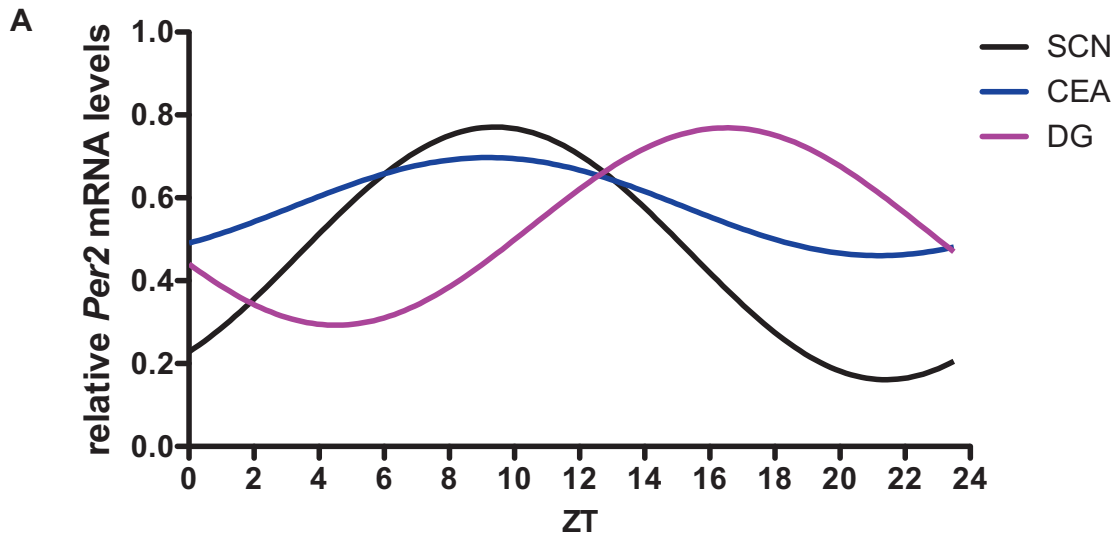


Figure 38. *Per2*. A) Sine-fitted *Per2* expression patterns in all 3 regions across 48 *zeitgeber* times. B) Amplitudes (mean number \pm SEM of relative *Per2* mRNA) measured from peak to trough, in each region. Symbol indicates statistical significance ($p < .05$) as follows: *: CEAI compared to all other regions.

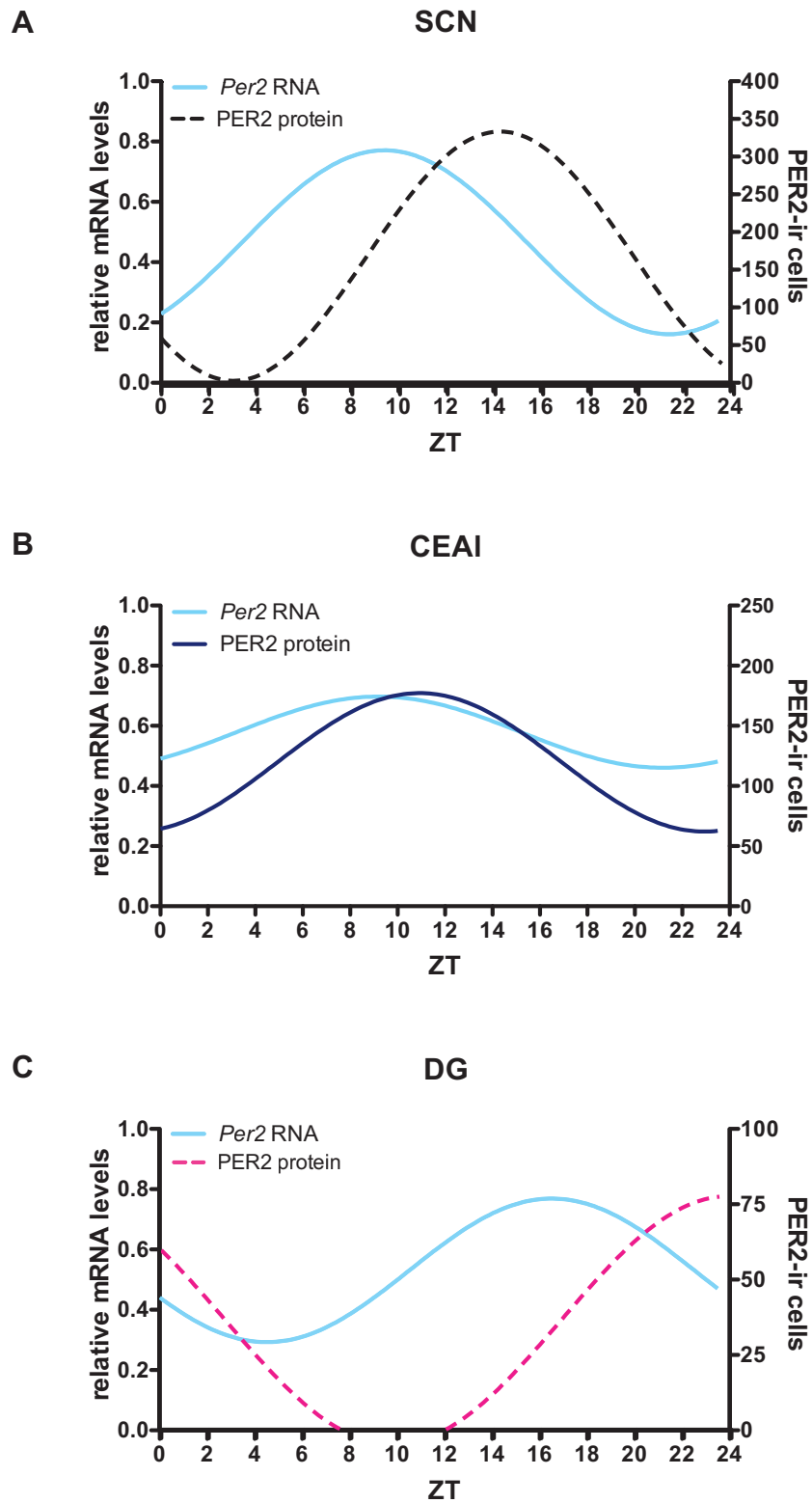


Figure 39. PER2 protein vs *Per2* mRNA. Sine-fitted *Per2* mRNA (light blue) versus PER2 protein expression in the A) suprachiasmatic nucleus B) central amygdala, lateral and C) dentate gyrus across 48 *zeitgeber* times. Solid lines: 24-hr fit, dotted lines: <28-hr fit.

Table 8. Correlations between the SCN, CEAI, and DG. Pearson r values comparing brain regions for Per2 (A), Bmal1 (B), and Dbp (C) expression across the 24-hr day. Values in bold are statistically significant ($p < .05$).

A) *Per2*

Region	CEAI	DG
SCN	0.40	0.02
CEAI		0.09

B) *Bmal1*

Region	CEAI	DG
SCN	0.30	-0.12
CEAI		0.09

C) *Dbp*

Region	CEAI	DG
SCN	0.52	0.33
CEAI		0.39

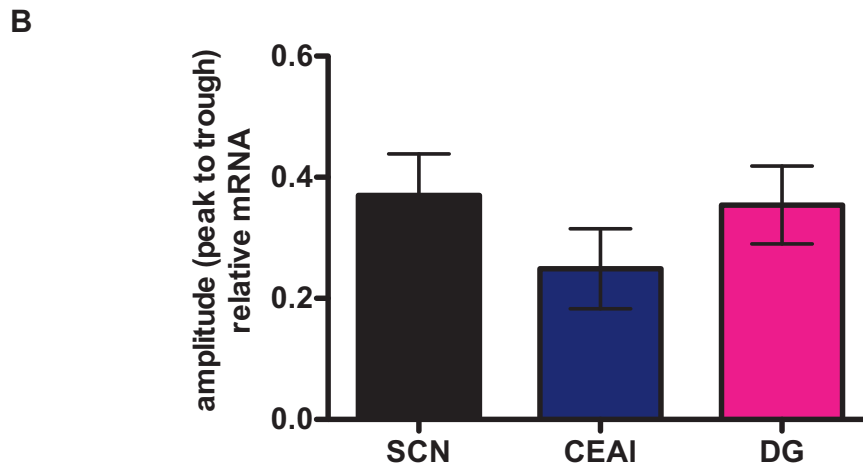
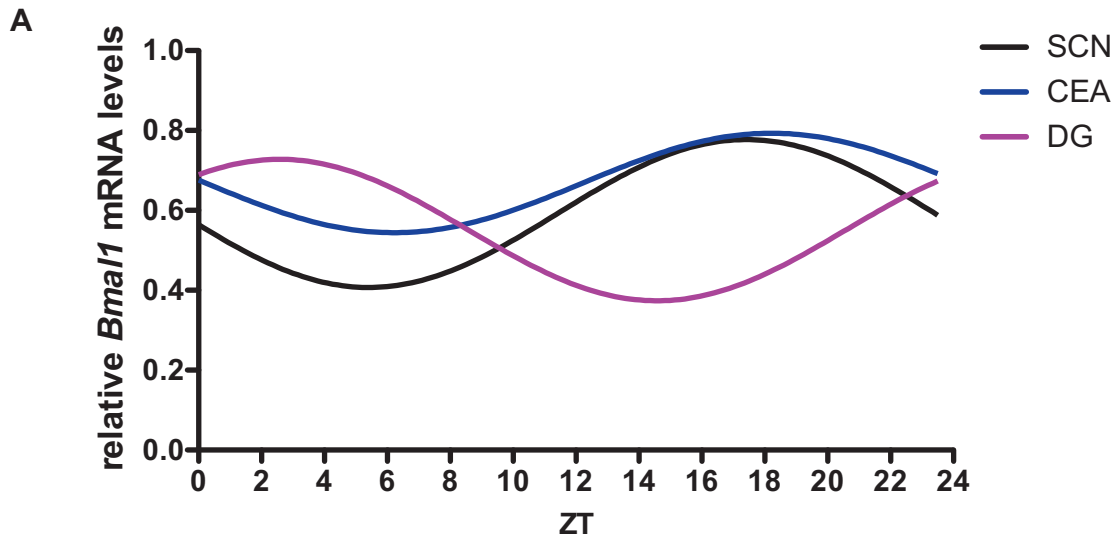


Figure 40. *Bmal1*. A) Sine-fitted *Bmal1* expression patterns in all 3 regions across 48 *zeitgeber* times. B) Amplitudes (mean number \pm SEM of relative *Bmal1* mRNA) measured from peak to trough, in each region.

Dbp

The phase relationships of *Dbp* expression in the SCN, CEAl, and DG differ only slightly compared to expression patterns of *Per2* and *Bmal1* in these regions. Specifically, the SCN and CEAl are almost in phase, with only a half hour difference in peak *Dbp* expression, but in contrast to the two clock genes, *Dbp* expression in the DG peaks only about 2-hrs later (Fig. 41A, 42C). Relative *Dbp* mRNA amplitude levels differ in these regions ($F_{(2,218)}=3.09, p<.05$), however, Bonferroni post-hoc tests did not find any significant differences (Fig. 41B). Finally, correlations of *Dbp* expression across the 24-hr day between the SCN, CEAl, and DG revealed moderate statistically significant relationships between all regions with Pearson r values ranging from .33 to .52 (see Table 8C).

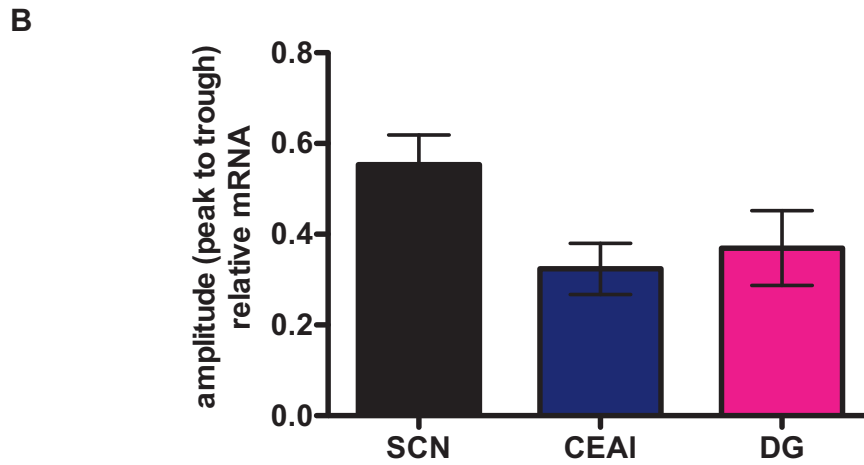
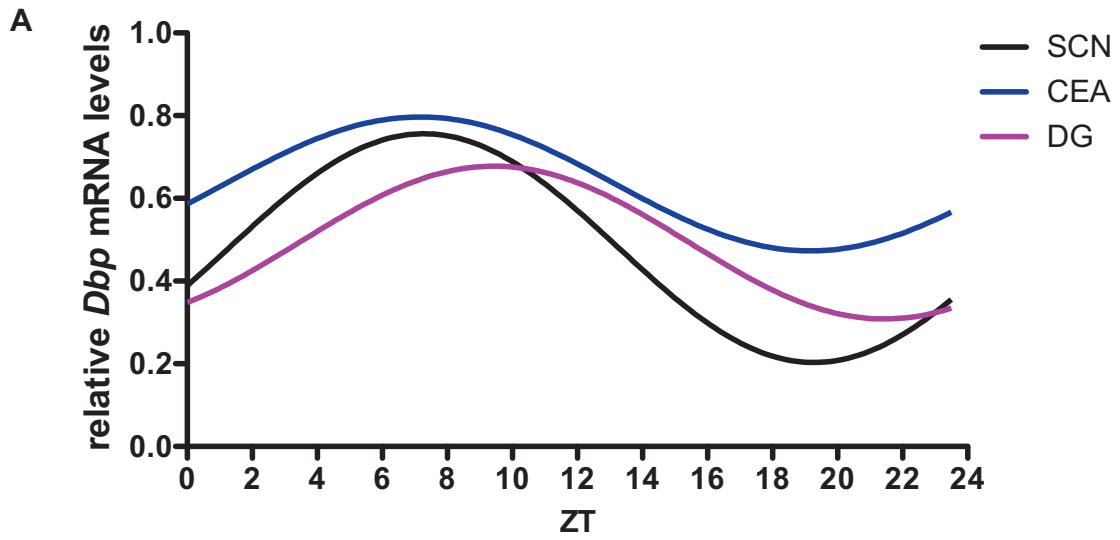


Figure 41. *Dbp*. A) Sine-fitted *Dbp* expression patterns in all 3 regions across 48 *zeitgeber* times. B) Amplitudes (mean number \pm SEM of relative *Dbp* mRNA) measured from peak to trough, in each region.

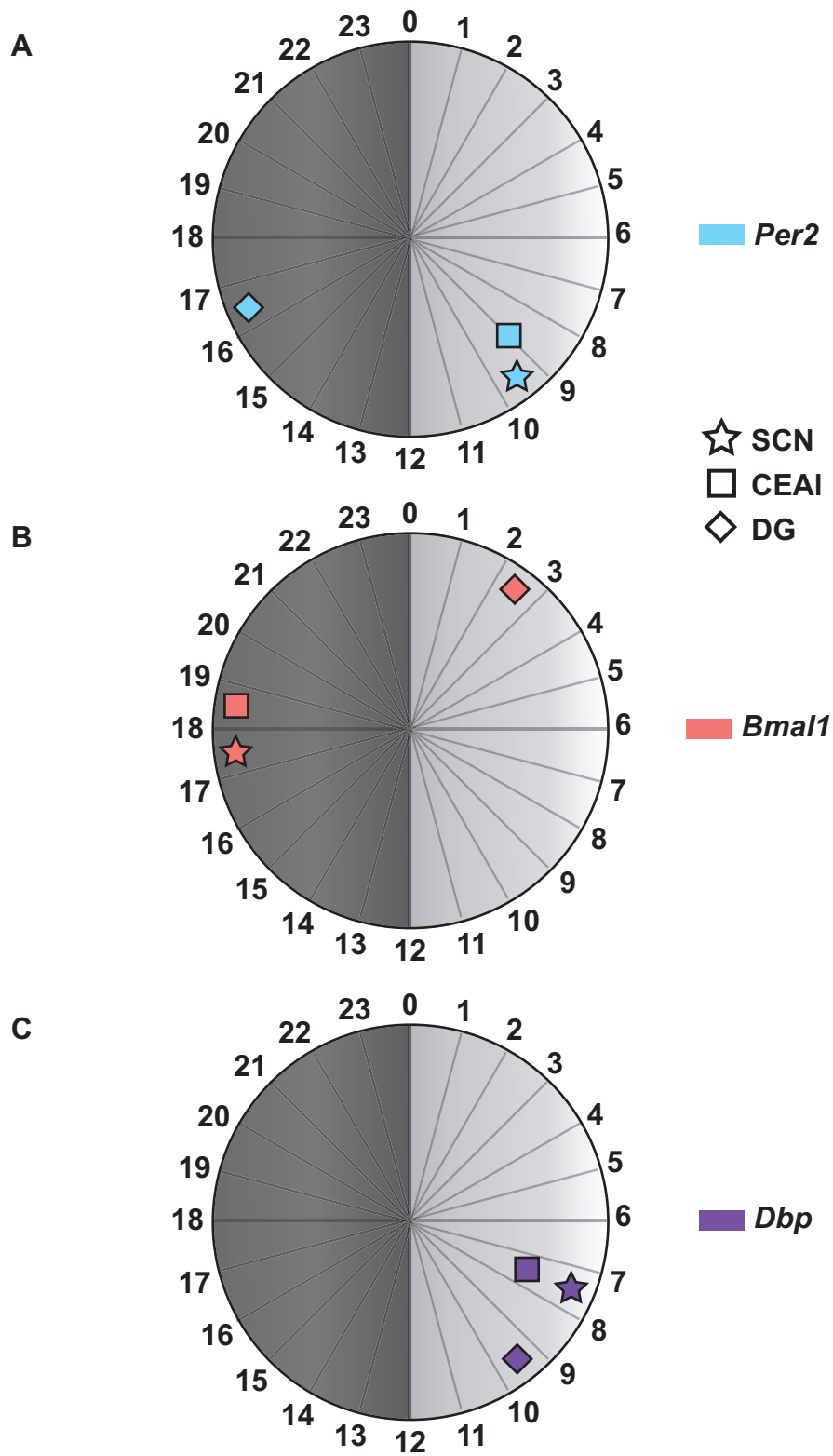


Figure 42. Summary: Comparing phase between regions. 24-hr circular diagram displaying peak *Per2* (A), *Bmal1* (B), and *Dbp* (C) expression in the SCN, CEAI, and DG. Numbers around the ‘clock’ are in *zeitgeber* time.

DISCUSSION

Using a high temporal resolution analysis of PER expression, the present thesis sought to re-examine the rhythms in previously characterized areas of the limbic forebrain, discover novel regions exhibiting rhythmic clock gene expression, and importantly, establish the phase relationships between the rhythms in these regions under basal conditions. In total, 22 sub-regions of the male rat forebrain were studied and we found that 20 of these regions showed measurable circadian rhythms. Analysis of these rhythms further revealed a multifaceted, region-specific distribution of peak PER2 expression patterns across the 24-hr day. These results suggest that a complex network of differently phased brain clocks interact to regulate basal physiology and behaviour in rodents.

The brain is a multi-oscillator organ

As previously reported, using a lower temporal resolution analysis, a number of areas of the rat brain show circadian oscillations in PER2 expression. The rhythms in these areas showed two opposing phases: one where peak expression occurs at the beginning of the dark portion of the LD cycle, in phase with the start of locomotor activity, as was seen in the SCN, BNSTov, and CEAl, the other occurring at the beginning of the light portion of the cycle, as was seen in the BLA, DG, and dorsal striatum (Amir, Harbour, & Robinson, 2006; Amir, Lamont, Robinson, & Stewart, 2004; Beaulé, Houle, & Amir, 2003; Lamont, Robinson, Stewart, & Amir, 2005).

The in phase- or in antiphase- to the SCN relationships previously observed were thought to reflect the general organization of extra-SCN oscillators. However, when

analyzed with a high temporal resolution and when including additional regions showing rhythmic PER2 expression, a more complex distribution of phases emerged. Four distinct clusters of cyclic expression can be observed within these 20 regions along with some regions that peak in isolation (see Fig. 32B). A phase “cluster” was defined as peak PER2 expression occurring in multiple regions within 30 min of each other. The BNSTov and CEAl form one cluster, and are the only regions that show peak PER2 expression during the light portion of the LD cycle, albeit at the very end, at ZT11. The AIp, EPd, ENTld, ENTls of the cortex and the CA1 of the hippocampus showed peak phases occurring between ZT21 and ZT21.5, forming a second cluster. PER2 expression in the BLA and NAc core peaks at ZT22.5 forming a third cluster. The four sub-regions of the dorsal striatum (ASd, ASm, PSd, PSm), the PIR2 of the cortex, and the DG and CA3 of the hippocampus peak 1 hour later, at ZT23.5, forming a fourth cluster. Finally, the rhythms in the ACAv of the cortex and, most notably, the SCN, do not form clusters with other regions but instead peak on their own at ZT17 and ZT14.5, respectively. However, the possibility remains that other regions that have not been examined in this thesis form clusters with the SCN and ACAv. It is especially intriguing that some regions within the same brain structure, which are anatomically interconnected and functionally related, are in different phase clusters. For example, in the hippocampus, PER2 expression in the CA1 peaks at a different time than in the DG and CA3, and the EPd, which is considered to be part of the piriform cortex, is in a different phase cluster than the PIR2.

In addition, mRNA expression of two core clock genes, *Per2* and *Bmal1*, and one clock-controlled gene, *Dbp*, were examined to further assess the circadian molecular machinery in the SCN and two limbic forebrain regions that have been shown to express

opposite patterns in PER2 protein. Although transcript levels of these genes were noisier than the PER2 protein data, they were all rhythmically expressed in the SCN, CEAl, and DG, consistent with the presence of a functional circadian clock in these regions.

Analysis of these rhythms across 24-hrs further revealed differential peak expression between the three genes and regions analyzed (see Fig. 42). Interestingly, the 3.5-hrs difference in phase between the SCN and CEAl seen at the PER2 protein level did not translate to the mRNA data. Here, peak *Per2* mRNA expression between the SCN and CEAl differed by only 30 min (ZT9.5 and ZT9, respectively). The pattern in *Per2* expression found in the SCN is consistent with previous reports of peak expression between ZT8 -10 (Bae et al., 2001; Reppert & Weaver, 2001). The SCN and CEAl differed by 1-hr in peak *Bmal1* expression (ZT17.5 and ZT18.5, respectively), and were identical in peak *Dbp* expression (ZT7.5). Peak *Per2* expression in the DG occurred 7-hrs later than in the SCN and CEAl, at ZT16.5, while *Bmal1* expression in the DG peaked at ZT2.5, which is 9 and 8-hrs later than in the SCN and CEAl, respectively. Conversely, the phase relationship between the DG and the SCN and CEAl differed by only 2-hrs for the *Dbp* data. It is interesting that the phase relationship between these regions is similar for the two core clock genes but differs for *Dbp*, a clock-controlled gene. This might suggest a functional difference in the regulation of this gene in the DG and points towards the possibility that the role of clock-controlled genes might be different across areas.

The SCN stands alone

Importantly, using a fine sampling interval of 30 min across the 24-hr day allowed us to accurately determine the timing of peak PER2 expression in the SCN. The data in the present thesis is in general agreement with peak PER2 occurring at the beginning of the dark portion of the LD cycle (Field et al., 2000; Reppert & Weaver, 2001). However, fitting a circadian sine wave function to these data established that peak PER2 expression occurs approximately 2-hrs later than previously found when examining fewer time-points in rats (Beaule, Houle, & Amir, 2003) and in mice (Reppert & Weaver, 2001). Furthermore, the phase difference between *Per2* mRNA and protein in the SCN was found to be 5-hrs, confirming the 4 to 6-hr lag in protein expression previously reported elsewhere (see Fig. 39A; Bae et al., 2001; Field et al., 2000; Reppert & Weaver, 2001). Interestingly, the results from this thesis show that the SCN stands alone, and that no other brain region peaks exactly in phase or in antiphase with the PER2 rhythm in the SCN, which is also in contrast to previous observations (Amir, Lamont, Robinson, & Stewart, 2004; Lamont, Robinson, Stewart, & Amir, 2005).

In contrast to previous work in our laboratory showing no differences in PER2 phase between the SCN core and shell when sampled every 3-hrs (Beaule, Houle, & Amir, 2003), the high temporal resolution analysis in the present thesis showed that PER2 expression in the core peaks slightly earlier than in the shell. This finding is not surprising given that the core receives environmental light cues and subsequently transmits this entraining information to the shell (Moore, Speh, & Leak, 2002). This suggests that under stable entrainment conditions *in vivo*, light regulates (i.e. entrains) rhythms in the SCN core, which then sets the phase for rhythms in the shell. The small phase difference in PER2 reported here may be a representation of such entrainment

properties. In agreement with this, it has been shown that the core and shell subdivisions have differential rates of re-entrainment to phase shifts in the LD cycle, with the shell lagging behind the core (Yan & Silver, 2002, 2004). In contrast, bioluminescence recordings of isolated SCN organotypic slices have shown opposite phase differences between the core and shell subdivisions, although similar in magnitude. In these studies, PER1 and PER2 protein and *Per1* mRNA have been shown to peak slightly earlier in the shell, rather than in the core (Evans, Leise, Castanon-Cervantes, & Davidson, 2011; Foley et al., 2011; Yamaguchi et al., 2003). The opposite direction in core-shell phase difference between our results and those obtained *in vitro* can possibly be explained by the latter data originating from free running isolated SCN cultures.

Validation of established clocks

Limbic forebrain

The present thesis confirmed previously reported results that the PER2 rhythms in the BNSTov and CEAl are in perfect phase with each other (Amir, Lamont, Robinson, & Stewart, 2004; Lamont, Robinson, Stewart, & Amir, 2005). However, the time of peak PER2 expression was found to occur at ZT11 in these regions, approximately 2-hrs earlier than previously described. The high correlation of .88 comparing PER2 expression patterns between the BNSTov and CEAl further confirms the similarities between these two regions. Interestingly, the phase difference between *Per2* mRNA and PER2 protein in the CEAl was only 2-hrs, in contrast to the usual 4 to 6-hr lag between mRNA and protein (see Fig. 39B). Furthermore, PER2 expression in the BLA remained 180° out of phase with the rhythms in BNSTov and CEAl as previously shown (Lamont, Robinson,

Stewart, & Amir, 2005), with a notable difference in peak expression now occurring at approximately ZT22.5. Peak PER2 expression in the DG, on the other hand, occurred 1 hour later than in the BLA, at ZT23.5, and is therefore not in perfect phase with this region as previously reported, and consequently, is also not in perfect antiphase with the rhythms in the BNSTov and CEAl. Peak *Per2* mRNA in the DG occurred at ZT16.5, 7-hrs earlier than the peak in PER2 protein (see Fig. 39C), which is in general agreement with the time lag usually seen between mRNA and protein expression (Reppert & Weaver, 2001).

Striatum

The dorsal striatum is a large structure with distinct segregations of afferent projections (Gerfen, 2004). Based on these previously described cortical afferents, four subdivisions of the dorsal striatum were examined (anterior dorsal, anterior medial, posterior dorsal, and posterior medial). These striatal subdivisions all displayed rhythmic PER2 patterns with peak expression occurring at the end of the dark phase, at approximately ZT23.5. The area that corresponds to the anterior dorsal division in this thesis has been previously shown to express peak PER2 levels at ZT1 when using fewer time-points (Amir, Harbour, & Robinson, 2006), which is slightly later than what is reported here, but is still in general agreement with peak expression occurring during the transition from dark to light for the striatum. The results show that these striatal subdivisions are virtually identical in amplitude and phase of PER2 expression, suggesting that under basal conditions, and in spite of the difference in afferent projections, the dorsal striatum shows homogeneous PER2 rhythms and does not need to

be subdivided based on rhythmic properties. This can be further confirmed by the high correlation values ranging from .83 to .91 comparing PER2 expression patterns between these regions. However, given the distinct distribution of cortical afferents to striatal sub-regions, it is conceivable that dissociations of PER2 rhythms could occur under specific conditions. In agreement with this, Willuhn and colleagues (2003) have shown differential regulation of *c-fos* and dynorphin among striatal subdivisions following cocaine administration, demonstrating the need to consider possible roles of different sub-regions within this large forebrain structure.

The NAc core showed a robust rhythm in PER2 expression with the largest amplitude after the SCN. The PER2 rhythm in the NAc core is similar in phase to those in the four sub-regions of the dorsal striatum, with peak expression occurring before light onset, at ZT22.5. Conversely, the NAc shell had low levels of PER2-ir cells randomly distributed across the 24-hr day, resulting in overall arrhythmic PER2 expression. This differs from mRNA data where *Per2* has been shown to be rhythmic in both subdivisions of the NAc (Li, Liu, Jiang, & Lu, 2009). However, it is well known that changes in mRNA do not always correlate with changes in protein, and vice versa (Anderson & Seilhamer, 1997; Gygi, Rochon, Franza, & Aebersold, 1999). Intriguingly, a rhythm in the NAc shell in both PER1 and PER2 protein has been reported in the diurnal grass rat (Ramanathan, Stowie, Smale, & Nunez, 2010b), suggesting a possible functional difference in this region between diurnal and nocturnal species.

Novel rhythms in PER2

Rhythms in PER2 expression were found in the CA1 and CA3 of the hippocampus, and all regions of the cortex examined: layer II of the piriform cortex (PIR2), the dorsal endopiriform (EPd) cortex, the ventral part of the anterior cingulate (ACAv), the posterior part of the anterior agranular insular cortex (AIp), and the superficial (I-III) and deep (IV-VI) layers of the lateral entorhinal cortex (ENTIs and ENTId, respectively). Although the presence of clock genes such as *Per1*, *Per2*, and *Clock* have previously been reported in most of these regions (Abe et al., 2002; Shieh, 2003; Yamamoto et al., 2001), this is the first time, to our knowledge, that actual rhythms have been characterized in these regions in a nocturnal rodent.

The PER2 rhythms in the CA1 and CA3 differed by 2-hrs, with peak expression occurring at ZT21.5 and ZT23.5, respectively. The majority of afferent information into the hippocampus flows from the DG, to the CA3, to the CA1. The CA1 acts as the major output of the hippocampus proper sending efferent signals to the ENT cortex and to multiple other cortical regions, including the AI, as well as the thalamus, hypothalamus, and the amygdala (Cenquizca & Swanson, 2006, 2007). Many of these areas also project back to the hippocampus (Pikkarainen, Ronkko, Savander, Insausti, & Pitkanen, 1999; Pitkanen, Pikkarainen, Nurminen, & Ylinen, 2000). In addition, the perforant path provides connections from the ENT cortex to all sub-regions of the hippocampal formation, including the three regions examined in the present thesis (Witter et al., 2000; Witter, Wouterlood, Naber, & Van Haefen, 2000).

Rhythms in PER1 and PER2 protein have been previously reported in the CA1 in the diurnal grass rat (Ramanathan, Stowie, Smale, & Nunez, 2010b). In this study, diurnal rats were sacrificed every 4-hrs, and peak expression for both proteins was found

to occur at ZT10. The difference in phase between the rhythm in PER2 between the current thesis and the data obtained in diurnal rodents is in agreement with the finding that the phase-relationship among extra-SCN oscillators is inverted between diurnal and nocturnal rodents (Ramanathan, Stowie, Smale, & Nunez, 2010a, 2010b).

The ENT cortex is both the major input and, together with the CA1 and subiculum, the major output system of the hippocampal formation, projecting mainly to the amygdala, especially the BLA, and the NAc, and to other cortical areas such as the anterior and posterior cingulate cortex (reviewed in Swards & Swards, 2003). The six layers of the ENT have been classically divided into superficial (I-III) and deep (IV-VI) layers, with the superficial layers acting as the primary 'input' station and the deep layers acting as the primary 'output' station (Burwell & Amaral, 1998; Kohler, 1988; Witter, Wouterlood, Naber, & Van Haefen, 2000), although there is some dispute to whether this still holds true (Swards & Swards, 2003; Canto, Wouterlood, & Witter, 2008). A slight difference in PER2 phase was found between the two subdivisions of the ENT1, with the superficial layers peaking 30 min after the deep layers at ZT21.5.

We found that in the PIR2, PER2 expression peaked at ZT23.5. In the grass rat study mentioned above, a rhythm in PER1 and PER2 protein was also found in the PIR, with peak expression occurring at ZT10 (Ramanathan, Stowie, Smale, & Nunez, 2010b). The PIR is also known as the primary olfactory cortex due to major afferent input from the olfactory bulb (OB). In addition to direct input from the OB, the PIR also receives projections from the basal forebrain, thalamus, hypothalamus, and brainstem (Loscher & Ebert, 1996). The PIR itself projects back to the OB, hypothalamus, and thalamus, and sends efferent projections to the insular cortex, ENT, and regions of the amygdala

(Loscher & Ebert, 1996). Besides playing a major role in olfactory processing, the PIR has also been implicated in fear memory (Pantazopoulos, Dolatshad, & Davis, 2011) and epileptogenesis (Loscher & Ebert, 1996).

Interestingly, PER2 expression in the EPd, which is described by some as layer IV of the PIR cortex due to its proximity and heavy interconnections (Haberly, 1990), peaks 2.5-hrs earlier than the PIR2, at ZT21. Like the PIR, the EP not only has connections with the olfactory system, but also possesses reciprocal connections with the ENT, insular cortex, cortical amygdaloid nuclei, thalamus, and NAc shell (Kowianski, Lipowska, & Morys, 1999). It is not clear what the exact function of the EPd is, however, it has been implicated in temporal lobe epileptogenesis (Behan & Haberly, 1999; Kowianski, Lipowska, & Morys, 1999).

We found that the rhythm in PER2 in the ACA_v peaked on its own, at ZT17. The ACA is important for a wide range of autonomic functions, including regulation of heart rate and blood pressure, and in motivation and goal-directed behaviours (Devinsky, Morrell, & Vogt, 1995). The ACA can be subdivided anatomically and functionally into ventral (emotional) and dorsal (cognitive) regions. The ACA_v has connections with the NAc core, amygdala, AI, and hypothalamus, and has been shown to be involved in the processing of salient emotional and motivational information (Cardinal, Parkinson, Hall, & Everitt, 2002; Neafsey, Terreberry, Hurley, Ruit, & Fryszak, 1993). Furthermore, both the anterior and posterior cingulate project to the deep layers of the ENT (Wyss & Van Groen, 1992).

The agranular insular (AI) cortex is part of the anterior portion of the insular cortex so named because of the missing granular layer IV (Kobayashi, 2011). We found

that the rhythm in PER2 in the posterior part of this region peaks at ZT21.5. The AI innervates the NAc core and shell, the BNST, and the amygdala, and itself receives large input from the CEAI as well as the ENTI and thalamus (McDonald, Shammah-Lagnado, Shi, & Davis, 1999; Reep & Winans, 1982a, 1982b). The AI also has reciprocal connections with the PIR and EP cortices. The insular cortex has been shown to be important in addiction, emotions, and motor control, as well as in homeostatic functions including visceral sensation and gustatory processing (Kobayashi, 2011; Krushel & van der Kooy, 1988).

PER2 is arrhythmic in certain brain regions

Two out of the 22 sub-regions analyzed failed to meet the criteria for rhythmicity. Although PER2-ir labeled cells were present in the NAc shell and posteriodorsal part of the medial amygdala (MEApd), their expression was evenly distributed across the 24-hr day, leading to the classification of these regions as arrhythmic. What does it mean that the NAc shell and MEApd contain PER2-ir cells that are non-rhythmic as a whole? There are two possibilities: either individual PER2 expressing cells within these regions are arrhythmic, which then begs the question of PER2's function in these regions, or, individual cells are still rhythmic but are not synchronized to each other, resulting in overall arrhythmicity. The latter is most probable given that it has been shown that individual cells within an arrhythmic SCN still oscillate with a period close to 24-hrs but are out of phase with each other (Welsh, Logothetis, Meister, & Reppert, 1995; Yoo et al., 2004; but see Webb, Angelo, Huettner, & Herzog, 2009).

These two regions are arrhythmic under basal conditions, which might lead one to wonder whether a rhythm in PER2 could be induced in these regions under different or abnormal conditions, as has been shown to occur in the dorsomedial hypothalamus (DMH). The DMH is known to show arrhythmic levels of PER2 and very low amplitude levels of PER1 under normal *ad libitum* conditions. However, when a rat is placed on a daily schedule of restricted feeding (RF), a robust rhythm in both these clock genes is induced (Mieda, Williams, Richardson, Tanaka, & Yanagisawa, 2006; Verwey & Amir, 2011; Verwey, Khoja, Stewart, & Amir, 2007). Notably, it has been shown that a 2-hr daytime RF schedule shifted the rhythms in PER1 protein by 6-hrs to ZT12 in both the NAc core and shell (Angeles-Castellanos, Mendoza, & Escobar, 2007). It would be interesting to see if a rhythm in PER2 could be induced in the NAc shell by this same schedule. Moreover, as previously mentioned, *Per1* and *Per2* have been differentially implicated in cocaine sensitization (Abarca, Albrecht, & Spanagel, 2002). Given the important role of the NAc shell in drug addiction, it would be interesting to see if a rhythm in PER2 could be induced in this region by daily drug administration. Interestingly, Li and colleague (2010) have shown that during morphine withdrawal, *Per1* mRNA in the NAc core and *Per2* mRNA in the NAc shell show inverted rhythms compared to basal patterns (Li, Liu, Jiang, & Lu, 2009).

Rhythmicity Index

The Rhythmicity Index is a valuable tool that allows for the comparison of rhythms in different regions with varying levels of PER2 expression. By taking into account the mean level of PER2 expression as well as the amplitude, the RI provides a

more meaningful analysis of the rhythms and, importantly, quantifies the strength of rhythms allowing for comparisons between regions. All regions were normalized to the SCN, which was given a value of 1. Interestingly, the RI revealed that PER2 rhythms in the DG and CA3 of the hippocampus and the PIR2 and AIP of the cortex are as robust as the rhythm of the SCN, with RI values of over .90. Large rhythms may suggest large day-night differences in the functional roles of these regions. For example, day-night differences in memory formation have been reported (Eckel-Mahan & Storm, 2009; Gerstner & Yin, 2010), consistent with the presence of functional clocks in the hippocampus.

Different expression patterns within sub-divisions of the same structure

The fact that sub-divisions of the same brain structure differ in PER2 amplitude and phase (especially in the NAc, and to a lesser degree in the SCN, piriform cortex, and ENT1) is particularly intriguing. Whether these phase and/or amplitude differences are a reflection of different information processing mechanisms by the subdivisions of the same structure remains to be elucidated. In particular, it will be important to study the consequence of altering the phasing or amplitude in one compartment for the overall functioning of the whole structure. At the very least, this underscores the importance for future research to properly identify which specific sub-region within a larger functional structure is under study.

Functional role of multi-oscillator organization

The SCN acts as a central coordinator, synchronizing oscillators throughout the organism to the 24-hr external environment. The present thesis further confirmed that the circadian system is comprised of numerous dispersed clocks “chiming” at different times of day. This complex temporal framework allows for great flexibility to subtle changes in the environment, such as alterations in seasonal day length, an adaptability important for survival (Yamazaki et al., 2000). However, this tightly knit organization is susceptible to disruption when faced with abrupt and large changes in environmental timing cues, such as can be seen with travel across time zones and rotating shift work.

In agreement with this, rodents experiencing large shifts in the LD cycle display temporary disruption of the phase relationship between the SCN and subordinate clocks throughout the rest of body. This disruption lasts for several days before the phase relationship is reestablished following stable re-entrainment to the new LD cycle. For example, whereas *Per1* rhythms in the SCN shift almost immediately following a 6-hr phase shift of the LD cycle, clocks in both peripheral tissues and brain structures take significantly longer (up to 6 days) before completely adjusting (Abe et al., 2002; Yamazaki et al., 2000). Our laboratory has also shown that re-entrainment of the PER2 rhythm in the BSNTov to an 8-hr delay or advance in the LD cycle lagged behind the SCN by several days before re-establishing its normal phase relationship (Amir, Lamont, Robinson, & Stewart, 2004). Furthermore, we have shown that prolonged exposure to a 26-hr LD cycle, which requires daily phase delays, uncoupled PER2 rhythms in the BNSTov and CEAl from the master SCN clock, while leaving other limbic forebrain regions unaffected, and led to the emergence of a new phase relationship between these regions (Harbour, Robinson, & Amir, 2011).

Together, the findings that large shifts in the entraining LD cycle are associated with differential rates of re-entrainment of clock gene rhythms in the SCN compared with those in other areas, suggest the existence of weak coupling between the master clock and subordinate oscillators in the brain and periphery. This highlights the susceptibility of extra-SCN oscillators to physiological and environmental perturbations. It may also simply be a function of a highly adaptable system that is better suited to respond to changes when oscillators have different phases. Pittendrigh and Daan in 1976 suggested that a clock with an endogenous period different from the external *zeitgeber* could entrain better than one where the period of the clock equals that of the time-cue (Pittendrigh & Daan, 1976a).

It is believed that one of the key roles of subordinate oscillators in the brain is to maintain the operational integrity of neural circuits by regulating basic processes at the cell and tissue levels (Tu & McKnight, 2006). Accordingly, changes in the timing of such processes within these multiple brain areas may affect communication between these and other behaviourally important networks and, ultimately, alter the way in which motivationally and emotionally significant stimuli are translated into appropriate behavioural and physiological responses. Appropriate alignment of central and peripheral circadian oscillations is thought to be critical for the proper temporal organization of physiology and behaviour. In agreement with this, disruptions in circadian rhythms have been implicated in sleep disorders, cognitive dysfunction, mood disorders, and general malaise as seen in jet lag and shift work (Boivin, 2000; Bunney & Potkin, 2008; Bunney & Bunney, 2000). Whether these disorders induce, or are the result of, disrupted phase relationships between brain clocks is unknown.

The present thesis provides a snapshot of PER2 rhythms under normal basal conditions in brain regions known to play important roles in a wide range of motivated and appetitive behaviours. The fact that the PER2 rhythms in multiple regions adopt differential patterns in peak expression suggests that it is the phase relationship between the clocks in these regions that establishes a healthy functioning system. Understanding the phase relationship between brain clocks in animals models of emotional and cognitive disorders will provide critical insights into the mechanisms responsible for the establishment of appropriate phase relationships and will provide a starting point for the development of behavioural or pharmacological treatment.

Although the SCN provides a necessary signal for rhythmicity, several other factors have been identified that can directly affect the phase of individual extra-SCN oscillators. As previously mentioned, rhythms in PER2 in some extra-SCN brain regions are sensitive to homeostatic and hormonal perturbations that can directly influence behaviour. Most notably, schedules of RF are able to entrain or shift rhythms in multiple subordinate oscillators, effectively overriding SCN signals (Angeles-Castellanos, Mendoza, & Escobar, 2007; Mieda, Williams, Richardson, Tanaka, & Yanagisawa, 2006; Waddington Lamont et al., 2007; Wakamatsu et al., 2001). Interestingly, PER2 rhythms in the BNSTov and CEAl have been shown to be selectively sensitive to a wide range of hormonal dysregulation, while other regions in the limbic forebrain remain unaffected (Amir & Stewart, 2009a, 2009b). Specifically, the rhythms in PER2 in these regions are modulated by rhythmic corticosterone (Segall & Amir, 2010), thyroid hormones (Amir & Robinson, 2006), and gonadal hormones (Perrin, Segall, Harbour, Woodside, & Amir, 2006). Understanding the nature of the signals that modulate clock-gene oscillations

observed in extra-SCN regions will provide another critical starting point for the understanding of the role of these clocks in normal and pathological conditions. The tissue specific functions of these clocks within this complex temporal framework remain to be defined.

Limitations

The data in this thesis were analyzed using least squares regression sine waves with imposed circadian frequencies. This was done in order to obtain empirical measures of phase, amplitude, and, to a lesser degree, period for the 22 brain regions examined. A limitation of the sampling duration arises from this method. We attempted to determine the best fit possible for both a 24-hr and <28-hr sine function on exactly 24-hrs (i.e. one day) of data. Due to the fact that these data are limited to one circadian cycle, it is very difficult to infer any information about period length. Most regions were fit with a fixed 24-hr sine wave, with the rationale being that the rats were stably entrained to a 24-hr day. However, for those regions where the <28-hr model was the most appropriate fit for the data, we can only describe the period as the frequency to which the curve fit the data and nothing more. It is possible that with sampling across multiple days, period length could be different from what we have reported. Having more than one cycle of 24-hrs would greatly improve precision and accuracy of the measurements derived from this function.

The possibility that extra-SCN clocks have periods that differ from 24-hrs under stable entrainment conditions is intriguing. For instance, when rhythmicity in peripheral organs and tissues is studied *in vitro*, each rhythmic structure has its own phase,

amplitude and, importantly, period, suggesting that the details of the molecular mechanism generating the circadian oscillation is tissue or region-specific (Yoo et al., 2004). It is conceivable that similar differences exist in the rhythmic properties between extra-SCN brain oscillators. Furthermore, changes in the regular temporal conditions of these oscillators may be an underlying mechanism in pathology. For example, it is well established that disruptions in circadian rhythms are associated with mood disorders such as bipolar disorder (BD). Interestingly, it has been found that BD patients have abnormally fast daily rhythms in a number of physiological processes, suggesting a phase advance in the circadian clock, and thus a shortened period (Linkowski et al., 1994; McClung, 2007a). In agreement with this, the mood stabilizer lithium, the most common treatment for BD, has been shown to lengthen the circadian period in several species, including humans (reviewed in McClung, 2007a). Thus, it seems that relief from BD symptoms may be linked, at least in part, to re-synchronization of circadian oscillators to the 24-hr environment and consequently the re-establishment of proper phase alignment between these clocks.

The nature of the data, that is, extracting one time-point from a given rat across the 24-hr day, introduces a limitation of inter-individual variability. The only way to increase the precision of the analysis of the expression of clock genes would be to sample continuously from the same rat. This is obviously impossible using IHC or qRT-PCR. Bioluminescence measurements would provide such high temporal resolution. However, at the present time, it is unfeasible to monitor clock gene-driven bioluminescence *in vivo* in the brain of intact animals, except for a few easily accessible areas (e.g. olfactory bulb; Abraham, Prior, Granados-Fuentes, Piwnica-Worms, & Herzog, 2005). That being said,

given the high temporal resolution analysis of sampling every 30 min across the 24-hr day, we are confident that the rhythms reported in this thesis are reliable.

The fact that the <28-hr model could not be fit to several regions is also somewhat problematic. However, this is the case only in regions where the peak in PER2 expression is ‘missed’ or ‘cut-off’ (i.e. the CA3, sub-regions of the striatum, and PIR2), occurring at the very end of the dark phase or beginning of the light phase. This is simply a factor of the way the data are graphed. For example, if re-plotted so that the X-axis begins at ZT12 and the peak of the rhythm is therefore moved to the middle of the graph, the <28-hr model can then be fit to the data. This was not done, however, because doing so would misalign the timing of the phases and comparisons would not be possible between these regions. Furthermore, for those regions that failed the Runs test (showing patterns in the spread of residuals from the curve), it is most likely due to the fact that PER2 levels were very low during some part of the day, creating a cluster near zero levels. For these regions, the sine fitted curve had to dip below zero to correctly fit the data, which violates the nature of the data as it is impossible to have negative amounts of PER2. Finally, given that the rats were entrained to a LD cycle, it must be noted that it is unknown whether the rhythms in the regions examined are endogenous. Rats would have to be put in constant conditions without any external *zeitgebers* present in order to address this. Replicating the experiment in rats housed in complete darkness would clarify this point.

Future studies are needed to determine the functionality of PER2 in specific brain regions. A tool that may prove useful to address this issue is RNA interference (RNAi), which temporarily knocks down a targeted gene or protein. Region specific knockouts

can also be created using viral vectors, which would allow for a more permanent silencing of a specific clock component. These methods, along with specific tissue mutations, have been previously used in peripheral organs such as the liver (Etchegaray et al., 2006) and heart (Ko et al., 2011) to investigate specific clock functions in these tissues. McClung et al have also used short hairpin RNA (shRNA), expressed in an adeno virus, in the brain to further investigate the importance of *Clock* in mania-like behaviours (McClung, 2007b; Mukherjee et al., 2010; Roybal et al., 2007). They showed that knockdown of *Clock*, specifically in the ventral tegmental area, resulted in similar behavioural phenotypes seen in *Clock* mutants (Mukherjee et al., 2010).

Injection of RNAi for PER2 into specific brain regions would allow for the study of behavioural and cognitive consequences of disrupted clock function in these areas (Gavrila et al., 2008). A crucial question still remaining would be whether it is specifically PER2 that is responsible for changes in physiology and behaviour, or whether is it the disruption of the molecular clockwork, itself, that is the cause. This could be addressed by silencing other clock genes (one at a time) in the same areas to see if any differences in phenotype occur.

Conclusion

In conclusion, our data demonstrate the presence of complex and previously unappreciated associations of PER2 expression both between functionally and anatomically distinct brain regions as well as between these brain areas and the master SCN clock. The multiple phases and, potentially, different periods observed in brain areas analyzed in the present thesis likely form the optimal organization needed for a

flexible multi-oscillatory system that is capable of being reset daily by environmental cues in order to yield adaptive behaviour.

REFERENCES

- Abarca, C., Albrecht, U., & Spanagel, R. (2002). Cocaine sensitization and reward are under the influence of circadian genes and rhythm. *Proc Natl Acad Sci U S A*, 99(13), 9026-9030.
- Abe, K., Kroning, J., Greer, M. A., & Critchlow, V. (1979). Effects of destruction of the suprachiasmatic nuclei on the circadian rhythms in plasma corticosterone, body temperature, feeding and plasma thyrotropin. *Neuroendocrinology*, 29(2), 119-131.
- Abe, M., Herzog, E. D., Yamazaki, S., Straume, M., Tei, H., Sakaki, Y., et al. (2002). Circadian rhythms in isolated brain regions. *J Neurosci*, 22(1), 350-356.
- Abraham, U., Prior, J. L., Granados-Fuentes, D., Piwnica-Worms, D. R., & Herzog, E. D. (2005). Independent circadian oscillations of Period1 in specific brain areas in vivo and in vitro. *J Neurosci*, 25(38), 8620-8626.
- Akashi, M., Ichise, T., Mamme, T., & Takumi, T. (2006). Molecular mechanism of cell-autonomous circadian gene expression of Period2, a crucial regulator of the mammalian circadian clock. *Mol Biol Cell*, 17(2), 555-565.
- Akashi, M., & Takumi, T. (2005). The orphan nuclear receptor RORalpha regulates circadian transcription of the mammalian core-clock Bmal1. *Nat Struct Mol Biol*, 12(5), 441-448.
- Alheid, G. F. (2003). Extended amygdala and basal forebrain. *Ann N Y Acad Sci*, 985, 185-205.
- Amir, S., Cain, S., Sullivan, J., Robinson, B., & Stewart, J. (1999). Olfactory stimulation enhances light-induced phase shifts in free-running activity rhythms and Fos expression in the suprachiasmatic nucleus. *Neuroscience*, 92(4), 1165-1170.
- Amir, S., Harbour, V. L., & Robinson, B. (2006). Pinealectomy does not affect diurnal PER2 expression in the rat limbic forebrain. *Neurosci Lett*.
- Amir, S., Lamont, E. W., Robinson, B., & Stewart, J. (2004). A circadian rhythm in the expression of PERIOD2 protein reveals a novel SCN-controlled oscillator in the oval nucleus of the bed nucleus of the stria terminalis. *J Neurosci*, 24(4), 781-790.
- Amir, S., & Robinson, B. (2006). Thyroidectomy alters the daily pattern of expression of the clock protein, PER2, in the oval nucleus of the bed nucleus of the stria terminalis and central nucleus of the amygdala in rats. *Neurosci Lett*, 407(3), 254-257.
- Amir, S., & Stewart, J. (2009a). Behavioral and hormonal regulation of expression of the clock protein, PER2, in the central extended amygdala. *Prog Neuropsychopharmacol Biol Psychiatry*, 33(8), 1321-1328.

- Amir, S., & Stewart, J. (2009b). Motivational Modulation of Rhythms of the Expression of the Clock Protein PER2 in the Limbic Forebrain. *Biological Psychiatry*, 65(10), 829-834.
- Anderson, D. R. (2008). *Model Based Inference in the Life Sciences: A Primer on Evidence*: Springer.
- Anderson, L., & Seilhamer, J. (1997). A comparison of selected mRNA and protein abundances in human liver. *Electrophoresis*, 18(3-4), 533-537.
- Angeles-Castellanos, M., Mendoza, J., & Escobar, C. (2007). Restricted feeding schedules phase shift daily rhythms of c-Fos and protein Per1 immunoreactivity in corticolimbic regions in rats. *Neuroscience*, 144(1), 344-355.
- Arble, D. M., Ramsey, K. M., Bass, J., & Turek, F. W. (2010). Circadian disruption and metabolic disease: findings from animal models. *Best Pract Res Clin Endocrinol Metab*, 24(5), 785-800.
- Bae, K., Jin, X., Maywood, E. S., Hastings, M. H., Reppert, S. M., & Weaver, D. R. (2001). Differential functions of mPer1, mPer2, and mPer3 in the SCN circadian clock. *Neuron*, 30(2), 525-536.
- Beaule, C., Houle, L. M., & Amir, S. (2003). Expression profiles of PER2 immunoreactivity within the shell and core regions of the rat suprachiasmatic nucleus. *Journal of Molecular Neuroscience*.
- Behan, M., & Haberly, L. B. (1999). Intrinsic and efferent connections of the endopiriform nucleus in rat. *J Comp Neurol*, 408(4), 532-548.
- Benedetti, F., Serretti, A., Colombo, C., Barbini, B., Lorenzi, C., Campori, E., et al. (2003). Influence of CLOCK gene polymorphism on circadian mood fluctuation and illness recurrence in bipolar depression. *American journal of medical genetics Part B, Neuropsychiatric genetics : the official publication of the International Society of Psychiatric Genetics*, 123(1), 23-26.
- Boivin, D. B. (2000). Influence of sleep-wake and circadian rhythm disturbances in psychiatric disorders. *Journal of psychiatry & neuroscience : JPN*, 25(5), 446-458.
- Boulos, Z., & Terman, M. (1980). Food availability and daily biological rhythms. *Neurosci Biobehav Rev*, 4(2), 119-131.
- Bunger, M. K., Wilsbacher, L. D., Moran, S. M., Clendenin, C., Radcliffe, L. A., Hogenesch, J. B., et al. (2000). Mop3 is an essential component of the master circadian pacemaker in mammals. *Cell*, 103(7), 1009-1017.
- Bunney, J. N., & Potkin, S. G. (2008). Circadian abnormalities, molecular clock genes and chronobiological treatments in depression. *British medical bulletin*.

- Bunney, W. E., & Bunney, B. G. (2000). Molecular clock genes in man and lower animals: possible implications for circadian abnormalities in depression. *Neuropsychopharmacology*, 22(4), 335-345.
- Burwell, R. D., & Amaral, D. G. (1998). Perirhinal and postrhinal cortices of the rat: interconnectivity and connections with the entorhinal cortex. *J Comp Neurol*, 391(3), 293-321.
- Canteras, N. S., Ribeiro-Barbosa, E. R., Goto, M., Cipolla-Neto, J., & Swanson, L. W. (2011). The retinohypothalamic tract: comparison of axonal projection patterns from four major targets. *Brain Res Rev*, 65(2), 150-183.
- Cardinal, R. N., Parkinson, J. A., Hall, J., & Everitt, B. J. (2002). Emotion and motivation: the role of the amygdala, ventral striatum, and prefrontal cortex. *Neurosci Biobehav Rev*, 26(3), 321-352.
- Cassone, V. M., Warren, W. S., Brooks, D. S., & Lu, J. (1993). Melatonin, the pineal gland, and circadian rhythms. *J Biol Rhythms*, 8 Suppl, S73-81.
- Cenquizca, L. A., & Swanson, L. W. (2006). Analysis of direct hippocampal cortical field CA1 axonal projections to diencephalon in the rat. *J Comp Neurol*, 497(1), 101-114.
- Cenquizca, L. A., & Swanson, L. W. (2007). Spatial organization of direct hippocampal field CA1 axonal projections to the rest of the cerebral cortex. *Brain Res Rev*, 56(1), 1-26.
- Cermakian, N., & Boivin, D. B. (2003). A molecular perspective of human circadian rhythm disorders. *Brain research Brain research reviews*, 42(3), 204-220.
- Chen, S. T., Choo, K. B., Hou, M. F., Yeh, K. T., Kuo, S. J., & Chang, J. G. (2005). Deregulated expression of the PER1, PER2 and PER3 genes in breast cancers. *Carcinogenesis*, 26(7), 1241-1246.
- Czeisler, C. A., Duffy, J. F., Shanahan, T. L., Brown, E. N., Mitchell, J. F., Rimmer, D. W., et al. (1999). Stability, precision, and near-24-hour period of the human circadian pacemaker. *Science*, 284(5423), 2177-2181.
- D'Agostino, R. B. (1986). Tests for Normal Distribution. In R. B. D'Agostino & M. A. Stepenes (Eds.), *Goodness-of-Fit Techniques*: Marcel Dekker.
- Dann, S., & Pittendrigh, C. (1976). A functional analysis of the circadian pacemakers in nocturnal rodents: II. The variability of phase response curves. *Journal of Comparative Physiology*, 106, 253.
- Davis, M. (1998). Are different parts of the extended amygdala involved in fear versus anxiety? *Biol Psychiatry*, 44(12), 1239-1247.

- Day, H. E., Badiani, A., Uslaner, J. M., Oates, M. M., Vittoz, N. M., Robinson, T. E., et al. (2001). Environmental novelty differentially affects c-fos mRNA expression induced by amphetamine or cocaine in subregions of the bed nucleus of the stria terminalis and amygdala. *J Neurosci*, *21*(2), 732-740.
- Day, H. E., Curran, E. J., Watson, S. J., Jr., & Akil, H. (1999). Distinct neurochemical populations in the rat central nucleus of the amygdala and bed nucleus of the stria terminalis: evidence for their selective activation by interleukin-1beta. *J Comp Neurol*, *413*(1), 113-128.
- Debruyne, J. P., Noton, E., Lambert, C. M., Maywood, E. S., Weaver, D. R., & Reppert, S. M. (2006). A clock shock: mouse CLOCK is not required for circadian oscillator function. *Neuron*, *50*(3), 465-477.
- Deindl, E., Boengler, K., van Royen, N., & Schaper, W. (2002). Differential expression of GAPDH and beta3-actin in growing collateral arteries. *Mol Cell Biochem*, *236*(1-2), 139-146.
- Devinsky, O., Morrell, M. J., & Vogt, B. A. (1995). Contributions of anterior cingulate cortex to behaviour. *Brain*, *118* (Pt 1), 279-306.
- Dheda, K., Huggett, J. F., Chang, J. S., Kim, L. U., Bustin, S. A., Johnson, M. A., et al. (2005). The implications of using an inappropriate reference gene for real-time reverse transcription PCR data normalization. *Anal Biochem*, *344*(1), 141-143.
- Dong, H. W., Petrovich, G. D., & Swanson, L. W. (2001). Topography of projections from amygdala to bed nuclei of the stria terminalis. *Brain Res Brain Res Rev*, *38*(1-2), 192-246.
- Dong, H. W., Petrovich, G. D., Watts, A. G., & Swanson, L. W. (2001). Basic organization of projections from the oval and fusiform nuclei of the bed nuclei of the stria terminalis in adult rat brain. *J Comp Neurol*, *436*(4), 430-455.
- Drouyer, E., LeSauter, J., Hernandez, A. L., & Silver, R. (2010). Specializations of gastrin-releasing peptide cells of the mouse suprachiasmatic nucleus. *J Comp Neurol*, *518*(8), 1249-1263.
- Dunlap, J., Loros, J., & DeCoursey, P. (2004). *Chronobiology: Biological Timekeeping*. Sunderland, Massachusetts, USA: Sinauer Associates, Inc. Publishers.
- Eckel-Mahan, K. L., & Storm, D. R. (2009). Circadian rhythms and memory: not so simple as cogs and gears. *EMBO Rep*, *10*(6), 584-591.
- Erb, S., Salmaso, N., Rodaros, D., & Stewart, J. (2001). A role for the CRF-containing pathway from central nucleus of the amygdala to bed nucleus of the stria terminalis in the stress-induced reinstatement of cocaine seeking in rats. *Psychopharmacology (Berl)*, *158*(4), 360-365.

- Erb, S., Shaham, Y., & Stewart, J. (2001). Stress-induced relapse to drug seeking in the rat: Role of the bed nucleus of the stria terminalis and amygdala. *Stress*, *44*, 289-303.
- Etchegaray, J. P., Yang, X., DeBruyne, J. P., Peters, A. H., Weaver, D. R., Jenuwein, T., et al. (2006). The polycomb group protein EZH2 is required for mammalian circadian clock function. *J Biol Chem*, *281*(30), 21209-21215.
- Evans, J. A., Leise, T. L., Castanon-Cervantes, O., & Davidson, A. J. (2011). Intrinsic regulation of spatiotemporal organization within the suprachiasmatic nucleus. *PLoS One*, *6*(1), e15869.
- Feillet, C. A., Ripperger, J. A., Magnone, M. C., Dulloo, A., Albrecht, U., & Challet, E. (2006). Lack of food anticipation in *Per2* mutant mice. *Current biology : CB*, *16*(20), 2016-2022.
- Field, M. D., Maywood, E. S., O'Brien, J. A., Weaver, D. R., Reppert, S. M., & Hastings, M. H. (2000). Analysis of clock proteins in mouse SCN demonstrates phylogenetic divergence of the circadian clockwork and resetting mechanisms. *Neuron*, *25*(2), 437-447.
- Foley, N. C., Tong, T. Y., Foley, D., Lesauter, J., Welsh, D. K., & Silver, R. (2011). Characterization of orderly spatiotemporal patterns of clock gene activation in mammalian suprachiasmatic nucleus. *Eur J Neurosci*, *33*(10), 1851-1865.
- Fu, L., Pelicano, H., Liu, J., Huang, P., & Lee, C. (2002). The circadian gene *Period2* plays an important role in tumor suppression and DNA damage response in vivo. *Cell*, *111*(1), 41-50.
- Funk, D., & Amir, S. (2000). Circadian modulation of fos responses to odor of the red fox, a rodent predator, in the rat olfactory system. *Brain Res*, *866*(1-2), 262-267.
- Gavrila, A. M., Robinson, B., Hoy, J., Stewart, J., Bhargava, A., & Amir, S. (2008). Double-stranded RNA-mediated suppression of *Period2* expression in the suprachiasmatic nucleus disrupts circadian locomotor activity in rats. *Neuroscience*, *154*(2), 409-414.
- Gerfen, C. (2004). Basal Ganglia. In G. Paxinos (Ed.), *The Rat Nervous System* (3rd ed., pp. 455-508). San Diego: Elsevier Academic Press.
- Gerstner, J. R., & Yin, J. C. (2010). Circadian rhythms and memory formation. *Nat Rev Neurosci*, *11*(8), 577-588.
- Gould, E., Tanapat, P., Hastings, N. B., & Shors, T. J. (1999). Neurogenesis in adulthood: a possible role in learning. *Trends Cogn Sci*, *3*(5), 186-192.

- Governale, M. M., & Lee, T. M. (2001). Olfactory cues accelerate reentrainment following phase shifts and entrain free-running rhythms in female *Octodon degus* (Rodentia). *J Biol Rhythms*, *16*(5), 489-501.
- Green, D. J., & Gillette, R. (1982). Circadian rhythm of firing rate recorded from single cells in the rat suprachiasmatic brain slice. *Brain Res*, *245*(1), 198-200.
- Groos, G., & Hendriks, J. (1982). Circadian rhythms in electrical discharge of rat suprachiasmatic neurones recorded in vitro. *Neurosci Lett*, *34*(3), 283-288.
- Guilding, C., & Piggins, H. D. (2007). Challenging the omnipotence of the suprachiasmatic timekeeper: are circadian oscillators present throughout the mammalian brain? *Eur J Neurosci*, *25*(11), 3195-3216.
- Gygi, S. P., Rochon, Y., Franza, B. R., & Aebersold, R. (1999). Correlation between protein and mRNA abundance in yeast. *Mol Cell Biol*, *19*(3), 1720-1730.
- Haberly, L. B. (1990). Olfactory cortex. In G. M. Shepherd (Ed.), *Synaptic Organization of the brain* (pp. 317-345). New York: Oxford University Press.
- Harbour, V. L., Robinson, B., & Amir, S. (2011). Variations in Daily Expression of the Circadian Clock Protein, PER2, in the Rat Limbic Forebrain During Stable Entrainment to a Long Light Cycle. *Journal of molecular neuroscience* *45*(2), 154-161.
- Harbour, V. L., Weigl, Y., Robinson, B., & Amir, S. (2010). Comprehensive mapping of PERIOD2 expression patterns in the rat brain across the 24-hour day. *Program No. 698.14. 2010 Abstract Viewer/Itinerary Planner, San Diego, CA: SfN, 2010. Online.*
- Harbour, V. L., Weigl, Y., Robinson, B., & Amir, S. (2011). PERIOD2 rhythms in 20 brain regions across 48 time-points. *Poster session presented at the meeting of Symposium of Circadian Rhythms Research in Canada, Montreal, QC.*
- Herzog, E. D., & Huckfeldt, R. M. (2003). Circadian entrainment to temperature, but not light, in the isolated suprachiasmatic nucleus. *J Neurophysiol*, *90*(2), 763-770.
- Herzog, E. D., Takahashi, J. S., & Block, G. D. (1998). Clock controls circadian period in isolated suprachiasmatic nucleus neurons. *Nat Neurosci*, *1*(8), 708-713.
- Hogenesch, J. B., Chan, W. K., Jackiw, V. H., Brown, R. C., Gu, Y. Z., Pray-Grant, M., et al. (1997). Characterization of a subset of the basic-helix-loop-helix-PAS superfamily that interacts with components of the dioxin signaling pathway. *J Biol Chem*, *272*(13), 8581-8593.
- Hogenesch, J. B., Panda, S., Kay, S., & Takahashi, J. S. (2003). Circadian transcriptional output in the SCN and liver of the mouse. *Novartis Found Symp*, *253*, 171-180; discussion 152-175, 102-179, 180-173 passim.

- Honma, S., Honma, K., & Hiroshige, T. (1984). Dissociation of circadian rhythms in rats with a hypothalamic island. *Am J Physiol*, 246(6 Pt 2), R949-954.
- Hood, S. (2010). *Regulation by endogenous dopamine of the expression of the clock protein, PERIOD2, in the forebrain of the male Wistar rat*. Unpublished Doctoral dissertation, Concordia University, Montreal.
- Hood, S., Cassidy, P., Cossette, M. P., Weigl, Y., Verwey, M., Robinson, B., et al. (2010). Endogenous dopamine regulates the rhythm of expression of the clock protein PER2 in the rat dorsal striatum via daily activation of D2 dopamine receptors. *The Journal of neuroscience*, 30(42), 14046-14058.
- Hua, H., Wang, Y., Wan, C., Liu, Y., Zhu, B., Yang, C., et al. (2006). Circadian gene mPer2 overexpression induces cancer cell apoptosis. *Cancer Sci*, 97(7), 589-596.
- Iitaka, C., Miyazaki, K., Akaike, T., & Ishida, N. (2005). A role for glycogen synthase kinase-3beta in the mammalian circadian clock. *J Biol Chem*, 280(33), 29397-29402.
- Imbesi, M., Yildiz, S., Dirim Arslan, A., Sharma, R., Manev, H., & Uz, T. (2009). Dopamine receptor-mediated regulation of neuronal "clock" gene expression. *Neuroscience*, 158(2), 537-544.
- Inouye, S. T., & Kawamura, H. (1979). Persistence of circadian rhythmicity in a mammalian hypothalamic "island" containing the suprachiasmatic nucleus. *Proc Natl Acad Sci U S A*, 76(11), 5962-5966.
- Jilg, A., Moek, J., Weaver, D. R., Korf, H. W., Stehle, J. H., & von Gall, C. (2005). Rhythms in clock proteins in the mouse pars tuberalis depend on MT1 melatonin receptor signalling. *Eur J Neurosci*, 22(11), 2845-2854.
- Jin, X., Shearman, L. P., Weaver, D. R., Zylka, M. J., de Vries, G. J., & Reppert, S. M. (1999). A molecular mechanism regulating rhythmic output from the suprachiasmatic circadian clock. *Cell*, 96(1), 57-68.
- Kalsbeek, A., Perreau-Lenz, S., & Buijs, R. M. (2006). A network of (autonomic) clock outputs. *Chronobiol Int*, 23(1-2), 201-215.
- Ko, C. H., & Takahashi, J. S. (2006). Molecular components of the mammalian circadian clock. *Hum Mol Genet*, 15 Spec No 2, R271-277.
- Ko, M. L., Shi, L., Tsai, J. Y., Young, M. E., Neuendorff, N., Earnest, D. J., et al. (2011). Cardiac-specific mutation of Clock alters the quantitative measurements of physical activities without changing behavioral circadian rhythms. *J Biol Rhythms*, 26(5), 412-422.
- Kobayashi, M. (2011). Macroscopic connection of rat insular cortex: anatomical bases underlying its physiological functions. *Int Rev Neurobiol*, 97, 285-303.

- Kohler, C. (1988). Intrinsic connections of the retrohippocampal region in the rat brain: III. The lateral entorhinal area. *J Comp Neurol*, 271(2), 208-228.
- Kowianski, P., Lipowska, M., & Morys, J. (1999). The piriform cortex and the endopiriform nucleus in the rat reveal generally similar pattern of connections. *Folia Morphol (Warsz)*, 58(1), 9-19.
- Krushel, L. A., & van der Kooy, D. (1988). Visceral cortex: integration of the mucosal senses with limbic information in the rat agranular insular cortex. *J Comp Neurol*, 270(1), 39-54, 62-33.
- Kume, K., Zylka, M. J., Sriram, S., Shearman, L. P., Weaver, D. R., Jin, X., et al. (1999). mCRY1 and mCRY2 are essential components of the negative limb of the circadian clock feedback loop. *Cell*, 98(2), 193-205.
- Lamont, E. W., Diaz, L. R., Barry-Shaw, J., Stewart, J., & Amir, S. (2005). Daily restricted feeding rescues a rhythm of period2 expression in the arrhythmic suprachiasmatic nucleus. *Neuroscience*, 132(2), 245-248.
- Lamont, E. W., James, F. O., Boivin, D. B., & Cermakian, N. (2007). From circadian clock gene expression to pathologies. *Sleep medicine*, 8(6), 547-556.
- Lamont, E. W., Robinson, B., Stewart, J., & Amir, S. (2005). The central and basolateral nuclei of the amygdala exhibit opposite diurnal rhythms of expression of the clock protein Period2. *Proc Natl Acad Sci U S A*, 102(11), 4180-4184.
- Leak, R. K., Card, J. P., & Moore, R. Y. (1999). Suprachiasmatic pacemaker organization analyzed by viral transynaptic transport. *Brain Res*, 819(1-2), 23-32.
- Leak, R. K., & Moore, R. Y. (2001). Topographic organization of suprachiasmatic nucleus projection neurons. *J Comp Neurol*, 433(3), 312-334.
- Lee, C. C. (2006). Tumor suppression by the mammalian Period genes. *Cancer causes & control : CCC*, 17(4), 525-530.
- Lee, Y., & Davis, M. (1997). Role of the hippocampus, the bed nucleus of the stria terminalis, and the amygdala in the excitatory effect of corticotropin-releasing hormone on the acoustic startle reflex. *J Neurosci*, 17(16), 6434-6446.
- Lehman, M. N., Silver, R., Gladstone, W. R., Kahn, R. M., Gibson, M., & Bittman, E. L. (1987). Circadian rhythmicity restored by neural transplant. Immunocytochemical characterization of the graft and its integration with the host brain. *J Neurosci*, 7(6), 1626-1638.
- Li, S. X., Liu, L. J., Jiang, W. G., & Lu, L. (2009). Morphine withdrawal produces circadian rhythm alterations of clock genes in mesolimbic brain areas and peripheral blood mononuclear cells in rats. *J Neurochem*, 109(6), 1668-1679.

- Linkowski, P., Kerkhofs, M., Van Onderbergen, A., Hubain, P., Copinschi, G., L'Hermite-Baleriaux, M., et al. (1994). The 24-hour profiles of cortisol, prolactin, and growth hormone secretion in mania. *Arch Gen Psychiatry*, *51*(8), 616-624.
- Livak, K. J., & Schmittgen, T. D. (2001). Analysis of relative gene expression data using real-time quantitative PCR and the 2(-Delta Delta C(T)) Method. *Methods*, *25*(4), 402-408.
- Lopez-Molina, L., Conquet, F., Dubois-Dauphin, M., & Schibler, U. (1997). The DBP gene is expressed according to a circadian rhythm in the suprachiasmatic nucleus and influences circadian behavior. *Embo J*, *16*(22), 6762-6771.
- Loscher, W., & Ebert, U. (1996). The role of the piriform cortex in kindling. *Prog Neurobiol*, *50*(5-6), 427-481.
- Lowrey, P. L., Shimomura, K., Antoch, M. P., Yamazaki, S., Zemenides, P. D., Ralph, M. R., et al. (2000). Positional syntenic cloning and functional characterization of the mammalian circadian mutation tau. *Science*, *288*(5465), 483-492.
- Lowrey, P. L., & Takahashi, J. S. (2000). Genetics of the mammalian circadian system: Photic entrainment, circadian pacemaker mechanisms, and posttranslational regulation. *Annu Rev Genet*, *34*, 533-562.
- Lucas, R. J., Stirland, J. A., Darrow, J. M., Menaker, M., & Loudon, A. S. (1999). Free running circadian rhythms of melatonin, luteinizing hormone, and cortisol in Syrian hamsters bearing the circadian tau mutation. *Endocrinology*, *140*(2), 758-764.
- Malberg, J. E., & Duman, R. S. (2003). Cell proliferation in adult hippocampus is decreased by inescapable stress: reversal by fluoxetine treatment. *Neuropsychopharmacology*, *28*(9), 1562-1571.
- Masubuchi, S., Honma, S., Abe, H., Ishizaki, K., Namihira, M., Ikeda, M., et al. (2000). Clock genes outside the suprachiasmatic nucleus involved in manifestation of locomotor activity rhythm in rats. *Eur J Neurosci*, *12*(12), 4206-4214.
- Maywood, E. S., Chesham, J. E., O'Brien, J. A., & Hastings, M. H. (2011). A diversity of paracrine signals sustains molecular circadian cycling in suprachiasmatic nucleus circuits. *Proc Natl Acad Sci U S A*, *108*(34), 14306-14311.
- McClung, C. A. (2007a). Clock genes and bipolar disorder: implications for therapy. *Pharmacogenomics*, *8*(9), 1097-1100.
- McClung, C. A. (2007b). Role for the Clock gene in bipolar disorder. *Cold Spring Harbor symposia on quantitative biology*, *72*, 637-644.
- McClung, C. A., Sidiropoulou, K., Vitaterna, M., Takahashi, J. S., White, F. J., Cooper, D. C., et al. (2005). Regulation of dopaminergic transmission and cocaine reward

by the Clock gene. *Proceedings of the National Academy of Sciences of the United States of America*, 102(26), 9377-9381.

- McDonald, A. J., Shammah-Lagnado, S. J., Shi, C., & Davis, M. (1999). Cortical afferents to the extended amygdala. *Ann N Y Acad Sci*, 877, 309-338.
- McEwen, B. S. (2001). Plasticity of the hippocampus: adaptation to chronic stress and allostatic load. *Ann N Y Acad Sci*, 933, 265-277.
- Mieda, M., Williams, S. C., Richardson, J. A., Tanaka, K., & Yanagisawa, M. (2006). The dorsomedial hypothalamic nucleus as a putative food-entrainable circadian pacemaker. *Proc Natl Acad Sci U S A*, 103(32), 12150-12155.
- Mistlberger, R. E. (1994). Circadian food-anticipatory activity: formal models and physiological mechanisms. *Neurosci Biobehav Rev*, 18(2), 171-195.
- Mistlberger, R. E., & Skene, D. J. (2005). Nonphotic entrainment in humans? *J Biol Rhythms*, 20(4), 339-352.
- Moga, M. M., & Moore, R. Y. (1997). Organization of neural inputs to the suprachiasmatic nucleus in the rat. *J Comp Neurol*, 389(3), 508-534.
- Moore, R. Y., & Lenn, N. J. (1972). A retinohypothalamic projection in the rat. *J Comp Neurol*, 146(1), 1-14.
- Moore, R. Y., & Speh, J. C. (1993). GABA is the principal neurotransmitter of the circadian system. *Neurosci Lett*, 150(1), 112-116.
- Moore, R. Y., Speh, J. C., & Leak, R. K. (2002). Suprachiasmatic nucleus organization. *Cell Tissue Res*, 309(1), 89-98.
- Morin, L. P., & Blanchard, J. H. (2001). Neuromodulator content of hamster intergeniculate leaflet neurons and their projection to the suprachiasmatic nucleus or visual midbrain. *J Comp Neurol*, 437(1), 79-90.
- Motulsky, H., & Christopoulos, A. (2003). *Fitting models to biological data using linear and nonlinear regression. A practical guide to curve fitting.*, from www.graphpad.com.
- Motulsky, H. J., & Brown, R. E. (2006). Detecting outliers when fitting data with nonlinear regression - a new method based on robust nonlinear regression and the false discovery rate. *BMC Bioinformatics*, 7, 123.
- Mrosovsky, N. (1996). Locomotor activity and non-photic influences on circadian clocks. *Biol Rev Camb Philos Soc*, 71(3), 343-372.
- Mukherjee, S., Coque, L., Cao, J. L., Kumar, J., Chakravarty, S., Asaithamby, A., et al. (2010). Knockdown of Clock in the ventral tegmental area through RNA

- interference results in a mixed state of mania and depression-like behavior. *Biol Psychiatry*, 68(6), 503-511.
- Neafsey, E. J., Terreberry, K. M., Hurley, K. M., Ruit, K. G., & Fryszak, R. J. (1993). Anterior cingulate cortex in rodents: connections, visceral control functions, and implications for emotion. In B. A. Vogt & M. Gabriel (Eds.), *Neurobiology of Cingulate Cortex and Limbic Thalamus: A Comprehensive Handbook* (pp. 206-233). Birkhauser, Boston.
- Pantazopoulos, H., Dolatshad, H., & Davis, F. C. (2011). A fear-inducing odor alters PER2 and c-Fos expression in brain regions involved in fear memory. *PLoS One*, 6(5), e20658.
- Partonen, T., Treutlein, J., Alpmann, A., Frank, J., Johansson, C., Depner, M., et al. (2007). Three circadian clock genes *Per2*, *Arntl*, and *Npas2* contribute to winter depression. *Annals of medicine*, 39(3), 229-238.
- Paxinos, G., & Watson, C. (2005). *The Rat Brain: In stereotaxic coordinates* (5th ed.): Elsevier.
- Perrin, J. S., Segall, L. A., Harbour, V. L., Woodside, B., & Amir, S. (2006). The expression of the clock protein PER2 in the limbic forebrain is modulated by the estrous cycle. *Proceedings of the National Academy of Sciences of the United States of America*, 103(14), 5591-5596.
- Petrovich, G. D., Canteras, N. S., & Swanson, L. W. (2001). Combinatorial amygdalar inputs to hippocampal domains and hypothalamic behavior systems. *Brain Res Brain Res Rev*, 38(1-2), 247-289.
- Petrovich, G. D., & Gallagher, M. (2003). Amygdala subsystems and control of feeding behavior by learned cues. *Ann N Y Acad Sci*, 985, 251-262.
- Pickard, G. E. (1985). Bifurcating axons of retinal ganglion cells terminate in the hypothalamic suprachiasmatic nucleus and the intergeniculate leaflet of the thalamus. *Neurosci Lett*, 55(2), 211-217.
- Pikkarainen, M., Ronkko, S., Savander, V., Insausti, R., & Pitkanen, A. (1999). Projections from the lateral, basal, and accessory basal nuclei of the amygdala to the hippocampal formation in rat. *J Comp Neurol*, 403(2), 229-260.
- Pitkanen, A., Pikkarainen, M., Nurminen, N., & Ylinen, A. (2000). Reciprocal connections between the amygdala and the hippocampal formation, perirhinal cortex, and postrhinal cortex in rat. A review. *Ann N Y Acad Sci*, 911, 369-391.
- Pittendrigh, C. S., & Daan, S. (1976a). A Functional Analysis of Circadian Pacemakers in Nocturnal Rodents: V. Pacemaker Structure: A Clock for All Seasons. *J. Comp. Physiol.*, 106, 333-355.

- Pittendrigh, C. S., & Daan, S. (1976b). A Functional Analysis of Circadian Pacemakers in Nocturnal Rodents: I. The stability and lability of spontaneous frequency. *J. Comp. Physiol.*, *106*, 223-252.
- Preitner, N., Damiola, F., Lopez-Molina, L., Zakany, J., Duboule, D., Albrecht, U., et al. (2002). The orphan nuclear receptor REV-ERB α controls circadian transcription within the positive limb of the mammalian circadian oscillator. *Cell*, *110*(2), 251-260.
- Prolo, L. M., Takahashi, J. S., & Herzog, E. D. (2005). Circadian rhythm generation and entrainment in astrocytes. *The Journal of neuroscience* *25*(2), 404-408.
- Radonic, A., Thulke, S., Mackay, I. M., Landt, O., Siegert, W., & Nitsche, A. (2004). Guideline to reference gene selection for quantitative real-time PCR. *Biochem Biophys Res Commun*, *313*(4), 856-862.
- Ralph, M. R., Foster, R. G., Davis, F. C., & Menaker, M. (1990). Transplanted suprachiasmatic nucleus determines circadian period. *Science*, *247*(4945), 975-978.
- Ralph, M. R., & Menaker, M. (1988). A mutation of the circadian system in golden hamsters. *Science*, *241*(4870), 1225-1227.
- Ramanathan, C., Stowie, A., Smale, L., & Nunez, A. (2010a). PER2 rhythms in the amygdala and bed nucleus of the stria terminalis of the diurnal grass rat (*Arvicanthis niloticus*). *Neuroscience Letters*, *473*(3), 220-223.
- Ramanathan, C., Stowie, A., Smale, L., & Nunez, A. (2010b). Phase preference for the display of activity is associated with the phase of extra-suprachiasmatic nucleus oscillators within and between species. *Neuroscience*, *170*(3), 758-772.
- Reep, R. L., & Winans, S. S. (1982a). Afferent connections of dorsal and ventral agranular insular cortex in the hamster *Mesocricetus auratus*. *Neuroscience*, *7*(5), 1265-1288.
- Reep, R. L., & Winans, S. S. (1982b). Efferent connections of dorsal and ventral agranular insular cortex in the hamster, *Mesocricetus auratus*. *Neuroscience*, *7*(11), 2609-2635.
- Refinetti, R., & Menaker, M. (1992). The circadian rhythm of body temperature. *Physiol Behav*, *51*(3), 613-637.
- Reick, M., Garcia, J. A., Dudley, C., & McKnight, S. L. (2001). NPAS2: an analog of clock operative in the mammalian forebrain. *Science*, *293*(5529), 506-509.
- Reppert, S. M., & Weaver, D. R. (2001). Molecular analysis of mammalian circadian rhythms. *Annu Rev Physiol*, *63*, 647-676.

- Reppert, S. M., & Weaver, D. R. (2002). Coordination of circadian timing in mammals. *Nature*, *418*(6901), 935-941.
- Ripperger, J. A., Schmutz, I., & Albrecht, U. (2010). PERsuading nuclear receptors to dance the circadian rhythm. *Cell Cycle*, *9*(13), 2515-2521.
- Roybal, K., Theobald, D., Graham, A., DiNieri, J. A., Russo, S. J., Krishnan, V., et al. (2007). Mania-like behavior induced by disruption of CLOCK. *Proceedings of the National Academy of Sciences of the United States of America*, *104*(15), 6406-6411.
- Ruby, N. F., Burns, D. E., & Heller, H. C. (1999). Circadian rhythms in the suprachiasmatic nucleus are temperature-compensated and phase-shifted by heat pulses in vitro. *J Neurosci*, *19*(19), 8630-8636.
- Rusak, B., & Zucker, I. (1979). Neural regulation of circadian rhythms. *Physiol Rev*, *59*(3), 449-526.
- Sahar, S., Zocchi, L., Kinoshita, C., Borrelli, E., & Sassone-Corsi, P. (2010). Regulation of BMAL1 protein stability and circadian function by GSK3beta-mediated phosphorylation. *PLoS One*, *5*(1), e8561.
- Sato, T. K., Panda, S., Miraglia, L. J., Reyes, T. M., Rudic, R. D., McNamara, P., et al. (2004). A functional genomics strategy reveals Rora as a component of the mammalian circadian clock. *Neuron*, *43*(4), 527-537.
- Schmutz, I., Ripperger, J., Baeriswyl-Aebischer, S., & Albrecht, U. (2010). The mammalian clock component PERIOD2 coordinates circadian output by interaction with nuclear receptors. *Genes & development*, *24*(4), 345-357.
- Segall, L. A., & Amir, S. (2010). Glucocorticoid regulation of clock gene expression in the mammalian limbic forebrain. *J Mol Neurosci*, *42*(2), 168-175.
- Segall, L. A., Perrin, J. S., Walker, C. D., Stewart, J., & Amir, S. (2006). Glucocorticoid rhythms control the rhythm of expression of the clock protein, Period2, in oval nucleus of the bed nucleus of the stria terminalis and central nucleus of the amygdala in rats. *Neuroscience*, *140*(3), 753-757.
- Serretti, A., Benedetti, F., Mandelli, L., Lorenzi, C., Pirovano, A., Colombo, C., et al. (2003). Genetic dissection of psychopathological symptoms: Insomnia in mood disorders and CLOCK gene polymorphism. *Am J Med Genet Part B Neuropsychiatr Genet*, *121B*, 35-38.
- Sewards, T. V., & Sewards, M. A. (2003). Input and output stations of the entorhinal cortex: superficial vs. deep layers or lateral vs. medial divisions? *Brain Res Brain Res Rev*, *42*(3), 243-251.

- Shearman, L. P., Jin, X., Lee, C., Reppert, S. M., & Weaver, D. R. (2000). Targeted disruption of the mPer3 gene: subtle effects on circadian clock function. *Mol Cell Biol*, 20(17), 6269-6275.
- Shearman, L. P., Sriram, S., Weaver, D. R., Maywood, E. S., Chaves, I., Zheng, B., et al. (2000). Interacting molecular loops in the mammalian circadian clock. *Science*, 288(5468), 1013-1019.
- Shieh, K. R. (2003). Distribution of the rhythm-related genes rPERIOD1, rPERIOD2, and rCLOCK, in the rat brain. *Neuroscience*, 118(3), 831-843.
- Silver, R., LeSauter, J., Tresco, P. A., & Lehman, M. N. (1996). A diffusible coupling signal from the transplanted suprachiasmatic nucleus controlling circadian locomotor rhythms. *Nature*, 382(6594), 810-813.
- Smale, L., Nunez, A., & Schwartz, M. D. (2008). Rhythms in a diurnal brain. *Biological Rhythm Research*, 39(3), 305-318.
- Spanagel, R., Pendyala, G., Abarca, C., Zghoul, T., Sanchis-Segura, C., Magnone, M. C., et al. (2005). The clock gene Per2 influences the glutamatergic system and modulates alcohol consumption. *Nature medicine*, 11(1), 35-42.
- Stephan, F. K. (1983). Circadian rhythms in the rat: constant darkness, entrainment to T cycles and to skeleton photoperiods. *Physiol Behav*, 30(3), 451-462.
- Stephan, F. K. (2002). The "other" circadian system: food as a Zeitgeber. *J Biol Rhythms*, 17(4), 284-292.
- Stephan, F. K., Swann, J. M., & Sisk, C. L. (1979). Entrainment of circadian rhythms by feeding schedules in rats with suprachiasmatic lesions. *Behav Neural Biol*, 25(4), 545-554.
- Stephan, F. K., & Zucker, I. (1972). Circadian rhythms in drinking behavior and locomotor activity of rats are eliminated by hypothalamic lesions. *Proc Natl Acad Sci U S A*, 69(6), 1583-1586.
- Swanson, L. W. (2003). The amygdala and its place in the cerebral hemisphere. *Ann N Y Acad Sci*, 985, 174-184.
- Swanson, L. W. (2004). *Brain Maps: Structure of the Rat Brain. A laboratory guide with printed and electronic templates for data, models and schematics*. (3rd revised ed.). Amsterdam: Elsevier.
- Toh, K. L., Jones, C. R., He, Y., Eide, E. J., Hinz, W. A., Virshup, D. M., et al. (2001). An hPer2 phosphorylation site mutation in familial advanced sleep phase syndrome. *Science* 291(5506), 1040-1043.

- Trudel, E., & Bourque, C. W. (2003). A rat brain slice preserving synaptic connections between neurons of the suprachiasmatic nucleus, organum vasculosum lamina terminalis and supraoptic nucleus. *J Neurosci Methods*, *128*(1-2), 67-77.
- Trudel, E., & Bourque, C. W. (2010). Central clock excites vasopressin neurons by waking osmosensory afferents during late sleep. *Nat Neurosci*, *13*(4), 467-474.
- Tu, B. P., & McKnight, S. L. (2006). Metabolic cycles as an underlying basis of biological oscillations. *Nat Rev Mol Cell Biol*, *7*(9), 696-701.
- Turek, F. W., Joshu, C., Kohsaka, A., Lin, E., Ivanova, G., McDearmon, E., et al. (2005). Obesity and metabolic syndrome in circadian Clock mutant mice. *Science (New York, NY)*, *308*(5724), 1043-1045.
- Ueda, H. R., Chen, W., Adachi, A., Wakamatsu, H., Hayashi, S., Takasugi, T., et al. (2002). A transcription factor response element for gene expression during circadian night. *Nature*, *418*(6897), 534-539.
- Uz, T., Akhisaroglu, M., Ahmed, R., & Manev, H. (2003). The pineal gland is critical for circadian Period1 expression in the striatum and for circadian cocaine sensitization in mice. *Neuropsychopharmacology*, *28*(12), 2117-2123.
- Van den Pol, A. N. (1980). The hypothalamic suprachiasmatic nucleus of rat: intrinsic anatomy. *J Comp Neurol*, *191*(4), 661-702.
- van der Horst, G. T., Muijtjens, M., Kobayashi, K., Takano, R., Kanno, S., Takao, M., et al. (1999). Mammalian Cry1 and Cry2 are essential for maintenance of circadian rhythms. *Nature*, *398*(6728), 627-630.
- van Esseveldt, K. E., Lehman, M. N., & Boer, G. J. (2000). The suprachiasmatic nucleus and the circadian time-keeping system revisited. *Brain Res Brain Res Rev*, *33*(1), 34-77.
- Vandesompele, J., De Preter, K., Pattyn, F., Poppe, B., Van Roy, N., De Paepe, A., et al. (2002). Accurate normalization of real-time quantitative RT-PCR data by geometric averaging of multiple internal control genes. *Genome Biol*, *3*(7), RESEARCH0034.
- Verwey, M., & Amir, S. (2011). Nucleus-specific effects of meal duration on daily profiles of Period1 and Period2 protein expression in rats housed under restricted feeding. *Neuroscience*, *192*, 304-311.
- Verwey, M., Khoja, Z., Stewart, J., & Amir, S. (2007). Differential regulation of the expression of Period2 protein in the limbic forebrain and dorsomedial hypothalamus by daily limited access to highly palatable food in food-deprived and free-fed rats. *Neuroscience*, *147*(2), 277-285.

- Vitaterna, M. H., King, D. P., Chang, A. M., Kornhauser, J. M., Lowrey, P. L., McDonald, J. D., et al. (1994). Mutagenesis and mapping of a mouse gene, Clock, essential for circadian behavior. *Science*, 264(5159), 719-725.
- Vitaterna, M. H., Selby, C. P., Todo, T., Niwa, H., Thompson, C., Fruechte, E. M., et al. (1999). Differential regulation of mammalian period genes and circadian rhythmicity by cryptochromes 1 and 2. *Proc Natl Acad Sci U S A*, 96(21), 12114-12119.
- von Gall, C., Garabette, M. L., Kell, C. A., Frenzel, S., Dehghani, F., Schumm-Draeger, P. M., et al. (2002). Rhythmic gene expression in pituitary depends on heterologous sensitization by the neurohormone melatonin. *Nat Neurosci*, 5(3), 234-238.
- Waddington Lamont, E., Harbour, V. L., Barry-Shaw, J., Renteria Diaz, L., Robinson, B., Stewart, J., et al. (2007). Restricted access to food, but not sucrose, saccharine, or salt, synchronizes the expression of Period2 protein in the limbic forebrain. *Neuroscience*, 144(2), 402-411.
- Waddington Lamont, E., Legault-Coutu, D., Cermakian, N., & Boivin, D. (2007). The role of circadian clock genes in mental disorders. *Dialogues in Clinical Neuroscience*, 9(3), 333.
- Wakamatsu, H., Yoshinobu, Y., Aida, R., Moriya, T., Akiyama, M., & Shibata, S. (2001). Restricted-feeding-induced anticipatory activity rhythm is associated with a phase-shift of the expression of mPer1 and mPer2 mRNA in the cerebral cortex and hippocampus but not in the suprachiasmatic nucleus of mice. *Eur J Neurosci*, 13(6), 1190-1196.
- Wald, A., & Wolfowitz, J. (1940). On a test whether two samples are from the same population. *Annals of Mathematical Statistics*, 11, 147-162.
- Watson, R. E., Jr., Wiegand, S. J., Clough, R. W., & Hoffman, G. E. (1986). Use of cryoprotectant to maintain long-term peptide immunoreactivity and tissue morphology. *Peptides*, 7(1), 155-159.
- Watts, A. G., & Swanson, L. W. (1987). Efferent projections of the suprachiasmatic nucleus: II. Studies using retrograde transport of fluorescent dyes and simultaneous peptide immunohistochemistry in the rat. *J Comp Neurol*, 258(2), 230-252.
- Webb, A. B., Angelo, N., Huettner, J. E., & Herzog, E. D. (2009). Intrinsic, nondeterministic circadian rhythm generation in identified mammalian neurons. *Proc Natl Acad Sci U S A*, 106(38), 16493-16498.
- Weigl, Y., Harbour, V. L., Robinson, B., Dufresne, L., & Amir, S. (2010). Large scale analysis of clock gene rhythms in rats housed under normal lighting conditions reveals tissue-specific variability in clock machinery and output. *Poster session*

presented at the meeting of Symposium of Society for Research on Biological Rhythms, Sandestin, FL.

- Weitzman, E. D., Fukushima, D., Nogeire, C., Roffwarg, H., Gallagher, T. F., & Hellman, L. (1971). Twenty-four hour pattern of the episodic secretion of cortisol in normal subjects. *J Clin Endocrinol Metab*, 33(1), 14-22.
- Welsh, D. K., Logothetis, D. E., Meister, M., & Reppert, S. M. (1995). Individual neurons dissociated from rat suprachiasmatic nucleus express independently phased circadian firing rhythms. *Neuron*, 14(4), 697-706.
- Williams, D. L., & Schwartz, M. W. (2005). Out of synch: Clock mutation causes obesity in mice. *Cell metabolism*, 1(6), 355-356.
- Willuhn, I., Sun, W., & Steiner, H. (2003). Topography of cocaine-induced gene regulation in the rat striatum: relationship to cortical inputs and role of behavioural context. *Eur J Neurosci*, 17(5), 1053-1066.
- Witter, M. P., Naber, P. A., van Haeften, T., Machielsen, W. C., Rombouts, S. A., Barkhof, F., et al. (2000). Cortico-hippocampal communication by way of parallel parahippocampal-subicular pathways. *Hippocampus*, 10(4), 398-410.
- Witter, M. P., Wouterlood, F. G., Naber, P. A., & Van Haeften, T. (2000). Anatomical organization of the parahippocampal-hippocampal network. *Ann N Y Acad Sci*, 911, 1-24.
- Wyss, J. M., & Van Groen, T. (1992). Connections between the retrosplenial cortex and the hippocampal formation in the rat: a review. *Hippocampus*, 2(1), 1-11.
- Xu, Y., Padiath, Q. S., Shapiro, R. E., Jones, C. R., Wu, S. C., Saigoh, N., et al. (2005). Functional consequences of a CK1delta mutation causing familial advanced sleep phase syndrome. *Nature*, 434(7033), 640-644.
- Yamaguchi, S., Isejima, H., Matsuo, T., Okura, R., Yagita, K., Kobayashi, M., et al. (2003). Synchronization of cellular clocks in the suprachiasmatic nucleus. *Science*, 302(5649), 1408-1412.
- Yamaguchi, S., Mitsui, S., Yan, L., Yagita, K., Miyake, S., & Okamura, H. (2000). Role of DBP in the circadian oscillatory mechanism. *Mol Cell Biol*, 20(13), 4773-4781.
- Yamamoto, S., Shigeyoshi, Y., Ishida, Y., Fukuyama, T., Yamaguchi, S., Yagita, K., et al. (2001). Expression of the Per1 gene in the hamster: brain atlas and circadian characteristics in the suprachiasmatic nucleus. *J Comp Neurol*, 430(4), 518-532.
- Yamazaki, S., Kerbeshian, M. C., Hocker, C. G., Block, G. D., & Menaker, M. (1998). Rhythmic properties of the hamster suprachiasmatic nucleus in vivo. *J Neurosci*, 18(24), 10709-10723.

- Yamazaki, S., Numano, R., Abe, M., Hida, A., Takahashi, R., Ueda, M., et al. (2000). Resetting central and peripheral circadian oscillators in transgenic rats. *Science*, 288(5466), 682-685.
- Yan, L., Miyake, S., & Okamura, H. (2000). Distribution and circadian expression of dbp in SCN and extra-SCN areas in the mouse brain. *J Neurosci Res*, 59(2), 291-295.
- Yan, L., & Silver, R. (2002). Differential induction and localization of mPer1 and mPer2 during advancing and delaying phase shifts. *European Journal of Neuroscience*, 16(8), 1531-1540.
- Yan, L., & Silver, R. (2004). Resetting the brain clock: time course and localization of mPER1 and mPER2 protein expression in suprachiasmatic nuclei during phase shifts. *Eur J Neurosci*, 19(4), 1105-1109.
- Yang, X., Downes, M., Yu, R. T., Bookout, A. L., He, W., Straume, M., et al. (2006). Nuclear receptor expression links the circadian clock to metabolism. *Cell*, 126(4), 801-810.
- Yoo, S. H., Yamazaki, S., Lowrey, P. L., Shimomura, K., Ko, C. H., Buhr, E. D., et al. (2004). PERIOD2::LUCIFERASE real-time reporting of circadian dynamics reveals persistent circadian oscillations in mouse peripheral tissues. *Proc Natl Acad Sci U S A*, 101(15), 5339-5346.
- Yu, W., Nomura, M., & Ikeda, M. (2002). Interactivating feedback loops within the mammalian clock: BMAL1 is negatively autoregulated and upregulated by CRY1, CRY2, and PER2. *Biochem Biophys Res Commun*, 290(3), 933-941.
- Zheng, B., Albrecht, U., Kaasik, K., Sage, M., Lu, W., Vaishnav, S., et al. (2001). Nonredundant roles of the mPer1 and mPer2 genes in the mammalian circadian clock. *Cell*, 105(5), 683-694.
- Zheng, B., Larkin, D. W., Albrecht, U., Sun, Z. S., Sage, M., Eichele, G., et al. (1999). The mPer2 gene encodes a functional component of the mammalian circadian clock. *Nature*, 400(6740), 169-173.

APPENDIX

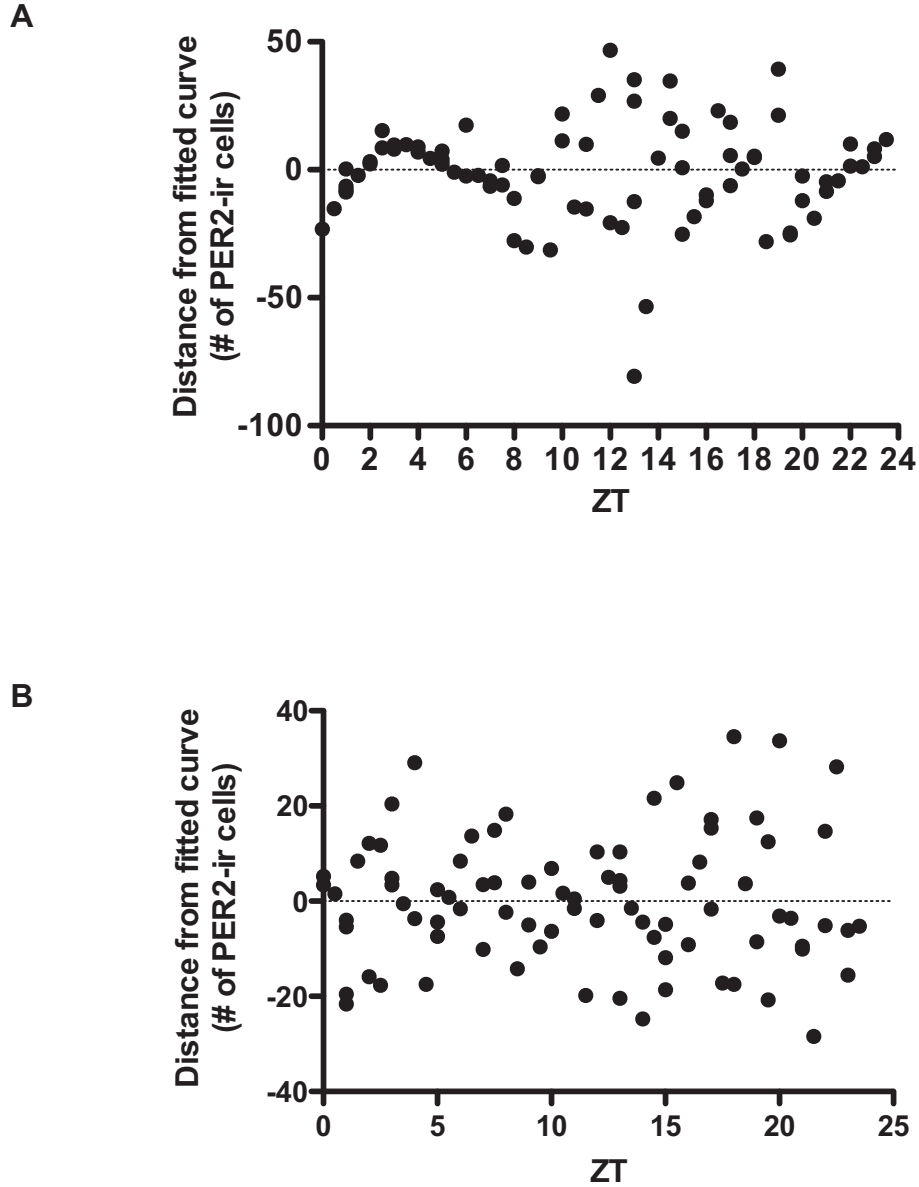


Figure A1. Suprachiasmatic Nucleus core. A) Residuals graph of SCNc showing the distance from the fitted curve (positive numbers above the curve, negative numbers below the curve) across 48 *Zeitgeber* times. This region failed the Runs Test, as can be seen by the pattern in the residuals. B) Residuals graph of a region that did not fail the Runs test (CA1) for comparison.

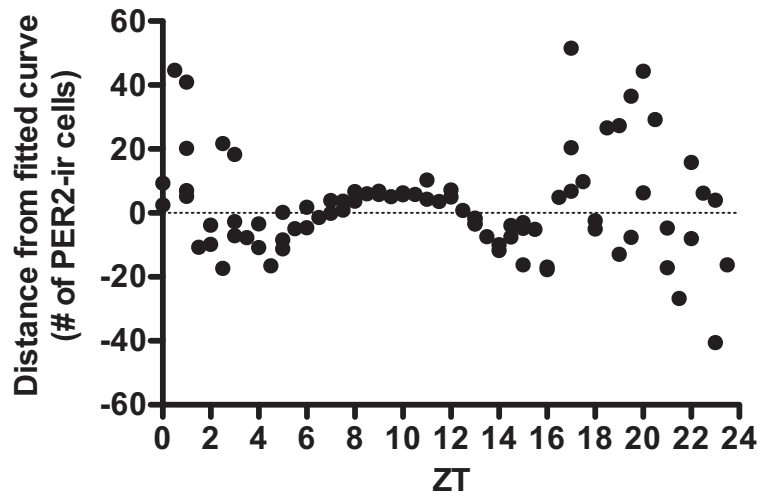


Figure A2. Dentate gyrus. Residuals graph of DG showing the distance from the fitted curve (positive numbers above the curve, negative numbers below the curve) across 48 *Zeitgeber* times. This region failed the Runs Test, as can be seen by the pattern in the residuals.

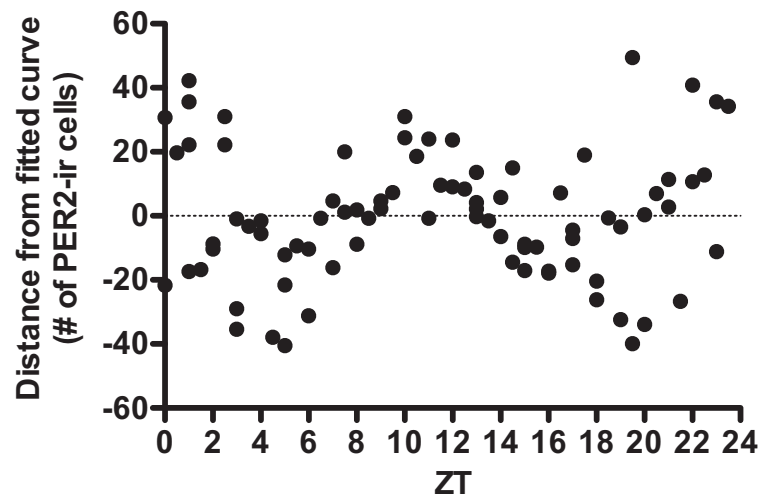


Figure A3. Anterior striatum, dorsal. Residuals graph of ASd showing the distance from the fitted curve (positive numbers above the curve, negative numbers below the curve) across 48 *Zeitgeber* times. This region failed the Runs Test, as can be seen by the pattern in the residuals.

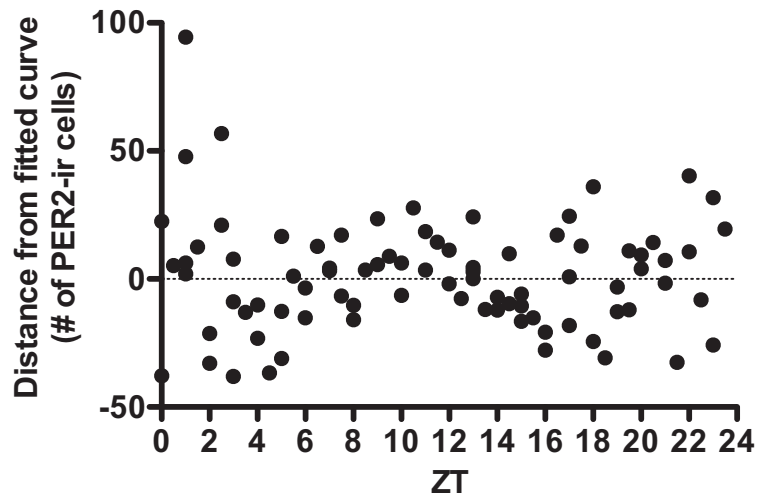


Figure A4. Posterior striatum, dorsal. Residuals graph of PSd showing the distance from the fitted curve (positive numbers above the curve, negative numbers below the curve) across 48 *Zeitgeber* times. This region failed the Runs Test, as can be seen by the pattern in the residuals.

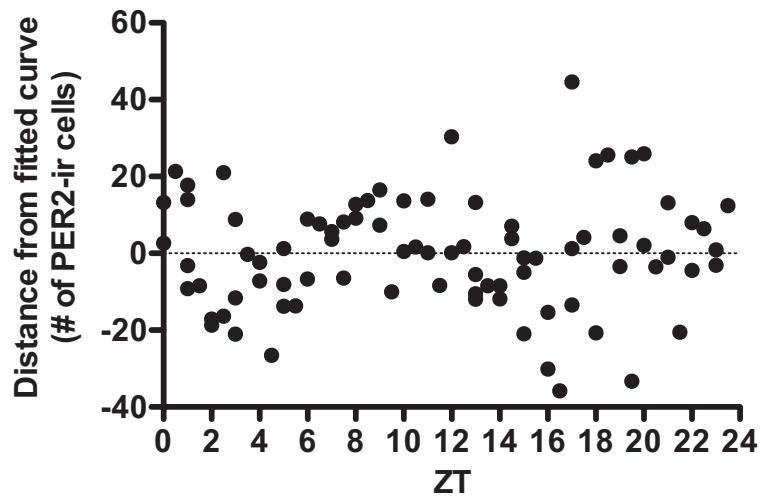


Figure A5. Endopiriform cortex, dorsal. Residuals graph of EPd showing the distance from the fitted curve (positive numbers above the curve, negative numbers below the curve) across 48 *Zeitgeber* times. This region failed the Runs Test, as can be seen by the pattern in the residuals.

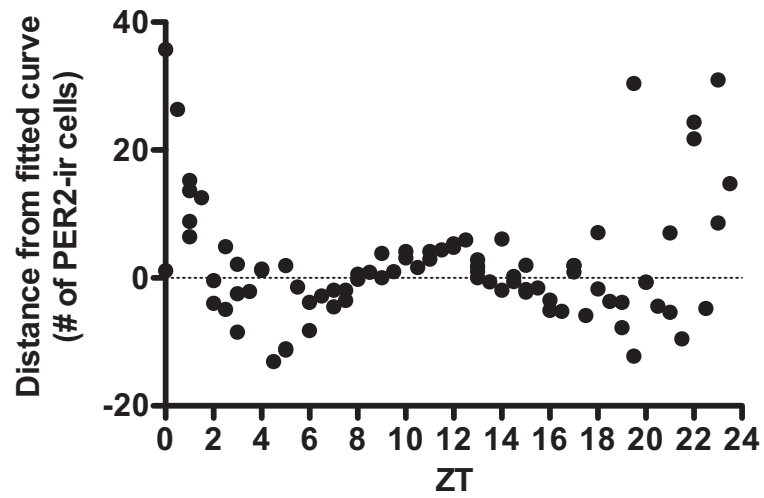


Figure A6. Piriform cortex, pyramidal layer. Residuals graph of PIR2 showing the distance from the fitted curve (positive numbers above the curve, negative numbers below the curve) across 48 *Zeitgeber* times. This region failed the Runs Test, as can be seen by the pattern in the residuals.